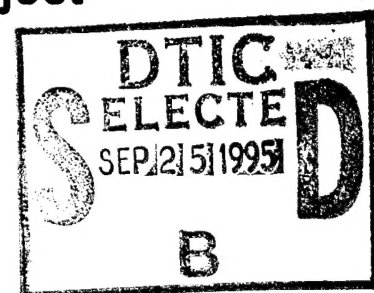
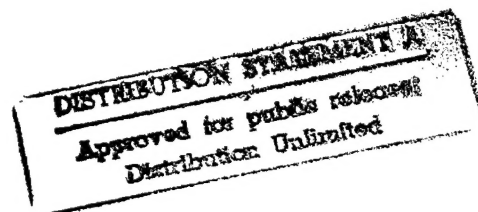


**Year 1**  
**Research and Development Status Report**  
**for**  
**GeoSAR**  
**A Radar Based Terrain Mapping Project**



*Contributors*

CALIFORNIA  
DEPARTMENT OF CONSERVATION

Integrated GeoData Management Unit  
Robert Yoha

Seismic Hazards Evaluation and Zonation Project  
Charles Real  
Rick Wilson  
Tim McCrink  
Emily Oatney  
Wayne Hayden  
Chris Wills

Farmland Mapping and Monitoring Program  
Molly Penberth

Timber Harvest Review Project  
Tom Spittler  
Mary Ann McKittrick

Office of Mine Reclamation  
Kit Custis

JET PROPULSION LABORATORY

Dr. Scott Hensley  
Dr. Jeff Klein  
Dr. Frank Webb  
Dr. Theirry Michel  
Dr. Ernesto Rodriguez  
Dr. Bijan Houshmand  
Dr. Thomas Thompson

CALGIS

Gerald Dildine  
Dr. Mushtaq Hussain  
Dr. Riad Munjy  
Dr. Jack Paris  
Jeffrey Seib  
Chris Bohain

**CLEARED**  
FOR OPEN PUBLICATION

SEP 15 1995 18

DIRECTORATE FOR FREEDOM OF INFORMATION  
AND SECURITY REVIEW (OASD-PA)  
DEPARTMENT OF DEFENSE

DTIC QUALITY INSPECTED 8

19950920 075

95-5-3676

**19950920 075**

**UNABLE TO GET PAGES 84 THRU 87 (FIG 3.1-21 THRU 3.1-25)**

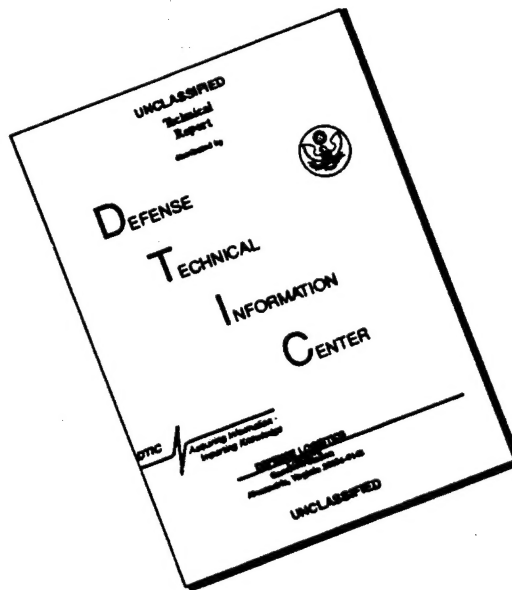
**AND PAGES 96 THRU 99 PER PATRICK RODELL(703) 696-0094**

**AT DEFENSE ADVANCED RESEARCH PROJECT AGENCY**

**ARLINGTON, VA.**

**MAY 22, 1996**

# DISCLAIMER NOTICE



**THIS DOCUMENT IS BEST  
QUALITY AVAILABLE. THE COPY  
FURNISHED TO DTIC CONTAINED  
A SIGNIFICANT NUMBER OF  
PAGES WHICH DO NOT  
REPRODUCE LEGIBLY.**

**19950920 075**

**UNABLE TO GET PAGES 84 THRU 87 (FIG 3.1-21 THRU 3.1-25)  
AND PAGES 96 THRU 99 PER PATRICK RODELL(703) 696-0094  
AT DEFENSE ADVANCED RESEARCH PROJECT AGENCY  
ARLINGTON, VA.**

**MAY 22, 1996**



# Contents

EXECUTIVE SUMMARY .....	ix
-------------------------	----

## Section 1: Introduction

1.1 PROJECT BACKGROUND .....	1
1.1.1 GeoSAR .....	1
1.1.2 Problem .....	1
1.1.3 Opportunity .....	2
1.1.4 Goals .....	3
1.2 GEOSAR TEAM .....	4
1.3 OVERVIEW OF YEAR 1 ACTIVITIES .....	5
1.3.1 Department of Conservation .....	5
1.3.2 Jet Propulsion Laboratory .....	5
1.3.3 Calgis .....	5
1.4 SITES AND USER EXPERIMENTS .....	6
1.4.1 Super Site #1 - Antioch Hills, Contra Costa County .....	8
1.4.2 Super Site #2 - Laurel Quad, Santa Cruz County .....	9
1.4.3 Test Site #3 - Gualala River Basin, Sonoma County .....	10
1.4.4 Test Site #4 - Iron Mountain Mine, Shasta County .....	11
1.4.5 Test Site #5 .....	12

## Section 2 : Data Collection and Support

2.1 JET PROPULSION LABORATORY .....	13
2.1.1 Mission Planning .....	13
2.1.1.1 Flight 1, Antioch Hills and Laurel Quad .....	13
2.1.1.2 Flight 2, Iron Mountain and Gualala River .....	14
2.1.2 Data Acquisition .....	14
2.1.2.1 Flight 1, Antioch Hills and Laurel Quad .....	14
2.1.2.2 Flight 2, Iron Mountain Mine and Gualala River .....	16
2.1.2.3 Flight 3, Northridge Area .....	16
2.1.2.4 Kinematic GPS .....	16
2.1.3 Overview of Interferometric Synthetic Aperture Radar and Processing .....	17
2.1.3.1 TOPSAR .....	22
2.1.3.2 Standard Processing .....	22
2.1.3.3 Calibration Activities .....	23
2.1.4.4 Land Cover Classification .....	23
2.2 CALGIS ACTIVITIES .....	24
2.2.1 Technical Assistance .....	24
2.2.2 Ground Truth .....	25
2.2.2.1 Site Preparation .....	25

☒  
☐  
☐  
*my letter*

Distribution	
Availability Codes	
Dist	Avail and/or Special
A-1	

2.2.2.1.1	Reconnaissance .....	25
2.2.2.1.2	Corner Reflector Deployment .....	25
2.2.2.1.2.1	Laurel Quad .....	25
2.2.2.1.2.2	Antioch Hills .....	26
2.2.2.1.2.3	Gualala River .....	26
2.2.2.1.2.4	Iron Mountain .....	26
2.2.2.2	Geodetic Control .....	26
2.2.2.2.1	Planning for Geodetic Control .....	26
2.2.2.2.2	Field Data Acquisition .....	29
2.2.2.2.3	Data Processing .....	29
2.2.2.3	Vegetation Transects .....	30
2.2.2.3.1	Test Grid A .....	30
2.2.2.3.2	Test Grid B .....	30
2.2.2.3.3	Test Grid C .....	31
2.2.2.3.4	Test Grid D .....	31
2.2.2.3.5	Test Grid E .....	31
2.2.3	Geometric Processing of Radar Data .....	32
2.2.3.1	Radar to GIS Conversion .....	32
2.2.3.2	Radar Mapping Coordinates to NAD83 Datum .....	32
2.2.3.3	Image and Height Resampling to NAD83 Datum .....	35
2.2.4	Multi-sensor Data for Land Use and Cover Mapping .....	36
2.2.4.1	Terrain Cover and Land Use Mapping .....	36
2.2.4.2	General Characteristics of TOPSAR Data .....	36
2.2.4.3	General Characteristics of Optical Data Used in the GeoSAR Program .....	38
2.2.4.4	Specific Approaches .....	39
2.2.4.4.1	Raster Conversion from 32-Bit Floating Point to 8-Bit Unsigned Integer .....	39
2.2.4.4.2	Decorrelation of MagdB8 and CorrPower8 Rasters .....	39
2.2.4.4.3	Aggregation of TOPSAR Rasters to Landsat TM Resolution .....	40
2.2.4.4.4	Proportional Indexing of Atmospherically-Corrected Landsat TM Rasters .....	40
2.2.4.4.5	Fusion of Landsat TM and SPOT Pan Rasters to TOPSAR .....	41
2.2.5	Photogrammetric Data Processing .....	41
2.2.5.1	Aerial Photography .....	41
2.2.5.2	Aerial Triangulation .....	42
2.2.5.2.1	Image Selection and Mensuration .....	42
2.2.5.2.2	Bundle Adjustment .....	43
2.2.5.3	Digital Orthophoto Production from SAR DEM .....	44

### Section 3: User Experiments

3.1	NON-VEGETATED HILLSLOPE DEM AND SLOPE HAZARDS EXPERIMENT .....	47
3.1.1	Abstract .....	47
3.1.2	Introduction .....	47
3.1.2.1	Purpose .....	47
3.1.2.2	Objectives .....	50
3.1.2.3	Site Description .....	51
3.1.3	User Experiment .....	52
3.1.3.1	Methodology .....	52
3.1.3.1.1	Landslide Inventory .....	53
3.1.3.1.1.1	Landslide Inventory Methodology .....	53
3.1.3.1.1.2	Results of Landslide Inventory .....	53

3.1.3.1.2	Soft Copy Photogrammetry .....	54
3.1.3.1.2.1	Stereo Models .....	57
3.1.3.1.2.2	Data Collection and DEM Building Process .....	57
3.1.3.2	Analysis .....	58
3.1.3.2.1	Background Data .....	58
3.1.3.2.2	Comparison .....	66
3.1.3.3	Results .....	67
3.1.3.4	Analysis of Radar Data with Systematic Bias Removed .....	83
3.1.4	Evaluation .....	99
3.1.4.1	Criteria .....	99
3.1.4.2	Discussion .....	100
3.1.4.2.1	Radar Imagery .....	100
3.1.4.2.2	Radar DEMs .....	101
3.1.4.2.3	Recommendations for Further Work .....	102
3.2	ANTIOCH HILLS, LAND USE AND LAND COVER EXPERIMENT, FARMLAND MAPPING PROGRAM .....	103
3.2.1	Abstract .....	103
3.2.2	Introduction .....	103
3.2.2.1	Purpose .....	103
3.2.2.2	Objective .....	104
3.2.2.3	Site Description .....	104
3.2.3	User Experiment .....	105
3.2.3.1	Methodology .....	105
3.2.3.2	Field Evaluation .....	107
3.2.3.3	Results .....	108
3.2.3.3.1	Image Enhancement .....	108
3.2.3.3.2	Automated Image Classification .....	110
3.2.3.3.3	JPL Automated Classifier .....	117
3.2.3.3.3.1	GML Classifier .....	117
3.2.3.3.3.2	Feature Vectors .....	117
3.2.3.3.3.3	Training Sets .....	118
3.2.4	Evaluation .....	118
3.2.4.1	Criteria .....	118
3.2.5	Discussion .....	119
3.3	VEGETATED HILLSLOPE DEM AND SLOPE HAZARDS EXPERIMENT .....	121
3.3.1	Abstract .....	121
3.3.2	Introduction .....	121
3.3.2.1	Purpose .....	121
3.3.2.2	Objectives .....	122
3.3.2.3	Site Description .....	122
3.3.3	User Experiment .....	125
3.3.3.1	Methodology .....	125
3.3.3.1.1	Landslide Inventories .....	125
3.3.3.2	Analysis .....	126
3.3.3.3	Results .....	126
3.3.4	Evaluation .....	126
3.3.4.1	Criteria .....	126
3.3.4.2	Discussion .....	128
3.3.5	Year 2 Work .....	128

3.4	GUALALA RIVER BASIN, TIMBER HARVEST EROSION EXPERIMENT, TIMBER HARVEST PLAN PROGRAM .....	129
3.4.1	Abstract .....	129
3.4.2	Introduction .....	129
3.4.2.1	Purpose .....	129
3.4.2.2	Objectives .....	129
3.4.2.3	Description .....	130
3.4.3	Year 2 Work Plans .....	130
3.5	SITE #4 - IRON MOUNTAIN MINE, CONTAMINATED MINE RUNOFF EXPERIMENT, OFFICE OF MINE RECLAMATION .....	131
3.5.1	Abstract .....	131
3.5.2	Introduction .....	131
3.5.2.1	Purpose .....	131
3.5.2.2	Objective .....	131
3.5.2.3	Site Description .....	132
3.5.3	Year 2 Work Plans .....	132
	APPENDIX A: REFERENCES .....	133
	APPENDIX B: ACKNOWLEDGMENTS .....	135

DOC conducted three end-user experiments, two in the Antioch Hills and one for the Laurel Quad test site, with JPL and Calgis providing technical support. The Seismic Hazards Evaluation and Zonation Project (SHEZP) conducted a non-vegetated DEM and slope hazards experiment in the grass covered rolling slopes of the Antioch Hills and, initiated a vegetated DEM and slope hazards assessment in the heavily forested mountainous Laurel Quad, with analysis of FOPEN technology planned for Year 2. The Farmland Mapping and Monitoring Program (FMMP) conducted a land use and land cover experiment in the urbanized and farmed region of the Antioch Hills that is planned to be continued into Year 2 for a change detection experiment.

## **Digital Elevation Model Results**

The IFSAR-derived DEM for Antioch Hills was found to be have a greater accuracy than the U.S. Geological Survey (USGS) 7.5 minute quadrangle based DEMs currently available for California. As a result, a more detailed and more precise analysis of terrain geometry would be possible using the radar-derived DEM than with a public domain USGS DEM. Another benefit that radar-based DEM production may demonstrate is increased production and reduced turnaround time compared to existing methods.

For the Antioch Hills detailed test area, a highly precise DEM was constructed using soft copy photogrammetry and 1:10,000 scale aerial photography specifically acquired to serve as ground truth and for analysis of the radar-derived DEM. SHEZP and Calgis determined a worst case standard deviation of 4.5m vertical which makes the radar-derived DEM suitable for creating maps with contour intervals of 15 to 20m. Horizontal ground resolution was found to be a factor of 6 times greater or 36 times the data density. These results were obtained according to National Map Accuracy Standards and procedures based on using a planimetric reference frame from an end-user's approach.

In order to evaluate the TOPSAR data from a sensor performance perspective, JPL performed a precise co-registration of a soft copy-derived photogrammetric reference DEM to the TOPSAR generated DEM. After removal of systematic miss registration errors that resulted from incomplete calibration of the TOPSAR instrument, JPL found a better level of RMSE accuracy by about 1m. This indicates that the TOPSAR instrument was performing as expected and after additional calibration, may ultimately permit attaining the target goal of 2 to 3m vertical accuracy with a 5m horizontal grid.

## **Land Use and Land Cover Results**

The IFSAR-derived ortho-rectified image for Antioch Hills was found to have an improved spatial accuracy over that of commercially available satellite imagery. A multi-sensor approach of combining the IFSAR data with spectral satellite imagery shows potential for improved mapping of agricultural land use change and urbanization in California.

The usefulness of radar imagery as an enhancement to multi-spectral satellite imagery was demonstrated in a comparison of four intensity, hue and saturation (IHS) enhanced images developed by FMMP and Calgis. Identification of urban, dry vegetation, and marsh land categories was improved by substituting an average of Thematic Mapper (TM) and radar principle component (PC1) for intensity in an IHS to red-green-blue (RGB) conversion, compared with using TM intensity alone. Discernment among dry vegetation categories was 25% closer to true ground control with the combined radar/TM compared to TM alone. However, the radar/TM combination effected a 15% decline in the ability to discern irrigated agricultural categories compared to TM. Other enhancement techniques which reduced the inherent noise and over saturation effects in the radar magnitude image are also being pursued.

Precision point placement tests indicate that the Antioch Hills radar imagery had the highest spatial accuracy compared to commercial satellite imagery, and would be suitable for FMMP's registration requirements for mapping farmland and urbanization. The 5m radar pixel makes it possible to discern the 4 hectare minimum mapping unit which must be measurable in 0.8 hectare increments for mapping and reporting agricultural and urban land use changes.

A five class automated land use and cover classifier was developed and demonstrated by JPL. Comparison between control land use and the automated classifier results was inconclusive concerning which band combinations were the most accurate for automated land use mapping. The inherent differences between the land use classes employed by FMMP and the automated classifier classes require further work to refine the classification methodology.

## **Executive Summary**

### **Background**

GeoSAR is a project to develop a commercial airborne, radar-based, terrain mapping system utilizing technology originally developed by NASA and ARPA for commercial and defense applications.

The project team consists of the Sensor Technology Office within the Federal Government's Advanced Research Projects Agency (ARPA), NASA's Jet Propulsion Laboratory (JPL) at the California Institute of Technology, Calgis Inc. a small business, and the California Department of Conservation (DOC) which brought together the GeoSAR team.

### **Multi-Year Program**

This report details the Year 1's efforts (March 1994 through June 1995) to investigate use of interferometric synthetic aperture radar (IFSAR) for mapping geologic hazards, and land use and land cover. The work plan is a 4 year end-user driven application and systems development and verification process, with the final goal being commercialization of the technology to serve the end-user community. Year 2's efforts will focus on development of foliage penetrating (FOPEN) capabilities for mapping true ground surface and expanding end-user applications. Years 3 and 4 will concentrate on systems' development and commercialization.

### **Year 1 Activities**

Year 1's activities focused on end-user experiments designed to test and validate IFSAR mapping capabilities using data acquired from JPL's airborne TOPSAR (Topographic Mapping Synthetic Aperture Radar) instrument flown aboard the NASA/JPL DC-8 research aircraft.

A ground campaign was conducted to establish geodetic control, set radar reflectors, and acquire ground truth for four test sites. The sites were chosen to represent environmental mapping problems from DOC line programs that could be solved using a GIS (geographic information system) enhanced with radar mapping technology. JPL oversaw flight planning, Calgis led the ground campaign with DOC providing end-user input and support. JPL conducted three TOPSAR flights that acquired radar data over five sites:

- Antioch Hills in the Sacramento Delta area serves three user experiments : (1) digital elevation model (DEM) verification; (2) slope hazards assessment; and, (3) land use and land cover analysis which will continue into Year 2 for change detection purposes.
- Laurel Quad, north of the town of Santa Cruz; is the primary site for foliated landslide mapping efforts initiated in Year 1 with the bulk of work on FOPEN image and DEM analysis to be done in Year 2.
- North fork of the Gualala River along California's north coast, for slope erosion analysis in a timber harvest site; data acquired for work planned in Year 2.
- The abandoned Iron Mountain Mine west of the town of Redding needs abatement of contaminated runoff; initial data acquired in Year 1; FOPEN DEM work planned in Year 2.
- An unforeseen opportunity developed to acquire a fifth IFSAR terrain data set over the San Fernando Valley after the January 1994 Northridge earthquake. The mosaiced IFSAR DEM is planned for use in a FEMA funded seismic hazards mapping project in 1995-96.

Radar data was processed by JPL for the Antioch Hills and Laurel Quad sites. The data were processed into three standard products: a radar-derived DEM with 5m horizontal postings; an orthorectified SAR image; and, a correlation map. The processed data were recompiled by Calgis and provided to DOC for end user experiments and analysis. Calgis developed software to transform the data from its spherical system of radar mapping coordinates used by JPL to the cartographic map projections and GIS format used by DOC.

## **Year 2 Plans**

### **FOPEN and Expanded Use**

Year 2 efforts will focus on development of foliage penetrating (FOPEN) capabilities for mapping true ground surface using improvements to the TOPSAR instrument and the aircraft inertial navigation system. In addition, end-user application will be expanded using real-world demonstration projects with other state and local government agencies, and university researchers.

### **Cost Study**

Additional work is necessary to evaluate a radar-derived DEM with that of a 1:40,000 scale photogrammetrically-derived DEM for a quadrangle sized area. The economics of cost, time, and accuracy of existing systems will be compared to using radar for DEM construction.

### **Automated Feature Detection**

A potentially valuable future topic is the development of automated landslide hazards and land use change detection algorithms using radar-derived DEMs and images. There exists the possibility to train the computer to recognize landslide features using this much more precise radar DEM data. Such a capability would significantly expedite the process of landslide inventory, quickly covering large areas, identifying candidate landslide features and allowing the analyst to concentrate on making final judgment calls. Along similar lines, radar-derived automated land use and cover change detection warrants additional investigation and will be pursued with a repeat flight over the Antioch Hills about 1 year later. It will employ image processing procedures.



## 1.1 PROJECT BACKGROUND

### 1.1.1 GeoSAR

GeoSAR (Geographic Synthetic Aperture Radar) is a project to develop a commercial airborne, radar-based, terrain mapping system utilizing defense technologies to identify geologic, seismic, and environmental hazards to increase public safety, and to improve environmental management.

GeoSAR came about as a result of an internal project begun in the fall of 1992 within the Department of Conservation's (DOC) Seismic Hazards Evaluation and Zonation Project (SHEZP) to investigate producing a digital elevation model (DEM) that would portray true ground surface for use in a geographic information system (GIS) for analysis of seismically induced slope failure. Various contacts were initiated within the photogrammetry and image processing community to develop an approach to deal with the known limitations of the standard U.S. Geological Survey (USGS) DEM. It was found that the Radar Sciences Group at the Jet Propulsion Laboratory (JPL) was conducting work using interferometric synthetic aperture radar (IFSAR) which had the potential for penetrating vegetation and creating a true ground surface DEM.

Several months into the investigation, an inquiry was received from a defense technology development group, inquiring about SHEZP's recent acquisition of a soft copy photogrammetry GIS workstation designed to be used for constructing highly precise DEMs and for 3-D stereo visualization. As events developed, a consortium was formed consisting of an end user (DOC), an application expert (JPL) and private enterprise (Calgis), which submitted an unsolicited proposal for the GeoSAR Project to the Advanced Sensor Technology Office within the Advanced Research Projects Agency (ARPA). The proposal's concept was approved and funding was provided by ARPA for the first year's validation and proof of concept efforts.

This report documents the first year's efforts of this consortium. To avoid confusion from different starting and ending dates for the Federal and State fiscal years, work begun in 1994 is referred to in this report as 'Year 1'. Likewise, work planned to be initiated in 1995 is referenced as Year 2, and so on. This report covers work beginning in March 1994 through June 30, 1995, hereafter referred to as 'Year 1'. Year 2 for GeoSAR begins on July 1, 1995.

### 1.1.2 Problem

Many of DOC's environmental management programs have come to rely on the use of GIS technology for their mapping needs. Use of GIS has spread widely, so much so that most all governmental agencies and private business utilize this technology, and share many of the same needs and problems as DOC's when using GIS for mapping and analyzing the environment.

A geographic information system, or GIS for short, is a combination of computer hardware and software designed to acquire, maintain, and analyze spatial (cartographic) data. In a broader sense, a GIS supports data base linkages to graphic elements that can then be analyzed and visually displayed with varying degrees of sophistication as fits the needs and capability of the user.

A major part of building a GIS data set is construction of the digital map base upon which the spatial data/information is shown and analyzed. It is most common for a GIS data set to be constructed using a 2-D planimetric map base that represents the earth's surface as a plane using a cartographic map projection, such as a Universal Transverse Mercator or Albers Equal Area projection. More often than not, these GIS projects are 'built flat' and do not take into account terrain. Often this is due to the lack of suitably accurate terrain elevation data.



Terrain elevations are an essential data layer in computerized maps and data models used for GIS analysis of environmental problems. With today's technology and complex environmental problems, it is often required that GIS mapping be done in 3-D rather than in 2-D. GIS base maps and data sets now need to take into account terrain. To illustrate this, modeling a forest fire burn can be more exact if terrain or slope is included within the data set. Another example is modeling of slope failure, which in addition to slope aspect and ratio, requires knowledge of cross slope and down slope curvature. For modeling slope failure in California's urbanized areas, slope geometry must be known to a high degree of both relative accuracy and absolute precision.

DEM data presently available from the U.S. Geological Survey (USGS) are limited in their use due to the inherent level of precision and accuracy. A DEM is a computerized mathematical model of the earth's surface. A DEM is commonly displayed on a computer screen as a wire frame model, which looks like a window screen molded over the earth's surface. Using today's technology, it is possible to drape a co-registered aerial photograph or satellite image over the DEM, to give it a more realistic appearance. The USGS produces a public domain series of DEM using various methods of construction. An older method is based on using the contour lines from published maps to derive the DEM. Another involves use of an analytical stereo instrument to profile stereo pairs and generate the DEM. Neither of these methods produces a DEM with a high degree of vertical accuracy. Use of USGS DEMs is limited to generalized applications.

Another problem is that USGS DEMs support a contour interval of 15 to 40m for maps at a scale 1:24,000, and have vertical intervals as large as 80m for large area maps at scales of 1:250,000. These rather gross vertical intervals make the standard USGS DEM unsuitable for terrain analysis. The surface represented in a DEM is not always the true ground surface. In places, the DEM surface reflects the tops of trees, buildings, etc. which are mapped where they obscure the ground. In addition, most terrain details fall within the smallest available vertical interval of 15m, and, as a consequence are masked and not apparent within of the DEM. Another problem with USGS DEMs is poor side-matching between models which creates discontinuities when mosaicing or tiling many DEMs together into a seamless surface. This presents a problem when attempting to model between multiple DEM map sheets.

A companion and not so apparent problem is the construction of orthophoto maps by the USGS. The approach is to use recent aerial photography, scan and digitize the image and then geometrically correct the image to place it into a planimetric map projection using the existing DEM to correct for relief displacement. The shortcoming noted above creates a degree of uncertainty as to the accuracy of the resultant orthophoto map.

### 1.1.3 Opportunity

Environmental mapping programs using GIS are plagued with this approximate ground surface problem inherent to USGS DEMs. DOC has several program areas that are in need of improved DEMs and also the companion technology that SAR also supports. Similar problems face other State of California agencies and organizations.

- The Seismic Hazards Evaluation and Zonation Project (SHEZP) must quantify terrain properties such as cross slope and down slope curvature and slope aspect in order to study landslides. An IFSAR DEM is much more accurate than a USGS DEM. Large areas can be mapped quickly and more accurately. A foliage penetration (FOPEN) DEM may more correctly show the ground surface.
- Satellite images alone are presently not suited for the mapping needs for the Farmland Mapping and Monitoring Program (FMMP). Co-registration of Synthetic Aperture Radar (SAR) imagery with multispectral imagery provides information not present in multispectral imagery.

With the addition of IFSAR data, it may be possible to map terra-planned subdivisions and to determine agricultural change such as removal of an orchard. Construction of orthoimage maps would be greatly enhanced if a more accurate IFSAR DEM were used to geometrically correct the aerial image. Coincident acquisition of the aerial image along with the IFSAR DEM would permit construction of an orthoimage map using a DEM with the same temporal time frame for both the terrain and image. Radar derived DEMs would be useful for this purpose even for concurrent imagery.

- Existing DEMs are not suited for studying slope erosion potential under the forest canopy, a problem dealt with by the Timber Harvest Plan Review Project (THPRP). Use of a FOPEN DEM would greatly speed up EIR (Environmental Impact Report) review and increase timber harvest production. Geologists presently only are able to identify and mitigate at most about 50% of the potential erosion sites in a timber harvest area. A FOPEN DEM would greatly improve analysis of potential erosion sites under the forest canopy by allowing identification of skid trails and potential slope failure sites.
- The Office of Mine Reclamation (OMR) needs microrelief data to locate and map mine sites and analyze contaminated surface runoff from mine tailings. Many mine sites are forested and in areas for which USGS has not yet compiled a DEM with sufficient accuracy for this level of application. As with most environmental features that have a height less than the DEM's vertical interval, mine tailings are vaguely portrayed in a DEM.

GeoSAR presents an opportunity for DOC to use advancements in terrain mapping presented by IFSAR and FOPEN technology to improve identification of geologic and environmental hazards, to integrate this technology into various DOC programs, and to increase public safety and improve environmental management.

#### 1.1.4 Goals

GeoSAR is a multi-year program intended to transfer advanced radar mapping technology from the government laboratories to the public sector. The following technical objectives were presented in the original proposal to ARPA, they were pursued beginning with Year 1.

- Develop a commercially viable high precision, mass production, digital terrain data-acquisition system based upon IFSAR.
- Research and develop a commercial foliage penetration (FOPEN) digital terrain acquisition system which provides for true ground surface.
- Develop an automated ortho-rectified image map and products based upon optical and radar sensory systems.
- Develop a suite of software map tools to maximize the utility of the above technologies.

GeoSAR program objectives are to use these advances in terrain mapping to improve identification of geologic and environmental hazards, to integrate this technology into various state and local agency programs, and to increase public safety and improve environmental management.

As originally envisioned, GeoSAR was to be a 4 year program based upon using the DOC as the end user test bed, coupled with expanding the technology, as it became proven, into other State agencies to demonstrate further applications. Figure 1.1-1 illustrates this 4 year knowledge building process and lists the technical objectives.

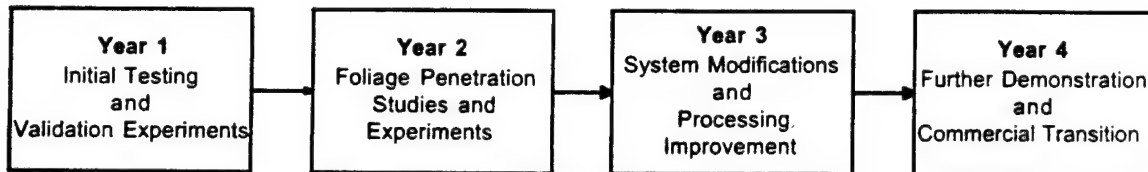


Figure 1.1-1: Four Year GeoSAR Program

## 1.2 GEOSAR TEAM

GeoSAR is a multi-participant development project. The GeoSAR team is made of ARPA's Sensor Technology Office, the California Department of Conservation (DOC), NASA's Jet Propulsion Laboratory (JPL), and private enterprise represented by Calgis, Inc., a California GIS integration company. Figure 1.2-1 illustrates the GeoSAR agency level organization structure. ARPA is the lead contracting agency, while JPL, DOC and Calgis make up the technical team.

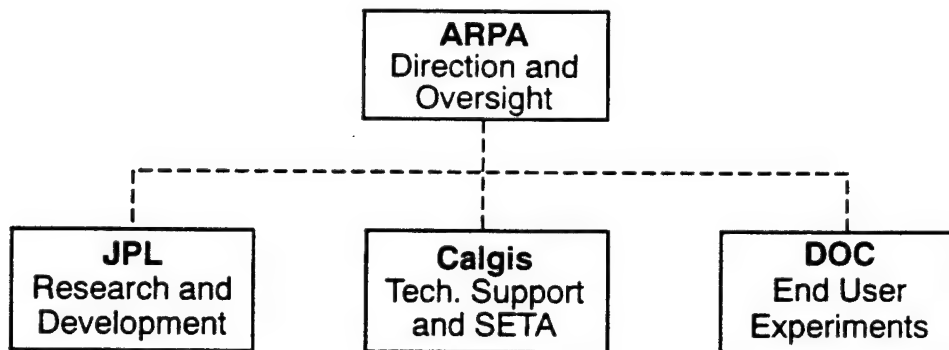


Figure 1.2-1: GeoSAR Organization

- ARPA's Advanced Sensor Technology Office oversees applicable technology transfer, providing funding, direction and oversight.
- DOC conceived this application and is the initial end-user and project coordinator for expansion into other State agencies.
- NASA's JPL is providing data acquisition and signal processing, hardware design and modifications, along with use of the DC-8 based AirSAR research radar, along with production of the radar derived DEM.
- Calgis is providing ground truth and technical support with photogrammetry and digital mapping. Calgis also is ARPA's Scientific Engineering and Technical Advisor (SETA) for the GeoSAR Project.

### 1.3 OVERVIEW OF YEAR 1 ACTIVITIES

GeoSAR's first year served to test and validate the GIS application of IFSAR's mapping capabilities in a real world situation.

The Year 1 program focused on end user experiments using data acquired from JPL's airborne AirSAR radar system flown in NASA's DC-8 aircraft. Radar data were collected by JPL for four sites during two flights, and processed for two sites. The data were reformatted by Calgis into a GIS format and provided to DOC for end user experiments and analysis.

#### 1.3.1 Department of Conservation

DOC's first efforts concentrated on learning and applying IFSAR technology to geologic hazards, land use and land cover mapping, as well as analyzing radar data for DOC application. Field reconnaissance was conducted for four test sites in support of JPL over flights and the Calgis ground campaign. Intensive geotechnical field investigations were conducted for two of the five sites in support for analyzing the companion IFSAR data. SHEZP then used and analyzed the radar data with a view toward integrating this technology into its geologic and land use mapping tasks. FMMP conducted a land use and cover analysis to monitor urbanization of agricultural land with the hopes of automating this task.

#### 1.3.2 Jet Propulsion Laboratory

JPL's role encompassed three main areas of activity in Year 1. First, JPL participated in site selection, ground truth, and data collection over five sites in California using the TOPSAR (Topographic Mapping Synthetic Aperture Radar) mapping instrument flown aboard the NASA/JPL DC-8 aircraft. These activities included corner reflector location determination, kinematic surveys of the ground sites, flight path planning, and kinematic GPS flight path reconstruction. Secondly, JPL processed TOPSAR data collected at the Laurel Quad and Antioch Hills sites. These activities included the first calibration of the TOPSAR instrument, and subsequent analysis of the collected data to assess overall instrument performance and help in interpreting results obtained by independent analysis of the data by DOC and Calgis. Finally, JPL worked on a modification to its existing aircraft interferometric processor to process L and P band repeat track aircraft data collected over Laurel Quad, Iron Mountain, and Gualala River. These data were collected to assess the possibility of generating DEM data beneath the vegetation canopy using lower frequency interferometric SAR data. Using algorithms developed under the ARPA AUTOMAP program, sample land cover classifications were provided to DOC for the Antioch Hills data.

#### 1.3.3 Calgis

Calgis conducted a four site ground campaign establishing precise geodetic control, acquired vegetative ground truth, developed a GIS earth based cartographic transform and file recompilation of the JPL radar data, and provided technical assistance to DOC. In addition, ground support was provided for a single overflight by a SAR aircraft from Stanford Research Institute (SRI). Calgis also served as ARPA's SETA contractor for GeoSAR. Calgis provided photogrammetric assistance to SHEZP and image processing and analysis to FMMP. Efforts were also begun on creating a radar DEM based orthophoto map using concurrently acquired aerial imagery that was scanned by SHEZP.

## 1.4 SITES AND USER EXPERIMENTS

Radar data were collected over five sites in northern, central, and southern California. Site #1-Antioch Hills and Site #2-Laurel Quad were flown first and serve as super sites for multiple applications in Years 1 and 2. Because of aircraft availability, it was decided to acquire data over Site #3-Gualala River Basin- and Site #4-Iron Mountain Mine-, and to process this for use in Year 2. The test sites and their proximity to NASA's Ames Research Center and Naval Air Station Moffet Field, home base to the NASA DC-8 aircraft, are shown in Figure 1.4-1. Sites #1 and #2 are referred to as "super sites" because they have multiple applications and end user experiments which required extensive supporting geodetic control and field work, far in excess of that planned for other test sites. A unforeseen yet fortuitous TOPSAR flight was conducted over the earthquake impacted Northridge area north of Los Angeles to take advantage of applying this technology in response to a major natural disaster for follow-up analysis and mitigation.

The test sites and their experiments were selected from existing DOC programs. They were chosen to represent environmental mapping problems and GIS applications with no present 'good' solution to them, for example:

- USGS DEMs not precise enough for detailed digital terrain modeling,
- A need for true ground surface DEM in forested sites; and,
- Satellite multi-spectral imagery alone does not provide enough spatial information to capture needed land use and land cover changes.

A second criterion was the test site's physical characteristics. Qualified sites had to present mapping problems not presently being solved with today's tools and that could potentially be solved by use of an improved DEM that represents true ground surface. In addition ancillary data from the radar including backscatter and correlation information may prove extremely useful in solving a number of DOC problems.

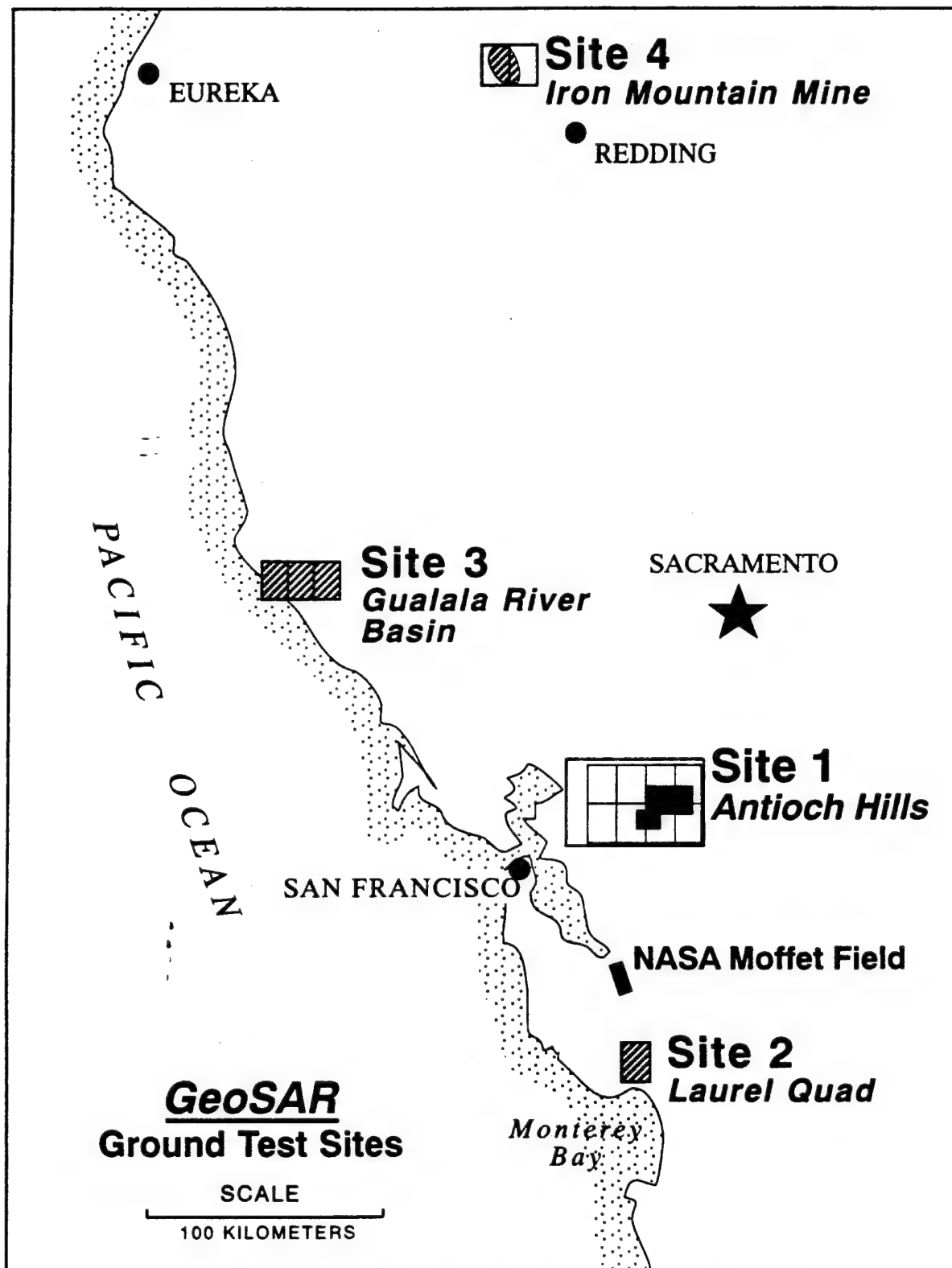


Figure 1.4-1: Location Map of four of GeoSAR Year 1 Test Sites

### 1.4.1 Super Site #1 - Antioch Hills, Contra Costa County

The Antioch Hills site is made of grassy rolling hills with localized urban and agricultural development in the adjacent valleys and Sacramento River delta. There are three objectives for this site.

- To compare the time, cost and efficiency of soft copy photogrammetry (SCP) versus IFSAR for building a DEM, and to compare the accuracy of the radar DEM to a SCP-derived DEM. This grassy hillside area serves as a control whereby no obscuring vegetation is present to degrade either DEM.
- An important end-user experiment is to analyze the ability to use the radar image and DEM to detect, map, and analyze well defined, non-vegetated slope failure (landslides).
- A second end-user experiment is the ability to use radar for land use and cover mapping with the goal being change detection in an urban and agricultural setting.

Figure 1.4-2 shows the Antioch Hills test sites which encompass portions of six USGS 7.5-minute quadrangle maps that are named in the Figure. The areas used for detailed geologic and land cover end user experiments are more to the east than originally planned. Extensive field reconnaissance found sites more suitable than those initially identified in the original project proposal.

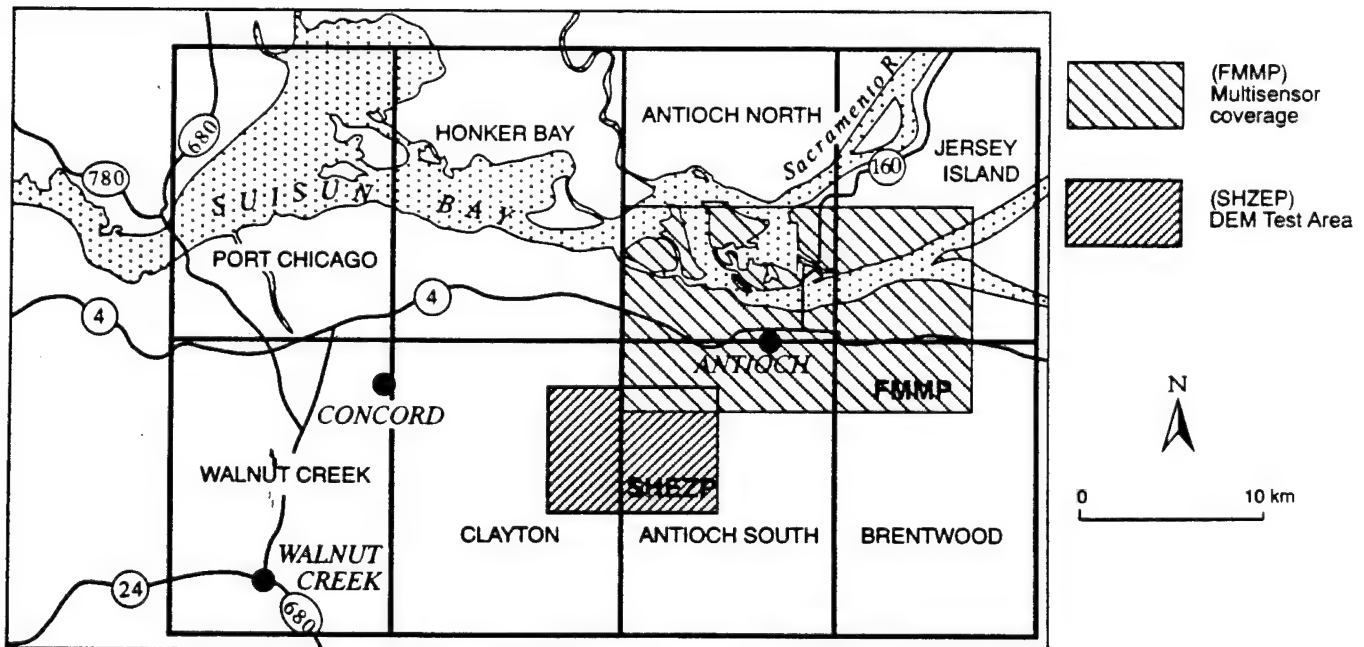


Figure 1.4-2: Super Site #1 - Antioch Hills

The Antioch Hills are part of the Mount Diablo Range, which lies about 48km northwest from San Francisco. The Sacramento River Transects the site from east to west, and empties into San Francisco Bay at the Carquinez Straits.

### 1.4.2 Super Site #2 - Laurel Quad, Santa Cruz County

The Laurel Quad consists of redwood and coastal shrub growth in semi-mountainous terrain directly northeast of the city of Santa Cruz. Super Site #2 is the location of the epicenter for the 1989 Loma Prieta earthquake where considerable damage occurred to dwellings from ground movement, in addition to widespread damage throughout the San Francisco Bay region. This site has had extensive field mapping of slope failure in well defined landslides with varying degrees of sloping terrain.

- The objective is to use FOPEN to create a true ground surface DEM from which to model terrain geometry and map landslide areas. This information will be used for identifying the hazard posed by seismically induced landslides to urbanized and developing areas.
- Field measurements and soft copy photogrammetry using vintage aerial photography taken after the forest was clear-cut in the 1930s will be used for comparison to the radar DEMs of the landslide sites.

Figure 1.4-3 shows the location of the Laurel Quad site, its boundaries are essentially the extent of the USGS 7.5 minute quadrangle.

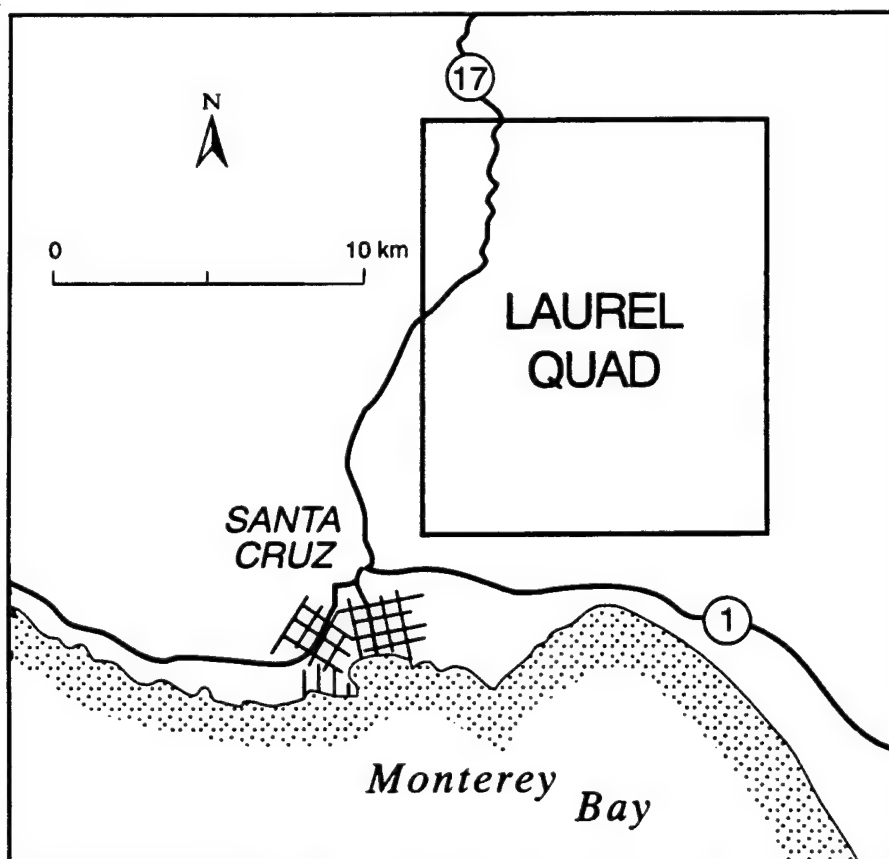


Figure 1.4-3: Super Site #2 - Laurel Quad

Santa Cruz is the nearest town and is immediately to the southwest, a 1 1/2 -hour drive along Highway 1 south from San Francisco.



### 1.4.3 Test Site #3 - Gualala River Basin, Sonoma County

The north fork of the Gualala River and its drainage basin are utilized for timber harvesting of redwood and other coastal trees. The Gualala River also supports a salmon spawning and rearing habitat. The site consists of mountainous coastal terrain covered with second growth redwood forest in various stages of regrowth and harvest, interspersed with other species of trees.

- The objective is to use FOPEN to create a true ground surface DEM to identify existing roads and skid trails under the forest canopy in areas planned for timber harvesting. Skid trails and dirt roads are prone to slope failure and soil erosion, and are major sources of sediment and debris discharges from timber harvest sites into streams.
- Forest biomass will also be identified by coincidentally mapping the forest canopy and ground surface. This combined knowledge will allow foresters and biologists to better manage fishery and forest habitats and stream channel sedimentation.

Figure 1.4-4 shows the location of the Gualala River site. The river basin meanders southwesterly across three USGS quadrangles and empties into the Pacific Ocean.

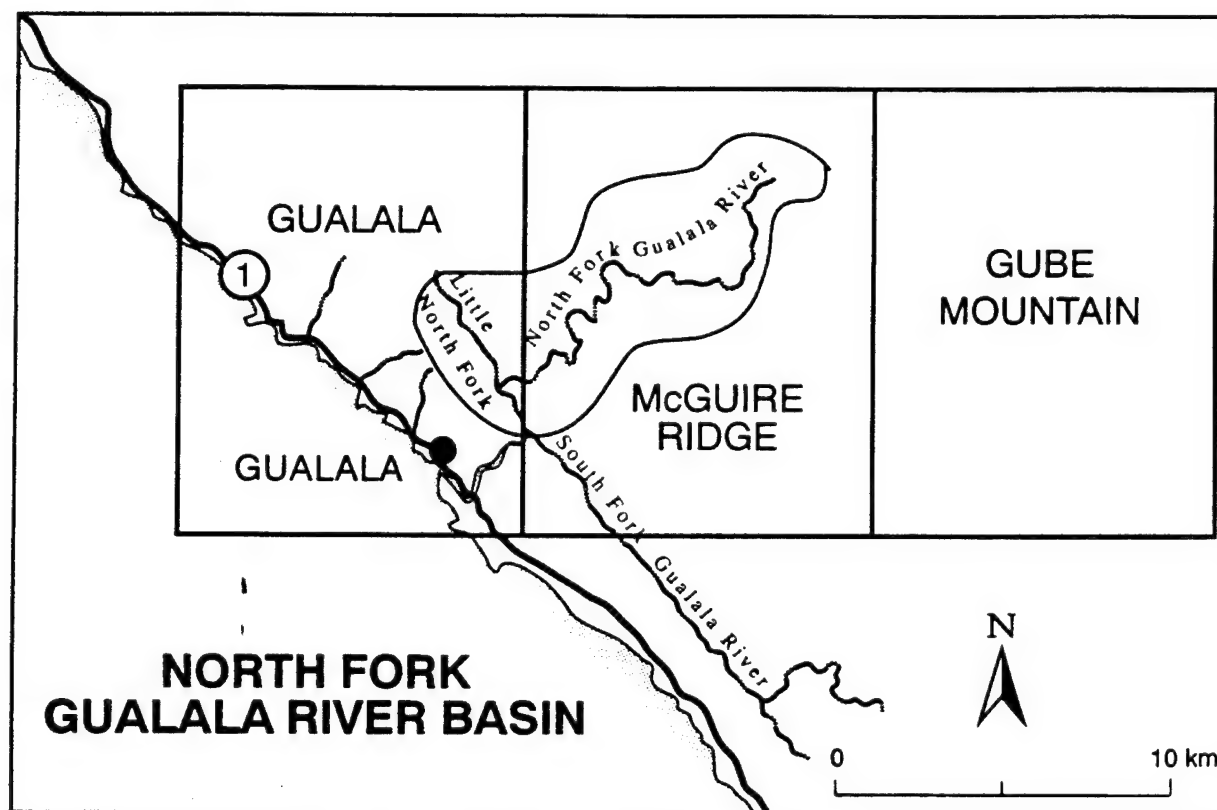


Figure 1.4-4: Test Site 3 – Gualala River Basin

The nearest town is Gualala located on a coastal bluff overlooking the Pacific Ocean, about 153km north of San Francisco and a 3 hour drive north along Highway 1. The region historically has supported a redwood timber harvest and salmon fishing industry.

#### 1.4.4 Test Site #4 - Iron Mountain Mine, Shasta County

Iron Mountain Mine dates back to the California Gold Rush and is on the EPA's Super Fund list due to toxic runoff from the mine site and its waste tailing piles. Pollution at this site is not yet fully abated and continues to pollute the Sacramento River, a major fishery and source of drinking water.

- The objective is to use FOPEN to model very fine terrain relief under the forest canopy for the upper and lower watershed. A radar DEM is critical for analysis of up-slope and down-slope runoff to and from the mine site, which leaches mine contaminants into the Sacramento River.
- Another important objective is to obtain multi-spectral data and co-register this to the radar DEM, to identify geologic formations, and contamination and degree of vegetative stress and vigor.

Figure 1.4-5 shows the location of the Iron Mountain Mine test site. The mine's drainage basin extends to the northwest from the approximate junction of four quadrangles.

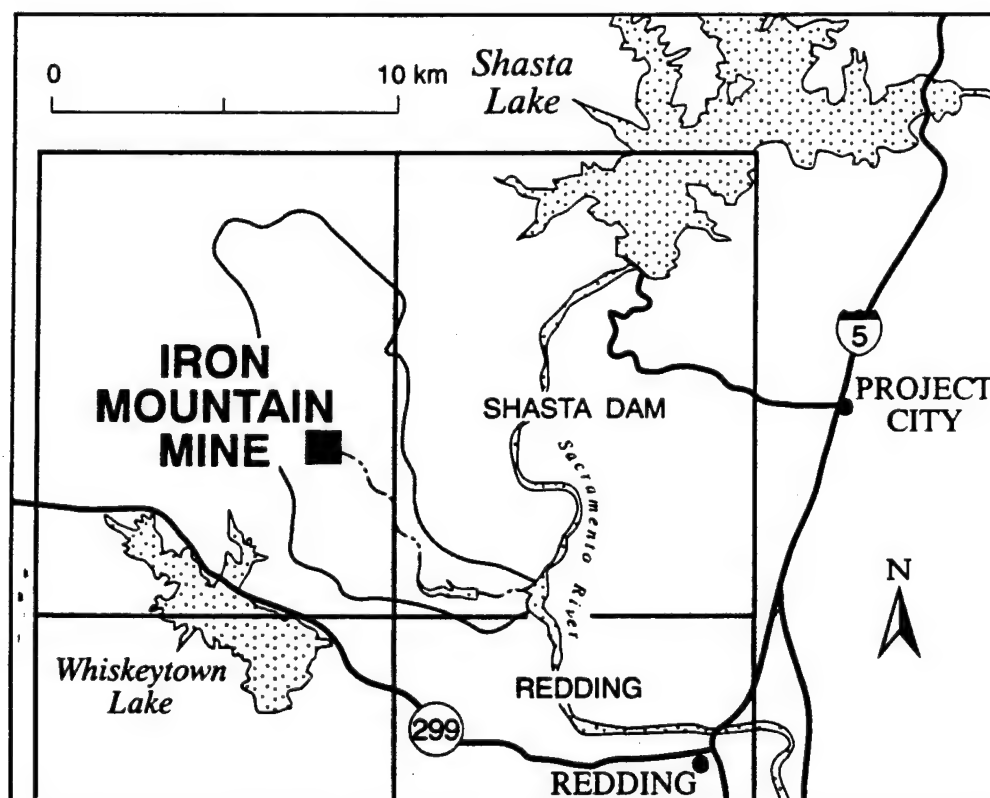


Figure 1.4-5: Test Site 4 – Iron Mountain Mine

The Iron Mountain Mine site is about 24km west of the town of Redding, which is approximately 265km north of Sacramento on Interstate Highway 5. The Mine site intercepts drainage from the mountains southwest of Lake Shasta, which flows to the southeast and into the Sacramento River.

### 1.4.5 Test Site #5 - Northridge Area

On January 17, 1994, a magnitude 6.7 earthquake centered below the city of Northridge in the San Fernando Valley, struck the Los Angeles urban area. This event provided a unique opportunity to acquire IFSAR data over a recently geologically active area. Widespread damage occurred to buildings, roads and other urban infrastructure. Extensive ground movement and slope failure occurred in the hills surrounding the San Fernando Valley. There are two major objectives for this data set.

- JPL will assemble a mosaic of the eight TOPSAR flight lines, using this exercise to develop and prototype a process to produce large area mosaics consisting of a radar-derived DEM with 5m horizontal postings, and a rectified image using the 5,600 square kilometers of data acquired over the Northridge Area.
- DOC will use the data to analyze terrain and identify areas of possible slope failure as part of a FEMA (Federal Emergency Management Agency) damage assessment project for the southern California area.

Figure 1.4-5 outlines the Northridge Area which encompasses about 35 USGS 7.5-minute 1:24,000 scale quadrangle map sheets and is approximately 80 by 70km.

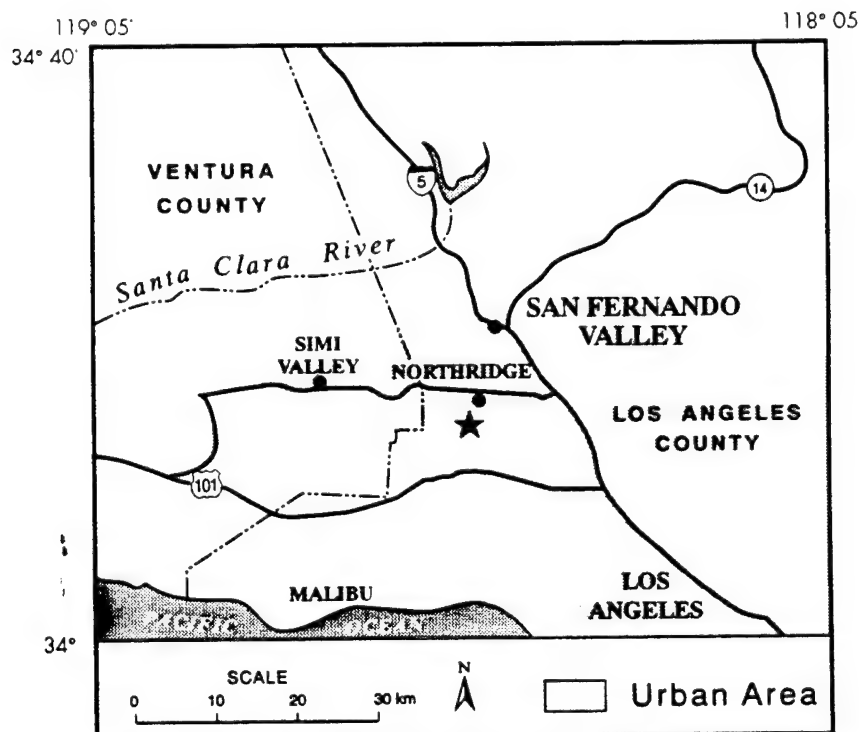


Figure 1.4-5: Northridge Area

The earthquake epicenter occurred below the city of Northridge. The Simi Valley is directly west of the San Fernando Valley damage. Damage occurred throughout the region and was most severe around Northridge and the northeastern edges of the San Fernando Valley.

## Section 2 : Data Collection and Support

### 2.1 JET PROPULSION LABORATORY

JPL participated in a number of activities necessary to collect, process and assess data over five sites in California. These activities included mission planning, data acquisition, data processing, and post processing of data for delivery to DOC and Calgis for subsequent analysis. Details for these activities are provided below.

#### 2.1.1 Mission Planning

Mission planning consisted of determining the flight lines for the TOPSAR instrument over each of the five sites, placement of corner reflectors to be used for ground truth and calibration, location and nature of additional ground-truth measurements such as vegetation transects and kinematic Global Positioning System (GPS) survey measurements to support experiment objectives over each of the five sites. Two of the five sites were categorized as "supersites" where additional ground truth data were to be taken in order to better assess interferometric accuracy and applicability to problems currently confronting applications in DOC.

##### 2.1.1.1 Flight 1, Antioch Hills and Laurel Quad

The objective for Flight 1 was to collect data over Antioch Hills and Laurel Quad, the two supersites for Year 1. Because of the lack of heavy vegetation in this area, only TOPSAR data were planned for collection over this site. Four passes, two running east-west and two running west-east were planned with a large amount of overlap between the east-west and west-east passes to be used for gap fill in regions of radar layover and radar shadow were selected. A planned flying altitude of 8000m was selected to provide good signal to noise and hence good height measurements. Four corner reflector locations in open areas were selected at the four corners of the planned data collection region. At each corner reflector site, corners were positioned pointing both north and south so each site would be visible from either the east-west or west-east passes. In addition to the corner reflectors a kinematic survey of the area using a JPL van equipped with a number of Turbo-Rogue differential GPS receivers would provide additional ground truth at points distributed throughout the area.

Laurel Quad was selected for the second supersite because of (1) the dense vegetation covering the region; (2) a number of prominent landslides both contained in the vegetation and in the open; (3) and the proximity of the epicenter of the Loma Prieta earthquake and landsliding related to seismic shaking. The main areas of interest lie between San Jose to the north and Santa Cruz to the south. Repeat passes at L and P bands are required in order to assess the ability to penetrate the foliage interferometrically. The JPL AIRSAR/TOPSAR system can simultaneously collect both C-band TOPSAR data as well as fully polarimetric L and P band data. However, starting in 1994, the AIRSAR system was prohibited from transmitting 40 MHz P-band data. In order to collect maximal resolution 40 MHz data as well obtain P-band repeat track data it was decided to collect 40 MHz TOPSAR and L-band data on four north-south passes and 20 MHz TOPSAR and L,P-band on four south-north passes. The pilot was instructed to repeat the flight lines as closely as possible, experience indicating the repeat tracks would be from 10-100m apart.

Corner reflectors were deployed at four locations around the site, each with corners facing east and west to be visible from either flight line. In addition several corner reflectors were deployed to support SRI aircraft activities. The corners for the JPL aircraft were all deployed in open areas, while those deployed for the SRI aircraft were deployed both inside and outside the vegetation canopy. Unfortunately, the JPL and SRI flight lines did not have the same heading, therefore the SRI corners are not visible in the JPL images. Kinematic GPS survey of the region from San Jose to Santa Cruz using the JPL equipped van was planned to increase the number of ground truth points and provide points for calibration. In order to obtain a quantitative assessment of the ability to generate sub-

canopy height maps using low frequency interferometry, a series of five vegetation transects 50 by 50m was collected across range. The transects were selected to be approximately homogeneous in vegetation content and thus allowed incidence angle effects to be studied in detail.

#### 2.1.1.2 Flight 2, Iron Mountain and Gualala River

The objective of Flight 2 was to collect data for the Iron Mountain and Gualala River sites. Data for the Iron Mountain site were collected on five southeast bound passes, four parallel northwest bound passes and one perpendicular northeast bound pass. Data for the Gualala River site were collected on four northeast bound passes, four parallel southwest bound passes and a final perpendicular southeast bound pass. The planned altitude at Iron Mountain was 7925m, and 8535m for Gualala River. The primary objective for these two sites was to obtain radar DEMs and images from the TOPSAR C-band interferometer as well as "repeat-pass" data at L- and P-band. A secondary objective was to obtain polarimetric L- and P-band data for Dale Shuler of the Naval Research Laboratory. Also, trucks were deployed at the Iron Mountain site for study of detection in the presence of forest growth.

### 2.1.2 Data Acquisition

Data acquisition of both TOPSAR and the kinematic GPS data for all sites was successfully completed, however a 3.5km offset between the desired and imaged swaths was observed at both Antioch Hills and Laurel Quad. This offset caused three major complications during the processing and analysis of the data. First, it was not possible to calibrate the TOPSAR data completely because at most two corner reflectors were visible in any of the imaged scenes. Calibration could be completed using other sources such as photogrammetric DEMs and kinematic GPS points. However these were not available until May 1995, too late for incorporation into this year's data analysis. Second, DOC had to alter its planned comparison region in the Antioch Hills area since one of the regions of interest was not in the imaged swaths. Finally, a major landslide concealed by vegetation in the Laurel Quad was on the edge of the swath and was not imaged at 40 MHz. Some specifics of each of the data acquisitions are provided below.

#### 2.1.2.1 Flight 1, Antioch Hills and Laurel Quad

The first flight on May 27, 1994 collected TOPSAR data for the Antioch Hills and Laurel Quad and repeat pass L,P band data for Laurel Quad. An operational flying altitude of approximately 8000 m was selected for both sites. Two east-west and two west-east passes were collected at Antioch Hills. Figures 2.1-1 and 2.1-2 show the southern west-east (Antioch 270-2) and east-west (Antioch 90-2) passes from Antioch Hills processed from the TOPSAR data. Here the data are displayed with the image intensity proportional to the radar backscatter and the height is encoded on a color wheel where one cycle of the color wheel represents a change in elevation of 100m. Hence, going from yellow to blue to red and back to yellow represents a height change of 100m. The area mapped is approximately 12 by 60km. The data for Laurel Quad were collected on four north-south passes using the 40 MHz TOPSAR mode and the L-band quad-pol mode and four south-north passes using the 20 MHz TOPSAR mode and L,P quad-pol mode. Figure 2.1-3 shows a 40 MHz TOPSAR pass of the Laurel region. The urban area at the top of the image is San Jose and the urban area at the bottom is Santa Cruz.

Kinematic GPS using measurements on board the aircraft were collected both for the Antioch Hills and Laurel Quad sites in order to obtain accurate flight path reconstruction on the order of 10cm for calibration and repeat track interferometry. Kinematic survey points were collected using the JPL GPS van in February 1995. Images of Laurel Quad and Antioch Hills were used to select regions at both sites that were easily identifiable in the radar imagery that were suitable kinematic surveys.

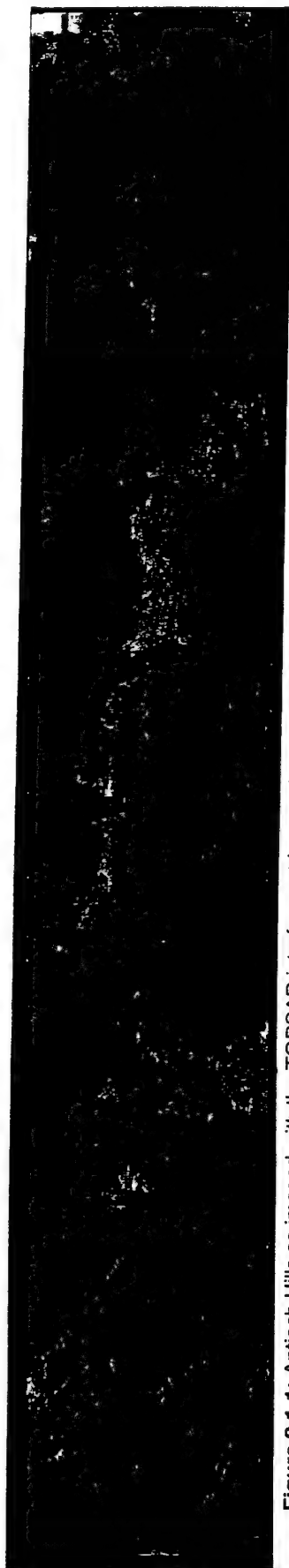


**Figure 2.1-1:** Antioch Hills as imaged with the TOPSAR interferometric mapping instrument. The data were collected on an east-west pass, north is on the right of the image and south is to the left. The image size is approximately 12 by 60km.



**Figure 2.1-2:** Antioch Hills as imaged with the TOPSAR interferometric mapping instrument. The data were collected on an east-west pass, south is on the right of the image and north is to the left. The image size is approximately 12 by 60km.

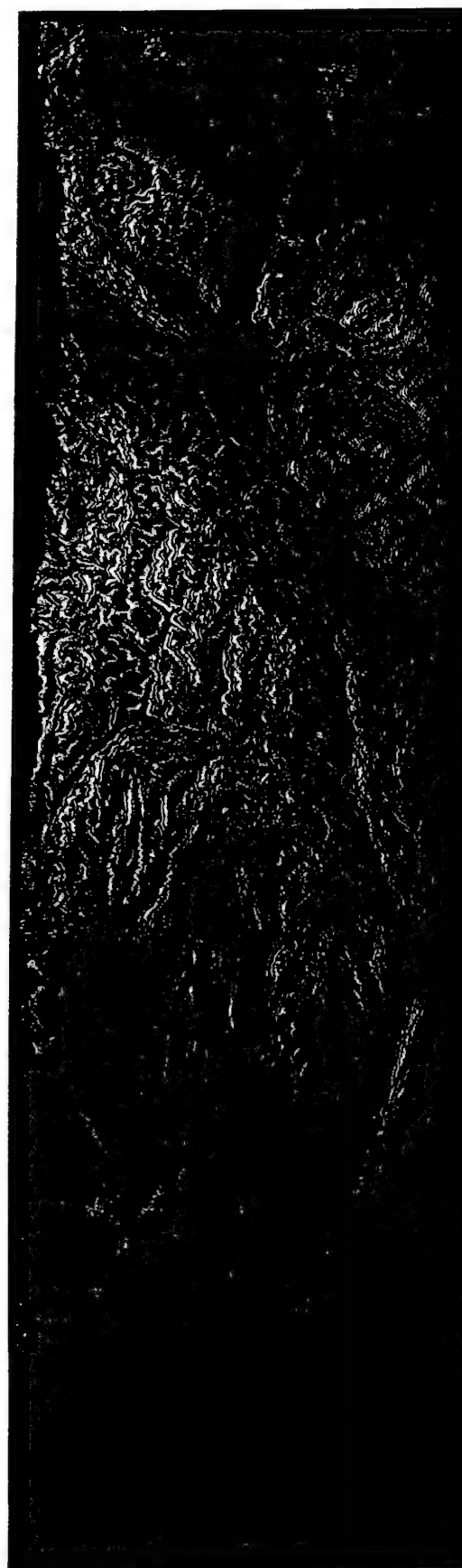


**Figure 2.1-3:** Laurel Quad as imaged with the TOPSAR interferometric mapping instrument. The data were collected on a north-south pass, north is on the top of the image and south is on the bottom. The image size is approximately 12 by 35km.



### 2.1.2.2 Flight 2, Iron Mountain Mine and Gualala River

Flight 2 on August 15, 1994 collected data for the Iron Mountain and Gualala River sites. Data for the Iron Mountain site were collected on five southeast bound passes, four parallel northwest bound passes and one perpendicular northeast bound passes. Data for the Gualala River site were collected on four northeast bound passes, four parallel southwest bound passes and a final perpendicular southeast bound pass. (A fifth planned southwest bound pass at Gualala River was lost because Air Traffic Control closed an air space immediately west of this site); Iron Mountain was flown at 7,925m while Gualala River was flown at 8535m.

Data for the Iron Mountain site were collected on five southeast bound passes with an aircraft track at 325° (35° west of north). In addition, four parallel northwest bound passes had a track at 145° (35° east of south). The final, perpendicular northeast bound pass had an aircraft track at 55° (35° north of east). The parallel passes at Iron Mountain had coverage from about 40° 26' to 40° 4' north latitude. The "Center-of-Image" for these passes was 40° 40' North, 122° 30' West, which was observed at 45° off nadir. Radar image widths are about 10-12km across-track; image lengths are about 60km along-track. The aircraft track directions were aligned with the major ridge lines in this area. Polarimetric L- and P-band images of the Iron Mountain site have been delivered to Dale Shuler of the Naval Research Laboratory.

Data for the Gualala River site were collected on four northeast bound passes with an aircraft track at 66° (24° north of east). Also, four parallel southwest bound passes had an aircraft track at 246° (24° south of west). A final perpendicular southeast bound pass with an aircraft track at 156° (24° east of south). The parallel passes at Gualala River had coverage from about 123° 45' to 123° 05' west longitude. The "Center-of-Image" for these passes was 38° 50' North, 123° 25' West, which was observed at 45° off nadir. Radar image widths are about 10-12km across-track; image lengths are about 60km along-track. The aircraft tracks directions were aligned with the major ridge lines in this area. Polarimetric L- and P-band images of the Iron Mountain site have been delivered to Dale Shuler of the Naval Research Laboratory.

### 2.1.2.3 Flight 3, Northridge Area

Flight 3 on August 5, 1994 was to collect data over a large urban area in the recently seismically active region of the Northridge earthquake. Data was collected on four east-west passes and 4 west-east passes covering the region from 119° 05' to 118° 05' west longitude (approximately 80km) and from 34° to 34° 40' north latitude (approximately 70km). This region encompasses about 35 USGS quadrangles over the Simi Valley, Northridge, and downtown Los Angeles. Two passes of the eight have been processed and one compared with a mosaic of USGS quads in the area. Major discontinuities in the USGS data were detected, some as large as 30 m. This data set when completed should provide an accurate DEM of the Northridge quake area that may prove extremely useful when combined with other data for assessing areas of potential risk in the future.

### 2.1.2.4 Kinematic GPS

Two types of kinematic survey data were collected and processed for the Antioch Hills and Laurel Quad sites. GPS data were collected on board the aircraft at 1 second intervals using a CA code Turbo-Rogue receiver. The raw pseudo-range measurements are combined with improved GPS satellite ephemeris data derived at JPL, models for ionospheric and tropospheric delays, clock drift, and ground based receiver measurements near the site to estimate the position of the aircraft with an accuracy of about 10cm.

Kinematic survey data for Laurel Quad and Antioch Hills were processed to obtain accurate and well-distributed ground truth points for both Antioch Hills and Laurel Quad. Preliminary results were obtained in May having an accuracy of 0.5m. The poor accuracy is a consequence of not yet completed algorithms for conducting kinematic surveys in urban environments where frequent loss of GPS satellites occurs. It is hoped that improved processing algorithms will improve the accuracy to the 10-20cm level. However, the 0.5m accuracy suffices for TOPSAR calibration and TOPSAR height comparison studies.

### 2.1.3 Overview of Interferometric Synthetic Aperture Radar and Processing

The basic principles of interferometric radars are described in detail by a number of sources, e.g. Zebker and Goldstein (1986) and Rodriguez and Martin (1992), so only a simplified discussion of the underlying principles will be provided here.

A single SAR image resolves targets in range by measuring the time it takes a radar pulse to propagate to the target and return to the radar. The azimuth location is determined from the Doppler frequency shift, the change in frequency which results whenever the relative velocity between the radar and target is not zero. Geometrically, this is the intersection of a sphere centered at the antenna with radius equal to the radar range and a cone with generating axis along the velocity vector and cone angle proportional to the Doppler frequency as shown in Figure 2.1-1. A target in the radar image could be located anywhere on the intersection locus which is a circle in the plane formed by the radar line of sight to the target and vector pointing from the aircraft to nadir. This still leaves the elevation angle undetermined. In order to obtain 3-dimensional position information, an additional measurement is used to obtain the elevation angle. Interferometry provides a means of determining this angle by using SAR images obtained from two antennas spatially separated in the cross track direction. Assume two identical antennas,  $A_1$  and  $A_2$ , are receiving radar echo signals from a single source as shown in Figure 2.1-2. The path length of the signals received by the two antennas will differ by

$$\text{Equation 1} \quad \Delta r = |\vec{r}_{2T}| - |\vec{r}_{1T}| = \hat{n}_{los} \cdot \vec{B} = |\vec{B}| \sin(\theta - \alpha)$$

where  $\vec{r}_{iT}$  indicates the vector from antenna  $i$  to the target,  $\hat{n}_{los}$  is a unit vector in the line of sight direction, the baseline vector,  $\vec{B}$ , is vector pointing from antenna 1 to antenna 2,  $\theta$  is the desired elevation angle and  $\alpha$  is the angle the baseline vector makes with respect to the horizontal. The range difference,  $\Delta r$ , may be obtained by measuring,  $\phi$ , the phase between the two interferometer signals, using the relation

$$\text{Equation 2} \quad \phi = -\frac{2 m \pi \Delta r}{\lambda}, \quad m = 1 \text{ or } 2$$

where  $\lambda$  is the radar wavelength and  $m$  equals 1 when the path length difference is associated with the one way path difference, as is the case for TOPSAR, or 2 for the two way path difference as is the case for repeat track interferometry.



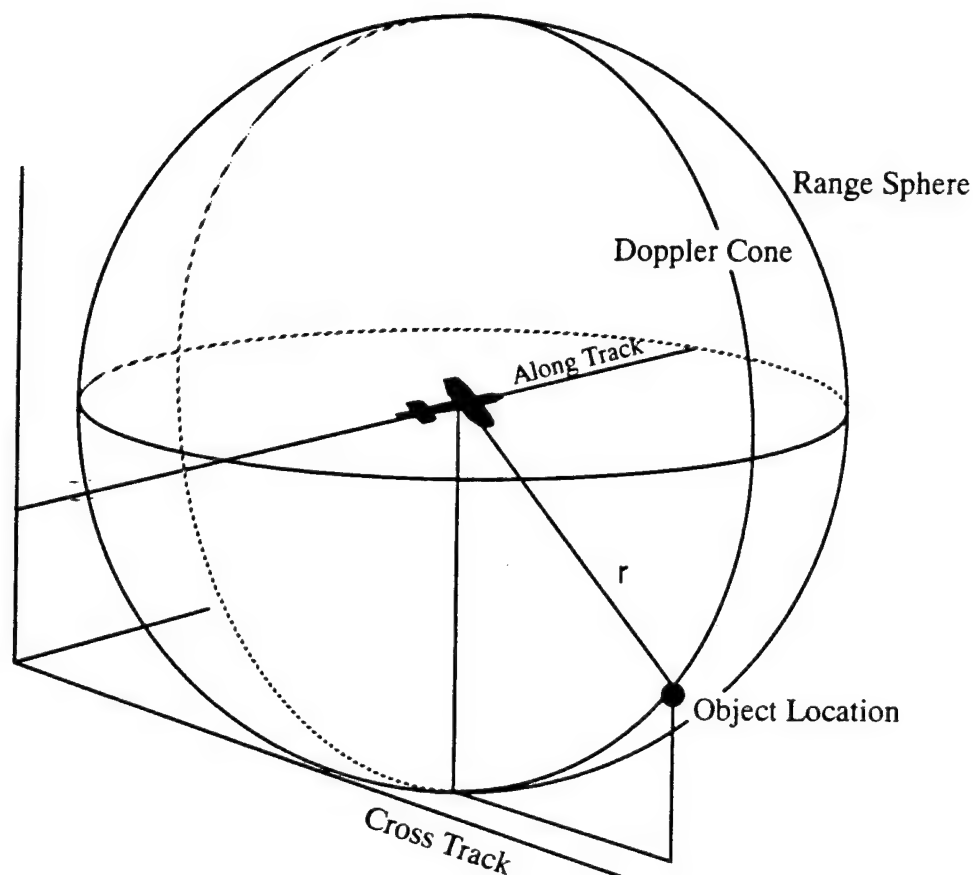


**Figure 2.1-1:** Target location in a SAR image could be anywhere on the intersection of a range sphere and Doppler cone thereby providing no information on the target's elevation.

Using the simplified geometry of Figure 2.1-2 the height of a target,  $h_t$ , is given by

Equation 3 
$$h_t = h - r_1 \cos(\theta)$$

where  $h$  is the altitude of the radar antenna and  $r_1$  is the slant range from the antenna to the target. Since the signal phase is sensitive to displacements between images of a fraction of a wavelength the interferometric technique provides a very accurate means of determining topographic heights.

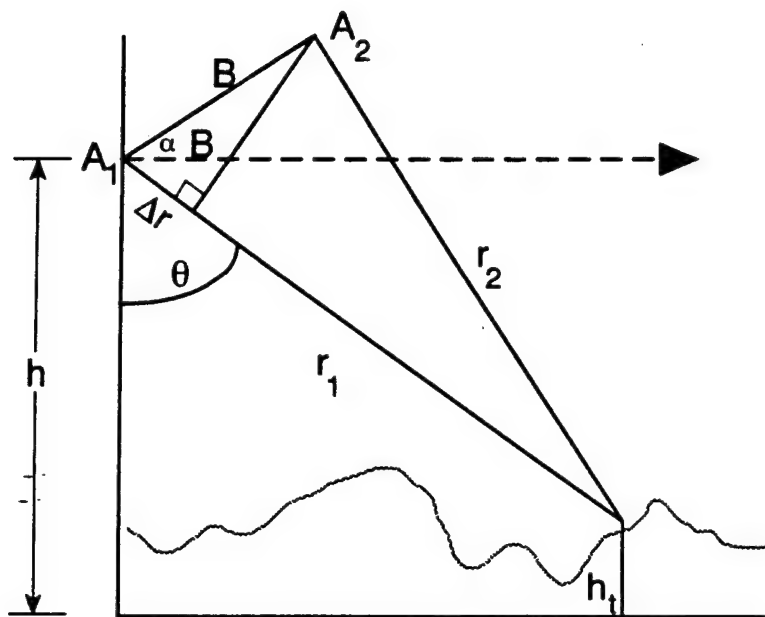


Figure 2.1-2: Simplified broadside looking radar interferometry geometry.

It can be shown that there is an upper value on the useful baseline known as the critical baseline. The critical baseline is reached when the amount of phase change per resolution element exceeds  $2\pi$  radians. This limitation is a result of the fact that the interferometric phase measurement is made only modulo  $2\pi$ . Thus as the baseline approaches the critical baseline the phase estimates from the two antennas become completely decorrelated. In general the decorrelation between the two channels is not only a function of the imaging geometry as discussed above but also a function of thermal noise, temporal changes between observations, and volume scattering effects. Then the amount of phase decorrelation between the two channels can be related to the amount of phase noise. The Cramer Rao bound relating the phase variance to the decorrelation coefficient,  $\gamma$ , (Rodriguez and Martin, 1992) is given by

$$\text{Equation 4} \quad \sigma_{\phi} = \frac{1}{\sqrt{2N_L}} \frac{\sqrt{1-\gamma^2}}{\gamma}$$

where  $N_L$  is the number of looks. From Equations 3 and 4 the height error as a function of the phase noise is given by

$$\text{Equation 5} \quad \sigma_h = \frac{\lambda r}{2\pi B} \frac{\sin(\theta)}{\cos(\theta-\alpha)} \sigma_{\phi}$$

Equations 4 and 5 allow the generation of an error map showing the local height accuracy in an interferometrically derived DEM.

One of the primary components of the TOPSAR system is the automatic generation of DEMs from interferometric SAR data. It is worthwhile to review the basic steps involved in interferometric SAR processing. Figure 2.1-3 shows a block diagram of the major steps in the DEM generation process, from raw data collection to generation of a digital topographic model. The description below will assume simultaneous collection of the two interferometric channels; however, with minor modification, the procedure outlined applies to repeat track processing as well.

The raw data are collected and stored on board for batch processing done on a mini-super computer. The first processing step is decoding the byte data, followed by range compression for each of the two interferometric channels. Using the aircraft motion information obtained from INU and GPS measurements, the data are compensated for perturbations in aircraft motion from a straight line path and azimuth compressed. This generates two single-look complex images. One of the single-look complex image pair is resampled to overlay the other, and an interferogram is formed by multiplying the complex pixel value in one image by the complex conjugate of the corresponding pixel in the second image. The resulting interferogram is multilooked (this is the optimal phase estimation as shown by Rodriguez, 1992) to reduce the amount of phase noise.

After the multilooked interferogram has been generated the phase for each complex sample is computed. Note that the phase measurement is made modulo  $2\pi$ . To generate a continuous height map, the 2-dimensional phase field must be unwrapped, that is, the correct multiple of  $2\pi$  must be added to the phase of each pixel so that the relative phase between the pixels will be correct. After the unwrapping process, there may still be an overall constant multiple of  $2\pi$  phase offset that needs to be added to each pixel so that the phase will have the correct relationship to the range shift as given in Equation 2. Estimating this overall phase constant is referred to as the absolute phase determination.

Subsequent to determining the absolute phase for each pixel in the interferogram and taking additional looks, the 3-dimensional target location is done using a target location algorithm that is outlined in Madsen (1993). In order to accurately position the targets, an accurate baseline estimate is required. In addition phase corrections are applied to the interferometric phase to account for tropospheric and ionospheric effects. A relief map is generated by gridding the unevenly sampled 3-dimensional target locations in a natural coordinate system aligned with the flight path. The gridded products include the target heights, the SAR image, a correlation map, and a height error map generated from the interferometric correlation using Equations 4 and 5. These four products will be referred to as primary mapping products. The resulting radar relief map may be measuring the heights above the ground, within the vegetation canopy or beneath the surface in arid regions. To convert this map into a true ground surface DEM corrections based on phenomenological studies must be incorporated into either the 3-dimensional location algorithms or into a post processing step.

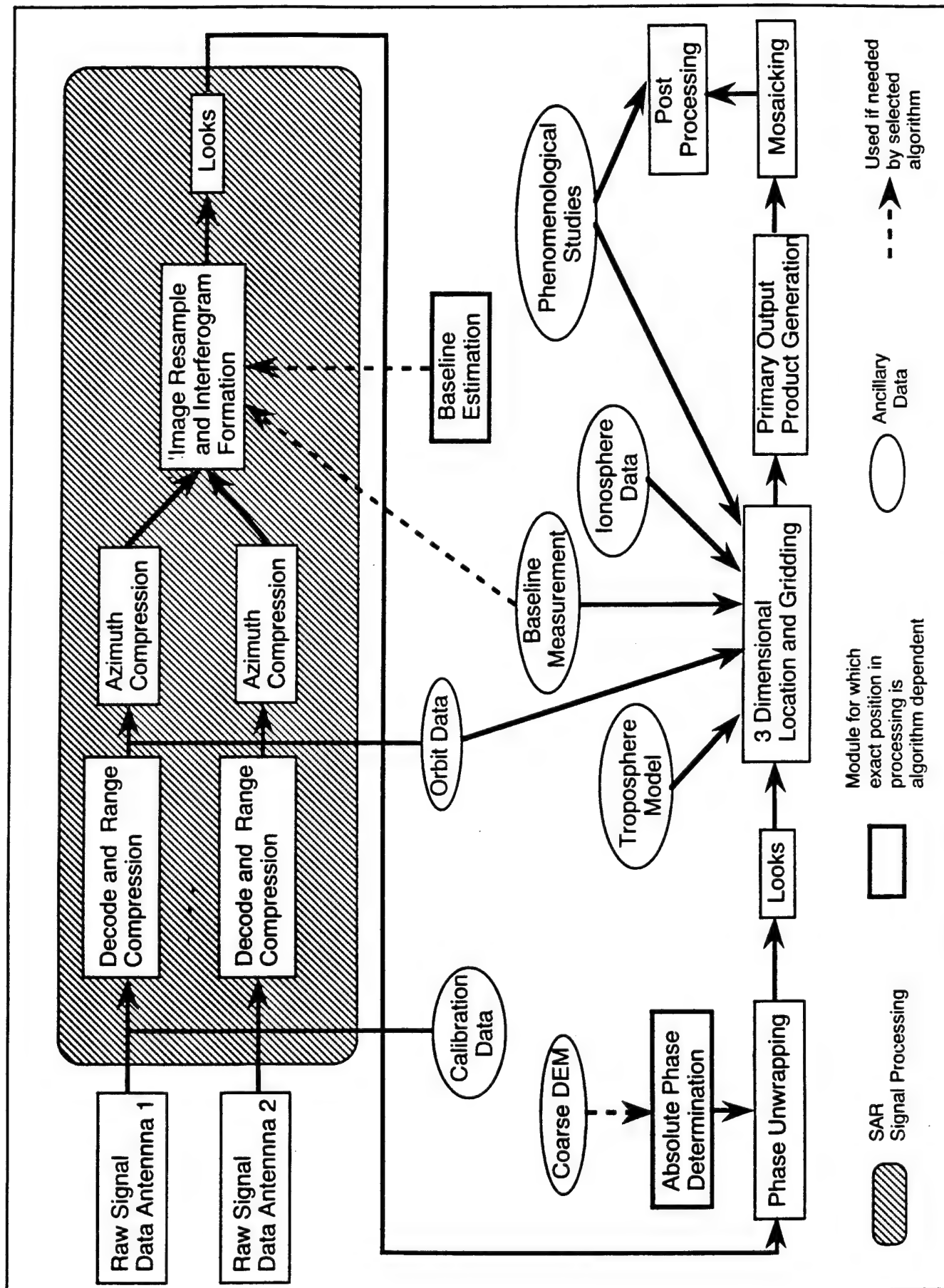


Figure 2.1-3: Data processing flow for an interferometric mapping system.

### 2.1.3.1 TOPSAR

Details of the TOPSAR radar system have been previously described in Zebker et al. (1992) and thus only the most important features will be discussed here. The TOPSAR radar system uses two C-band antennas which are flush mounted on the left side of the JPL/NASA DC-8. The antennas are mounted at the same position along the aircraft fuselage with a spatial separation (baseline) of 2.5m in the cross track direction. The electrical boresight of the antennas is 45° with respect to the vertical with one antenna used for transmission and both receiving returned echoes. The ground swath width of the TOPSAR is currently 12km in the 40 MHz mode. The range resolution of the system is limited by the transmitted bandwidth (40 MHz) or 3.75 m which projects to a ground resolution of approximately 5m at the center of the swath. Table 2.1-1 summarizes the key TOPSAR parameters.

Table 2.1-1 TOPSAR Parameters

Radar Parameter	Value
Frequency	5.3 Ghz
Range Bandwidth	40 Mhz
Peak Transmit Power	1000 W
Pulse Repetition Rate	3.9 pulses/m
Antenna Length	1.5 m
Antenna Elevation Beamwidth	30°
Baseline Length	2.50 m
Baseline Angle wrt Horizontal, $\alpha$	65.3°
Operating Altitude	8000 m
Look Angles, $\theta$	36°-64°
Slant Range near/far	9913 - 18361 m
Processed Ground Swath	12 km

The DC-8 and TOPSAR system are equipped with four independent motion measurement systems. The Digital Avionics Data System (DADS) includes the aircraft inertial navigation system, a barometric altimeter, a radar altimeter, as well as some additional navigation systems allowing the system to be updated during flight. The second system is the radar inertial navigation system, LASERREF, used to get high frequency motion data at a 50 Hz rate. The third system added to TOPSAR in 1994, a new Honeywell 764G combined p-code GPS receiver and INU were added to the radar avionics. The final system is a global positioning system (GPS). Both the DADS and GPS systems are quite accurate (GPS accuracy is 50 - 75 m) but the update rate is only 1 Hz. Because the LASERREF is not locked to any other system and biases in position and velocity tend to increase with time the two data sets are blended as described in zebker, et al. (1992) to produce the aircraft ephemeris. Differential GPS measurements are possible with an independent Turbo-Rogue GPS receiver on board the plane. These data are typically post processed using updated satellite ephemeris data in order to achieve position measurement accuracy of 10 cm along each axis. In summary, the combined motion measurement systems can yield aircraft locations with 10 cm accuracy at a 50 Hz rate.

### 2.1.3.2 Standard Processing

Standard processing of TOPSAR data generates a DEM, orthorectified SAR image and correlation map of an image strip in a coordinate system that is well suited to the radar imaging geometry. Until this year the on board INU was not accurate enough to absolutely position scatterers, so the resulting

DEM would generally have both planimetric errors as well as tilts in both the along track and cross track directions. Typically these errors were removed through the use of tie points. Initially one Laurel Quad run and all the Antioch Hills runs were delivered using the standard processing without any tilts or biases removed. These data did not prove particularly useful to DOC because their analysis was aimed at examination of data that had a high degree of absolute position accuracy. Later deliveries of the Laurel Quad and Antioch Hills data corrected this problem as described below.

### 2.1.3.3 Calibration Activities

One of the major changes to the TOPSAR system in 1994 was the incorporation of new Inertial Navigation Unit (INU), the Honeywell H764g, a combined p-code GPS receiver and ring laser gyro INU. The accuracy of the unit is 10 m spherical error and .001 degree attitude accuracy. The addition of the Honeywell INU made possible the absolute calibration of the TOPSAR instrument for the first time. A brief description of the calibration activities follows.

Since the Honeywell INU was acquired too late for incorporation into the standard radar data stream a specialized system operating on a PC was used to collect and store key output messages from the INU. Due to software error in the buffering logic the INU messages were scrambled such that time tag, position, and velocity information were not always in sync. This necessitated writing a program to realign the time tag, position, and velocity data so that it would be kinematically consistent. It was not possible to recover the Honeywell data at the full 50 Hz update rate. The effective message update rate was approximately 35 Hz, which was adequate for motion compensation.

After correcting for the misalignment, the Honeywell data were compared with the existing LASERREF INU and with differential GPS measurements from the Turbo-Rogue system to validate the Honeywell INU performance. Analysis showed that the position accuracy was within 3m rms on all three axes and the attitude measurements matched the LASERREF INU to within the accuracy of the LASERREF INU and an overall bias term. Since there is no means for independently assessing the accuracy of the Honeywell attitude measurement data, it was assumed to be working properly.

In order to calibrate the TOPSAR system a series of surveyed corner reflectors arranged in both the cross track and along track directions or an accurate photogrammetrically derived DEM is required to solve for all the calibration parameters. Since these data were not available in time to be provided to DOC for this year, they were partially calibrated using the two corner reflectors visible in the Laurel Quad data. (This did not permit solving for the full set of 13 calibration parameters; instead JPL solved for four of the 13 parameters.) The planimetric accuracy was found to be approximately 2.5 m in both along track and cross track. The vertical positions were observed to have a .05° slope in the cross direction resulting in up to 10 m of height error at the extreme edges of the swath.

### 2.1.4.4 Land Cover Classification

Although JPL's GeoSAR task plan did not include land cover classification studies, this type of work is being funded by ARPA under the AUTOMAP program. Data for the Antioch Hills site was made available to the AUTOMAP team to generate a land cover classification map based on algorithms developed at JPL. These data were then provided to DOC for comparison with its internally generated land cover classification maps from the TOPSAR data. JPL's land cover classification algorithm uses four classifications of land cover; these are water, fields, trees, and urbanized land. As JPL did not have access to ground truth data for this area no quantitative assessment of the classification accuracy was made. This assessment will be made in Year 1 by independent testing by Calgis and DOC.

## 2.2 CALGIS ACTIVITIES

### 2.2.1 Technical Assistance

Calgis has played a key role in completing the work plan for GeoSAR Project Year-1 activities. The technical assistance provided by Calgis as described below:

- **Project Coordination:** Calgis coordinated a range of project activities between ARPA, JPL, DOC, and Calgis. These included the coordination for the radar and photo flights, collection of ground truth, technical training, data acquisition and processing.
- **Ground Truth:** Calgis deployed radar targets for JPL and SRI radar flight missions, and provided surveyed 3-dimensional coordinate values in WGS-84 system for all radar targets. Additionally, detailed topographic surveys were completed for vegetation transect grid sites and data provided to DOC and JPL.
- **Technology Transfer:** Calgis provided technical expertise in support of digital soft-copy photogrammetric technology in use at DOC. Assistance supplementing training arranged by DOC through Intergraph. Calgis provided additional theoretical training in Photogrammetric Principles to DOC personnel, which was followed by practical demonstration at the ImageStation.
- **Photogrammetric Assistance:** Included precise GPS surveys for establishment of ground control for aerial triangulation, deploying photogrammetric targets, acquisition of aerial photography at four different scales, and completing the bundle adjustment of aerial photogrammetric blocks for each scale. Calgis also demonstrated the use of radar DEM data for the generation of orthophotos from aerial or radar imagery.
- **Radar Data Processing:** Calgis developed algorithms and software for the transformation of TOPSAR image and DEM data from the spherical coordinate system used by JPL to the NAD-83 California State Plane Coordinate System which is used by DOC and most other user communities for geologic, geophysical analysis and GIS. Similar data on UTM coordinate system were also provided for FMM Project of DOC.
- **Radar Image Processing:** Calgis carried out detailed analysis of the TOPSAR image data to assess its potential in the use for farmland and land use mapping and management. This analysis also involved multi-sensor data by combining the radar data with TM and SPOT data.
- **DEM Accuracy Analysis:** Calgis carried out a detailed comparative analysis of the geometric quality of radar DEM data by comparing it with the corresponding DEM data generated from aerial photogrammetric models. This analysis is presented in Section 3.1, this volume.



## 2.2.2 GROUND TRUTH

### 2.2.2.1 Site Preparation

Site preparation for the radar flights included initial reconnaissance and site selection, corner reflector deployment and monitoring, vegetation transect site selection, coordination of vehicle movement during the flight, and recording ground weather conditions during the flights.

#### 2.2.2.1.1 Reconnaissance

Reconnaissance visits were conducted for the Laurel Quad, Antioch Hills, Gualala River, and Iron Mountain sites to determine suitable locations for corner reflectors. Corner reflector sites to be used for registration were selected in open areas with unobstructed sky visibility above 30 degrees in orientations perpendicular to the flight lines. The sites were chosen in areas which were close to those selected from the flight maps during planning sessions. An attempt was made to select sites that had a minimum of cultural features or sharp breaks in topography to avoid spurious returns in the radar signal. Other considerations in selecting the sites were: accessibility, suitability as photogrammetric control points, suitability for GPS control, and cooperation of the property owner.

#### 2.2.2.1.2 Corner Reflector Deployment

The settings of corner reflectors at all sites were recorded at the time of deployment and again later, before the flight, and at the time of removal to check for any errors or disturbances of the reflectors. The rear corner of each reflector was centered over a 1.6cm diameter rebar with a plastic cap stamped "SEIBLS 5509." The recorded settings included the depression angle, roll, azimuth, height of the rear corner above the monument and the ground, and the height of the front edge above the ground. A "Corner Reflector Site Report" was completed for each reflector location, which included the property owner's name, address, and telephone number, directions to the site, a site description including reference ties to prominent objects to aid in monument recovery, reflector settings, and photographs. Corner reflector positions which were later used for major GPS control points were subsequently remonumented with a 7.6cm diameter aluminum monument, 76cm long set in concrete, with 8.9cm diameter aluminum caps on top stamped with DOC's logo, control point designation, and the date, as seen in Figure 2.2-1.

##### 2.2.2.1.2.1 Laurel Quad

A total of 21 corner reflectors were deployed on the site. Points near the four corners of the planned JPL swath were used as registration points. Each of these four locations had two 2.4m trihedral corner reflectors, one facing due east and one facing due west (see Figure 2.2-2). These eight corner reflectors were set for depression angles of 35 degrees. Five reflectors were set in the open across the SRI swath as calibration points. The first, third, and fifth reflectors were 2.4m trihedral corner reflectors and the second and fourth were 2.4m square reflectors. Two additional reflectors in the SRI swath were placed in the open, one 2.4m square and one 2.4m trihedral. Six reflectors in the SRI swath were placed under foliage for the foliage penetration experiment, five 2.4m squares and one 2.4m trihedral. All the reflectors in the SRI swath were oriented S 26° E, perpendicular to the flight line. The two reflectors in the far range of the swath in the calibration array were set for 35 degree depression angles, while the remaining 11 reflectors were set for 45 degree depression angles.



#### 2.2.2.1.2.2 Antioch Hills

Eight 2.4m trihedral corner reflectors were deployed in the open around the perimeter of the project site. All reflectors were set for depression angles of 35 degrees and oriented perpendicular to the flight paths. The reflectors in the southeast and southwest corners were oriented due north and those in the northeast and northwest corners were oriented due south. Two sets of reflectors were placed in the center east and center west portions of the project, each set having one reflector oriented due north and one due south.

#### 2.2.2.1.2.3 Gualala River

Eight 2.4m trihedral corner reflectors were deployed in the open near the four corners of the project area. At each of the locations, two reflectors were deployed, oriented perpendicular to the flight path, one at an azimuth of 336 degrees and the other at an azimuth of 156 degrees. All reflectors were set at 35 degree depression angles.

#### 2.2.2.1.2.4 Iron Mountain

Eight 2.4m trihedral corner reflectors were deployed in the open near the four corners of the project area. At each of the locations, two reflectors were deployed, oriented perpendicular to the flight path, one at an azimuth of 55 degrees and the other at an azimuth of 235 degrees. All reflectors were set at 35 degree depression angles.

### 2.2.2.2 Geodetic Control

The primary requirement for geodetic control was to establish the spatial position of those terrain points which had earlier been selected to serve as control points for the following three entirely different objectives.

- a. Points occupied by corner reflectors during radar flights at various sites. Their position was required to be accurate within 1m. These points had been monumented on the ground.
- b. Points selected to serve as control for the bundle adjustment of aerial triangulation. Such ground control was needed only for the Antioch Hills site. However, this site was covered by four different scales of photography ranging from the scale of 1:6,000 through 1:40,000. The aerial coverage varied for each scale, and the number, spatial distribution and the positional precision of the control points needed also varied according to each scale of photography. All the points had been monumented and had to be targeted before flying, and the optimal design and the size of the target was also dictated by each photo scale. The 3-dimensional positional precision needed varied from 3cm for the 1:6,000 scale to 20 cm for the 1:40,000 photo scale.
- c. Points selected to serve as control for the completion of field surveys for vegetation transects and for surveying the location of vehicles used in foliage penetration studies. These points were also monumented on the ground. The positional precision for such points was about 10 to 15cm.

#### 2.2.2.2.1 Planning for Geodetic Control

The planning considerations for providing the above geodetic control included the selection of a suitable geodetic datum, design and optimization of the geodetic networks and the methodology for geodetic positioning.

The geographic reference for the radar image data is provided by the airborne GPS data collected during radar flight mission. Consequently, it was decided to use the WGS-84 as the datum, which is the datum in which GPS data are reduced, for all types of field surveyed geodetic control. Subsequently, the DEM test data and the topographic data for the vegetation transect sites were expressed in the related NAD-83 California State Plane coordinate system. The datum connection was achieved through ties to the existing California High Precision Geodetic Network (HPGN) stations in and around the project area which were supplemented by ties to NGS first-order stations.



Figure 2.2-1: Primary Control Monument

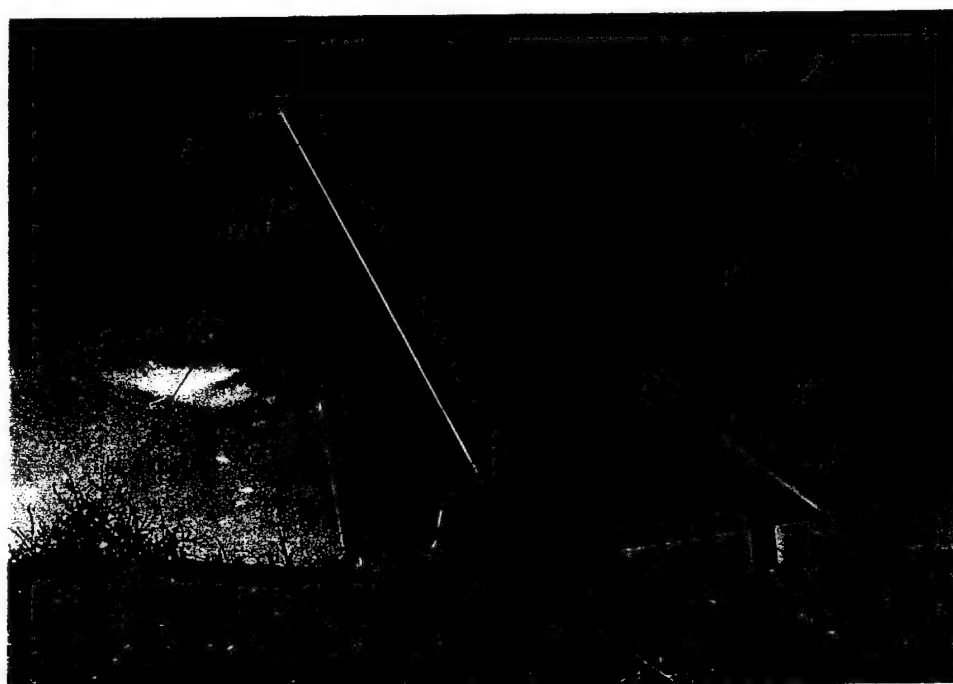


Figure 2.2-2: Eight-foot Trihedral Corner Reflector

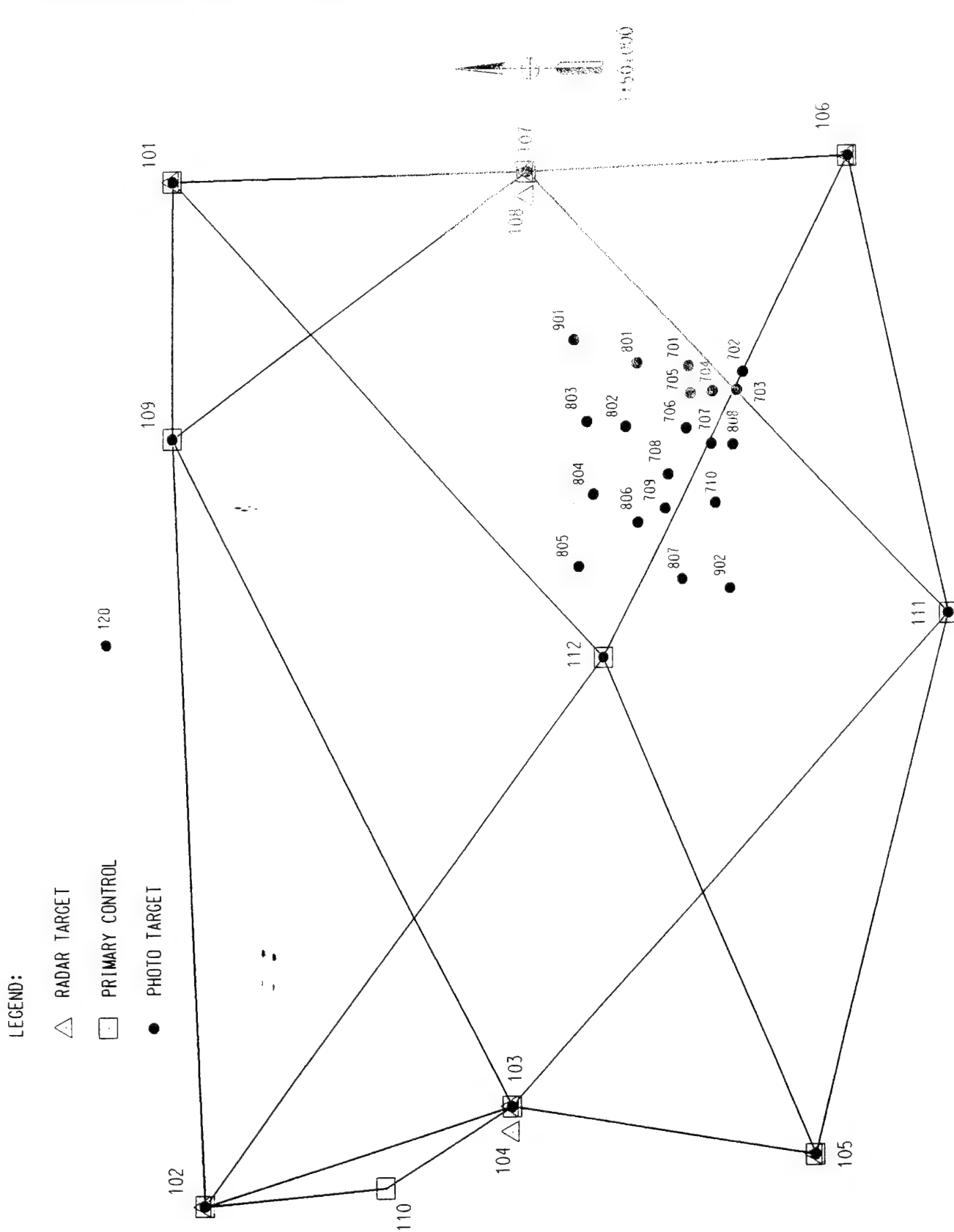


Figure 2.2-3: Control Network for Antioch Hills Site.

The distribution of photogrammetric control for the Antioch Hills site was planned to optimize the control layout for the aerial triangulation adjustment for all four different photo scale blocks, while maximizing the use of the control points falling in the common block coverage for more than a single photo block. Since formal permission from the property owners is essentially required, every effort was made to locate as many points as possible on state or public property. The geodetic control network is shown in Figure 2.2-3.

The considerations which established the superiority of GPS positioning method over the conventional EDM traversing were: (1) the relative positional accuracy requirements for widely spaced corner reflector targets, (2) the extent of the project area covered by geodetic control (more than 1,000 square kilometers), (3) the freedom from line-of-sight constraints imposed by the undulating and forested terrain, and (4) the ease with which control can be carried across dense urban areas. It was planned to carry out GPS surveys to meet the Federal Geodetic Control Committee GPS Relative Positioning Standard for Type C, First-order network, which specifies relative baseline accuracy of not less than 1:100,000.

#### 2.2.2.2.2 Field Data Acquisition

The primary network was established through static GPS positioning techniques. Using three dual-frequency Trimble 4000 Series Geodetic GPS Receivers, code and carrier phase measurement data were collected in sessions ranging from 60 to 120 minutes depending on the length of the base lines. The observation sessions were planned to increase: (1) the number of baselines measured more than once, and (2) the number of independent loops in the network.

The satellite availability and Positional Dilution of Precision (PDOP) requirement to be under 5 was easily satisfied for the generally open Antioch Hills site. For the Laurel Quad, Gualala River, and Iron Mountain forested sites, however, some of the stations had to be occupied for longer time to collect sufficient amount of data from more than four satellites meeting the PDOP requirements. One of the existing HPGN stations occupied during Gualala River site GPS survey was near the edge of the SR 101 pavement, and the regular flow of traffic along the highway resulted in strong multi-path effects. The extension of the data collection session, until a significant change in satellite geometry had occurred, resulted in providing satisfactory positioning data.

The secondary control network was observed for providing the tie between the pair of corner reflectors required at various sites, and for the aerial triangulation of 1:6,000 and 1:10,000 scale photo blocks in the Antioch Hills area. This control was established using the rapid-static GPS positioning technique based on ties made to the primary GPS control network. The data were collected using Ashtech Z-12 dual-frequency GPS Receivers and the rover receiver collected data at each station for 10 to 15 minutes, while another receiver continuously occupied one of the primary control stations as the base. The GPS satellite availability was excellent and PDOP remained mostly under 4.

#### 2.2.2.2.3 Data Processing

The multi-baselines observed in each GPS data collection session of the primary network were reduced using the Trimble TRIMVEC software, while holding as fixed the position of any HPGN or First-order NGS station included in the session. After the data for all sessions were successfully reduced, loop closures were checked for all independent loops in the network, formed by baselines reduced from different sessions. The loop closures ranged from 0.2 parts per million (ppm) to 3.4ppm. This result is well within the intended standards.

The entire primary net was then adjusted simultaneously using a minimally constrained least squares adjustment with the GEOLAB software. The HPGN station Mount Diablo Ecc. was the only point held fixed in this adjustment. The results showed the adjustment correction to the baselines ranged from 0.4ppm to 3.2ppm. This clearly shows the internal consistency of the GPS data is well within the Type C-Class I GPS relative positioning standard.

The net was adjusted again, this time constraining the WGS-84 coordinates of all the tied HPGN and NGS First-order stations to be fixed. As a result of this constrained adjustment solution, the adjustment corrections to the measured baselines ranged from 1.8ppm to 6.3ppm. This shows that the intended precision standards were adequately met while maintaining consistency with the existing National Geodetic Control Network. The spatial coordinates for all the control points were computed as latitude, longitude and ellipsoidal height in WGS-84 coordinate system and were transformed to WGS-84 geocentric coordinates for supply to JPL.

The rapid-static GPS observations were reduced using the Ashtech PNAV software and holding the WGS-84 coordinates of the base station of the primary network as fixed. This processing software provides the capability to process each baseline in the forward and the backward direction. This provides an excellent check on the integer ambiguity solution, and the resulting standard errors in the computed baseline established the reliability of the computed coordinates to 2cm in position and 3 cm in height. The adjustment resulted in latitude, longitude and ellipsoidal height in WGS-84 system. These results were transformed to the NAD-83 California State Plane Coordinates for CA Zone 3 for use in photogrammetric data reduction and for topographic field surveys. The information about the vehicle positions for penetration studies were supplied to JPL as WGS-84 geocentric coordinates.

### 2.2.2.3 Vegetation Transects

Calgis personnel performed detailed mapping of five 2,500 square meter 'test grid' sites within the Laurel Quad to provide additional ground truth for foliage penetration experiments. An attempt was made to select test grid sites which were evenly spaced across the width of the swath and which had similar terrain and vegetation characteristics. GPS control was established in the vicinity of each test grid from which detailed topographic surveys were accomplished using electronic total stations with data collectors. The ground surfaces were determined by surveying breaks in terrain and spot positions throughout each grid. The base position and tops of all trees were surveyed and attribute data including species, trunk diameter, drip line, and height of the bottom of the canopy were noted. The location of all other undergrowth was noted and attribute data including species, diameter and height were recorded. The locations and attributes for all other features such as trails, roads, rocks, stumps, and logs were also surveyed and recorded. Digital terrain models and contour maps for both the ground and canopy surfaces were produced for each test grid. The data were provided digitally in MGE GIS format. A summary of each test grid site follows:

#### 2.2.2.3.1 Test Grid A

The northwest corner of the grid is located at 37°07'05" north latitude and 121°59'13" west longitude (NAD83). The site slopes easterly with an average grade of 35%.

The dominant species within the grid are Coast Redwoods, Pacific Madrones, and Tan Oaks, with light undergrowth of Redwood and Tan Oak seedlings. Within the grid there are: 29 Redwoods with trunk diameters ranging from 10 to 81cm, with the average being 46cm and heights ranging from 4 to 41m with the average being 27m; 30 Tan Oaks with trunk diameters ranging from 13 to 68cm with the average being 40cm, and heights ranging from 8.2 to 32m with the average being 23m; 17 Pacific Madrones with trunk diameters ranging from 15 to 50cm with the average being 33cm and heights ranging from 3.6 to 24m with the average being 18m.

#### 2.2.2.3.2 Test Grid B

The northwest corner of the grid is located at 37°05'24" north latitude and 121°57'10" west longitude (NAD83). The site slopes easterly with an average grade of 40%.

The dominant species within the grid are Coast Redwoods, Pacific Madrones, and Tan Oaks, with light undergrowth of Redwood and Tan Oak seedlings. Within the grid there are: 59 Redwoods with trunk diameters ranging from 13 to 152cm with the average being 66cm and heights ranging

from 4.2 to 32m with the average being 21m; 18 Tan Oaks with trunk diameters ranging from 10 to 43cm and heights ranging from 4.2 to 32m with the average being 21m; and six Pacific Madrones with trunk diameters ranging from 25 to 100cm and heights ranging from 8 to 19m with the average being 17m.

#### 2.2.2.3.3 Test Grid C

The northwest corner of the grid is located at 37°03'29" north latitude and 121°55'33" west longitude (NAD83). The site slopes easterly with an average grade of 40%.

The dominant species within the grid are Coast Redwoods, Pacific Madrones, and Tan Oaks, with light undergrowth of Redwood and Tan Oak seedlings. Within the grid there are: 19 Redwoods with trunk diameters ranging from 15 to 91cm and heights ranging from 5 to 32m with the average being 20m; 42 Tan Oaks with trunk diameters ranging from 10 to 56cm with the average being 30cm and heights ranging from 3.3 to 30m with the average being 18m; and two Pacific Madrones with trunk diameters of 25 and 30cm and heights of 17.6 and 18.2m.

#### 2.2.2.3.4 Test Grid D

The northwest corner of the grid is located at 37°00'37" north latitude and 121°54'26" west longitude (NAD83). The site slopes easterly with an average grade of 50%.

The dominant species within the grid are Coast Redwoods, Pacific Madrones, and Tan Oaks, with light undergrowth of Redwood and Tan Oak seedlings. Within the grid there are: 27 Redwoods with trunk diameters ranging from 20 to 89cm with the average being 61cm, and heights ranging from 11 to 41m with the average being 32m; 53 Tan Oaks with trunk diameters ranging from 10 to 53cm with the average being 61cm and heights ranging from 2.3 to 9.4m with the average being 23m; and four Pacific Madrones with trunk diameters ranging from 30 to 47cm and heights ranging from 18 to 28m.

#### 2.2.2.3.5 Test Grid E

The northwest corner of the grid is located at 37°01'29" north latitude and 121°52'58" west longitude (NAD83). The site slopes easterly with an average grade of 40%.

The dominant species within the grid are Coast Redwoods, Pacific Madrones, and Tan Oaks, with light undergrowth of Redwood and Tan Oak seedlings. Within the grid there are: 79 Redwoods with trunk diameters ranging from 10 to 91cm with the average being 47cm and heights ranging from 7.6 to 41m with the average being 27.5m; 40 Tan Oaks with trunk diameters ranging from 13 to 46cm with the average being 25cm and heights ranging from 6 to 26m with the average being 20m; and six Pacific Madrones with trunk diameters ranging from 20 to 46cm with the average being 31cm and heights ranging from 15 to 26m with the average being 21.5m.

## 2.2.3 GEOMETRIC PROCESSING OF RADAR DATA

### 2.2.3.1 Radar to GIS Conversion

The primary focus of the GeoSAR Year 1 experiments is to investigate the feasibility of the use of TOPSAR image and DEM data for GIS applications in engineering, geology, seismic hazard, land-use planning, and resource management. It is, therefore, necessary that the radar data be referenced to the horizontal and vertical datum that is most commonly used for such applications. Most applications are currently based on the geographic data derived from USGS 7.5-minute quad sheets, which have adopted the NAD83 for planimetric data and, although NAVD88 has been adopted for height data, most current elevation data are still available as orthometric elevations based on National Geodetic Vertical Datum 1929 (NGVD29). Calgis developed the software for the transformation of the radar image data from the spherical system of radar mapping coordinates to the NAD83 California State Plane Coordinate system and the transformation of radar elevations to orthometric heights based on (NGVD29).

### 2.2.3.2 Radar Mapping Coordinates to NAD83 Datum

The JPL radar mapping coordinates are defined relative to the sphere tangent to the ellipsoid at a peg point longitude ( $\lambda_0$ ) and latitude ( $\phi_0$ ), having a radius  $r_a$  which is the radius of curvature in the along track direction given by (written communication, 1993):

$$\text{Equation 1} \quad r_a = \frac{r_e(\phi_0) r_n(\phi_0)}{r_e(\phi_0) \cos^2 n + r_n(\phi_0) \sin^2 n}$$

$$\text{Equation 2} \quad r_e(\phi) = \frac{a}{(1 - e^2 \sin^2 \phi)^{1/2}}$$

$$\text{Equation 3} \quad r_n(\phi) = \frac{a(1 - e^2)}{(1 - e^2 \sin^2 \phi)^{3/2}}$$

where:

$n$ : track angle

$r_e$ : east principal radius of curvature

$r_n$ : north principal radius of curvature

The radar mapping coordinates ( $s, c, h$ ) are (See Figure 2.2-4):

$s$ : distance along the reference curve from the peg point

$c$ : distance from the reference curve along a meridian at a distance  $s$  from the pegpoint

$h$ : height above the approximating sphere

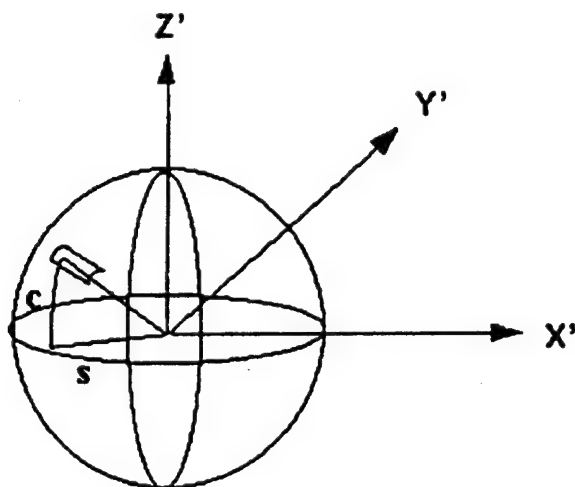


Figure 2.2-4: Approximating Radar sphere.

The geocentric coordinates for the approximating radar sphere  $(x', y', z')$  are:

$$\text{Equation 4} \quad \begin{bmatrix} x' \\ y' \\ z' \end{bmatrix} = \begin{bmatrix} (r_a + h) \cos c_\phi \cos s_\lambda \\ (r_a + h) \cos c_\phi \sin s_\lambda \\ (r_a + h) \sin c_\phi \end{bmatrix}$$

where:

$$c_\phi = \frac{c}{r_a}$$

$$s_\lambda = \frac{s}{r_a}$$

The transformation from  $(x', y', z')$  to the WGS-84 coordinates  $(x, y, z)$  is a 3-dimensional conformal transformation defined as follows:

$$\text{Equation 5} \quad \begin{bmatrix} x \\ y \\ z \end{bmatrix} = M_{x'y'z'}^{xyz} \begin{bmatrix} x' \\ y' \\ z' \end{bmatrix} + 0$$

where:

$M_{x'y'z'}^{xyz}$  : is an orthogonal transformation matrix

0 : translation vector



The transformation from WGS-84 geocentric coordinates  $(x, y, z)$  to geodetic coordinates, longitude, latitude, and height  $(\lambda, \phi, h)$  is given by:

$$\lambda = \begin{cases} \tan^{-1} \frac{y}{x} & x \geq 0 \\ \text{sign } y \tan^{-1} \frac{y}{x} + \pi & x < 0 \end{cases}$$

$$p = \sqrt{x^2 + y^2}$$

Equation 6

$$\alpha = \tan^{-1} \left[ \frac{z}{p} \frac{1}{\sqrt{1 - e^2}} \right]$$

$$\phi = \tan^{-1} \left[ \frac{z + \frac{e^2}{1 - e^2} b \sin^3 \alpha}{p - e^2 a \cos^3 \alpha} \right]$$

$$h = \frac{P}{\cos \phi} - r_e(\phi)$$

where:

$a$ : ellipse semi-major axis

$b$ : ellipse semi-minor axis

$c$ : ellipse eccentricity

$$e^2 = \frac{(a^2 - b^2)}{a^2}$$

$$r_e(\phi) = \frac{a}{(1 - e^2 \sin^2 \phi)^{3/2}}$$

The WGS84 geodetic longitude and latitude can now be transformed to NAD83 California State Plane coordinates by using well-known transformation algorithms.

### 2.2.3.3 Image and Height Resampling to NAD83 Datum

The projection of spherical surface onto a plane requires a varying degree of realignment within the image raster. The degree of relocation of the pixels within the raster is a function of radar image strip heading and the geographic location of the project.

The pixel locations in the spherical radar image from which the output pixels are drawn, do not fall on exact raster position. In other words, the output image will lie "between pixels" in the original image. In general, the new output pixel will fall between 4 pixels in the spherical radar image.

There are several methods to obtain a brightness value for the pixel in the rectified image, these are:

1. Nearest Neighbor:

The intensity of the pixel in the output image is assigned the intensity value of the pixel nearest in the input image. This simple method is fast, and does the least smoothing of the resulting image (which may be important to preserve edges), but often produces "jaggies" in which lines appear broken up or Moire effects appear.

2. Bi-linear Interpolation:

This interpolation utilizes the intensity values of the four immediate neighbor pixels. The brightness is assumed to vary linearly between the points above and below, and left and right of the interpolated coordinates of the pixel. The intensity of the output pixel at position (x, y) is computed using:

$$\text{Equation 7} \quad p(x, y) = a1 + a2x + a3y + a4xy$$

where a1, a2, a3, a4 are the polynomial coefficients which can be expressed as functions of the size of the raster and the pixel intensity. The resulting image is quite smooth, and lines do not show aliasing effects, but edges are somewhat smoothed by the procedure.

3. Cubic Convolution:

Cubic convolution interpolation uses the 16 nearest neighbor pixel intensities in interpolating the intensity value of the pixels in the output image. This is represented by a 16-term bi-cubic polynomial in which all possible cubic terms involving x, y and their products appear. The precision of the cubic convolution requires significantly more computer resources than either bi-linear or the nearest neighbor interpolation techniques.

The bi-linear interpolation was used for image intensity and the height data for this project, because it provides smooth interpolation with very good results and less computational overhead. To further decrease the amount of I/O operation, the image and height data files were divided into small overlapping tiles.

## 2.2.4 Multi-sensor Data for Land Use and Cover Mapping

### 2.2.4.1 Terrain Cover and Land Use Mapping

As a demonstration of potential uses of an advanced radar terrain mapping system like JPL's TOPSAR, Calgis provided technical support to DOC for its FMMP. The FMMP application differs markedly from others in the GeoSAR Program, in that FMMP is involved primarily in mapping land use from an agricultural point of view rather than in mapping terrain elevation *per se*. This does not mean that elevation information has no role in FMMP assessments. Indeed, elevation and derived terrain properties of slope and aspect are considerations in the determination of land use. The distinction here is one of FMMP's emphasis on terrain land cover and land use mapping.

Since the FMMP emphasis differs from other GeoSAR program elements, the FMMP component to the GeoSAR Program provides a unique insight to the needs of other California state agencies that are also interested in improving their capabilities regarding land use or land cover mapping. This aspect to the GeoSAR Program was made quite evident during the Multi-Agency Coordination Meeting held at DOC on May 24, 1995 with representatives of non-DOC California agencies. Most of these agencies have responsibilities which involve land use or land cover mapping.

Beyond the consideration of various TOPSAR applications, Calgis was also responsible for training FMMP personnel in the use of TOPSAR data. In the context of the FMMP application, non-TOPSAR remotely-sensed data have been or are being considered as an aid to land cover and land use mapping. While TOPSAR data may be used alone for some aspects of land-cover and land-use mapping, TOPSAR data can be combined with other-sensor data, e.g., with Landsat Thematic Mapper (TM), with SPOT data, and/or with polarimetric radar data for the same purpose. Thus, the Calgis training for FMMP personnel extended beyond TOPSAR to other sensor data. Furthermore, the development of approaches for using TOPSAR, TM, and/or SPOT data was being carried out within the context of the use of an Intergraph system for data processing, display, and analysis.

Beyond new-technology and training considerations, Calgis also has an overall responsibility in the GeoSAR Program in promoting commercial development of a TOPSAR-like system. Toward this end and toward needs of FMMP, Calgis developed preprocessing shell programs to convert TOPSAR data provided by JPL to forms compatible with standard Intergraph data structures. This responsibility will be expanded in Year 2 of the GeoSAR Program as other agencies are brought into the program. Beyond its expertise with Intergraph, Calgis staff also have extensive knowledge of the capabilities of other image processing software packages. This knowledge will be helpful when state agencies that use other software join the GeoSAR Program.

### 2.2.4.2 General Characteristics of TOPSAR Data

Recall that TOPSAR data consist of three accurately geocoded rasters with 5m spacing between raster cells (see Sections 2.1.3.1 and 2.1.3.2). These rasters are produced from raw TOPSAR data as 32-bit floating-point data. Since image processing software packages often expect 8-bit unsigned integer rasters, well-considered preprocessing algorithms are necessary to convert the floating-point raster values to 8-bit unsigned integer values. Another challenging characteristic of TOPSAR data is the existence of a significant number of undefined pixels scattered throughout the raster. These pixels are marked by special raster values called, in some contexts, null values. Undefined pixels arise at places where the confidence in the estimated elevation is low (i.e., the height-error is large). This happens when the backscattered signal is low, when geometric conditions are inappropriate for elevation estimation, and/or when the surface object exhibits complex scattering behavior (e.g., in volume-scattering objects like trees). Raster processing software needs to ignore null-valued cells in

processes that produce new rasters from original TOPSAR rasters. In summary, many raster-data processing issues had to be addressed in enabling the use of TOPSAR data on a standard image processing system like the Intergraph system.

While a threshold of 0.45 in the correlation raster layer from TOPSAR was used to define null pixels, it is likely that a higher threshold would be selected in the final analysis. Thus, more null pixels would be present and would have to be considered in any subsequent analyses.

It is also important to keep in mind the fact that the TOPSAR uses microwaves having a free-space wavelength of 5.67cm (in the C-band) with vertical polarization (V). Thus, TOPSAR microwaves do not penetrate farther than a centimeter or so into solid or liquid surface materials. Many land-cover types have well defined (hard) surfaces (e.g., bare soil, roof tops, roadways, sides of buildings, open water). Other land-cover types have ill-defined (soft) surfaces (e.g., trees, shrubs, and thick grasses). While these properties may cause difficulties in elevation estimation, they also represent ways of characterizing land cover. The implications of these properties will be discussed later.

The primary TOPSAR raster is the floating-point digital terrain elevation raster (DtmF). The numeric value of DteF represents elevations (in meters) above a defined spherical surface (local earth sphere) in a stated map coordinate system projection. This raster, like the other two TOPSAR rasters, is a 32-bit floating-point number on a 5-m posting. In hard-surface cases, DtmF is the elevation of basically the same surface seen by a human eye (or in a typical air photo). In soft-surface cases, DteF represents an elevation below the visible surface. With the TOPSAR being based on the C-band VV mode of operation (VV means vertical transmit, vertical receive polarization combination), TOPSAR microwaves do not often penetrate more than a few centimeters. For some surfaces (i.e., level, smooth surfaces like open water under calm wind conditions), the backscattered energy is so low that the signals received by TOPSAR's two receiving antennas and receiver systems cannot be correlated well enough to solve the elevation-estimation geometric problem. For soft surfaces, the object being mapped presents a confused radar signature to the two antennas; this also frustrates the elevation-estimation geometry. In either case, the estimated values of DteF have great uncertainty. Fortunately, other information in the form of rasters registered with the DteF raster is provided to the user as a result of raw TOPSAR data processing.

The second TOPSAR raster represents the backscattering coefficient (dimensionless) for each 5m cell; this raster is called the floating-point magnitude raster (MagF). While MagF is related to the absolute strength of the signal received by TOPSAR's dual antenna system, it has been corrected for known effects of slant-range (the 2-way inverse-square law loss of power effect) and antenna gain. Thus, MagF represents an estimate of the backscattering coefficient of the surface for each TOPSAR pixel. Since TOPSAR data are taken from an aircraft platform (NASA DC-8 aircraft flying at about 8,230m altitude), the incident angle of irradiance varies over the TOPSAR image swath from about 20 degrees (measured from nadir) to 62 degrees. Therefore, C-VV (MagF) would likely vary greatly for similar surface objects as a function of scene position (across track or range position).

With the estimated DteF information, the planimetric (map) location of each original TOPSAR image pixel has been corrected for relief displacement. Thus, MagF is an orthorectified image of the landscape. Also, DtmF and CorrF (see below) are orthorectified information about the landscape. Indeed, the orthorectified nature of TOPSAR data is a great strength of the data set.

The third TOPSAR raster, called CorrF, is a measure of elevation accuracy on a scale from 0 to 1. It may also be thought of as a measure of confidence in the estimated DteF value. Another interpretation is that CorrF represents the softness of the surface; this would be the case if JPL were to remove known effects of signal-to-noise (S/N) and poor geometry from the CorrF raster. This preprocessing operation is planned by JPL. Until that time however, the somewhat confused nature of CorrF will remain. In the Calgis approach to the use of CorrF and MagF, an attempt was made to decorrelate the two types of

data via a Principal Components (PC) analysis. It is clear that MagF and CorrF, while highly correlated, contain independent kinds of information about the nature of the surface materials (at whatever elevation). This is key to the application of TOPSAR data to the FMMP mapping objective.

JPL uses initial CorrF values to set a threshold of confidence on DteF (and on MagF). Specifically, if CorrF is less than 0.45, all pixels in the three raster set are set to null values (MagF = 0, DteF = -10000, CorrF = 0). This threshold was determined by JPL empirically. The concept of the designation of undefined pixels as null values, while common in some software packages, is not present in Intergraph. In its place, one can use a pixel mask to prevent processing of "null" pixels. The use of a detailed null mask was not explored during Year 1 of the GeoSAR Program; it will be explored in Year 2.

#### 2.2.4.3 General Characteristics of Optical Data Used in the GeoSAR Program

One approach to the use of TOPSAR data for an application like the FMMP is to combine TOPSAR data with other commonly-available data. Even if TOPSAR were the only data being used in a land-cover mapping effort, it is still useful to compare results of its use with the results of the use of non-TOPSAR data. The most commonly-available non-TOPSAR data are from photographic cameras or electro-optical scanners. Since FMMP personnel are using one form of optical data (high-altitude CIR photos) in the current approach, it is useful to understand the nature of these optical data. In general, all of these non-microwave devices can be classified as optical imaging devices. They differ by spectral coverage, spectral resolution, and spatial resolution.

In fact, the GeoSAR Program is concerned only about optical data from panchromatic aerial photography, color infrared (CIR) photography, the Landsat Thematic Mapper (TM), and the SPOT panchromatic scanner (Pan).

CIR photography covers three parts of the spectrum in green-light, red-light, and near infrared (NIR) (color coded in a positive transparency by blue, green, and red dyes, respectively). Relative to other non-photographic optical sensors used in the GeoSAR Program, CIR imagery is high resolution. Recall that FMMP personnel use CIR photography as on a light table under simple magnification (10X). Nevertheless, spatial features can be recognized in CIR that cannot be recognized in Landsat TM data, the only other multispectral data considered in the GeoSAR Program.

The TM collects seven digital image data sets (8-bit unsigned integer) with an instantaneous field of view (IFOV) of 30m for the shortwave bands (TM1, TM2, TM3, TM4, TM5, and TM7) and with an IFOV of 120m for the thermal IR band (TM6). Original TM data are processed into rasters with resampled cell spacing of 25m or 30m (customer specified). Six TM bands cover parts of the shortwave optical region with three bands devoted to the visible region (TM1 for blue-light, TM2 for green-light, and TM3 for red-light) and three bands designed for the shortwave infrared (IR) region (TM4 for the NIR, TM5 and TM7 for two parts of the middle IR: 1.65 micrometers and 2.21 micrometers).

SPOT Pan collects one digital image data set (8-bit unsigned integer) with an IFOV of 10m. The data are not resampled (unless requested). The SPOT Pan band covers the non-blue part of the visible spectrum (an average of green- and red-light).

Very-high resolution panchromatic photography was collected for the GeoSAR Program for stereo photogrammetric data reduction (at scales ranging from 1:6,000 to 1:40,000). For the purpose of correcting truth maps of land-cover and land-use, these data, taken on August 10, 1994, were used to update FMMP products originally produced from the 1993 CIR photographs. These data were not used with TOPSAR, TM, or SPOT Pan digital data (all or parts of which were fused in various ways).

Before leaving a general discussion of optical data, it should be noted that atmospheric haze affects all optical data in the visible and NIR. At first order, the effect of atmospheric haze (and other molecular scattering) is to add a bias to each band to what would have been recorded had there been no

atmosphere in the path between the sensor and the ground. Haze effects (and molecular scattering effects) are greatest for the shortest wavelengths. Thus, haze has a significant effect on TM1, TM2, and TM3, on SPOT Pan, on panchromatic photography, and on some components of CIR photography. Beyond this, in digital optical imagery, the sensor gain for each band controls how the digital brightness data are related to surface reflectance characteristics. In addition, in topographically non-level sites like the one used for the FMMP evaluation, shading effects caused by combinations of slope and aspect affect optical image brightness. To first order, the effects of topography on optical data are the same for all bands and can be considered to be multiplicative.

#### 2.2.4.4 Specific Approaches

##### 2.2.4.4.1 Raster Conversion from 32-Bit Floating Point to 8-Bit Unsigned Integer

From an inspection of TOPSAR histograms, one sees that all three rasters are highly skewed. MagF is skewed toward low values; CorrF is skewed toward high values; and DteF is skewed toward low values. Calgis was interested in performing a Principal Components (PC) analysis of MagF and CorrF to decorrelate the data into two independent measures. This requires 8-bit unsigned integer raster data in the Intergraph software package (as is the case for other packages). At first, a set of linear transformations was tried as follows:

$$\text{Mag8} = (\text{MagF} - \text{MagFMin}) * 255 / (\text{MagFMax} - \text{MagFMin})$$

$$\text{Corr8} = (\text{CorrF} - \text{CorrFMin}) * 255 / (\text{CorrFMax} - \text{CorrFMin})$$

Min and Max can be taken to be the absolute minimum (non-null) value and absolute maximum value in the linear equation. Alternatively, one can set the minimum and maximum at a low and high percentile level in the data distribution.

After the initial transformation to 8-bit data, a raster correlation / scatterplot examination showed that a high, but non-linear relationship exists between Mag8 and Corr8. Thus, a PC analysis will not be very successful in creating two rasters that show independence. Therefore, Calgis explored the idea that the data should be deskewed during the process of conversion from floating-point to 8-bit.

For the MagF raster, the simple approach was to convert MagF to decibels (i.e., to MagdB8) first. Then, a suitable level for Min and Max was determined (using 1 percentile and 99 percentile points in the distribution). After that, a similar linear transformation was done. This worked well for the MagF raster. In fact, an Intergraph shell program was written to allow the user (e.g., FMMP personnel) to perform this multistep conversion process.

For the CorrF raster, a simple linear transformation was used. In mid-May 1995, however, a different deskew algorithm was devised and used on CorrF data. This algorithm was based on a power-law transformation which moves the median of the CorrF values (equal to about 0.933 for the TOPSAR 090 data) to mid-range (i.e., to 128) in the CorrPower8 raster. This approach has not so far been fully tested.

The linear transformation method was used for the DteF raster. It is likely that a power-law deskew procedure would be useful here; however, this was not done in Year 1.

##### 2.2.4.4.2 Decorrelation of MagdB8 and CorrPower8 Rasters

As indicated above, a decorrelation of the transformed MagdB8 and CorrPower8 rasters (or just Corr8) can be done by using PC analysis. Qualitatively, this process produces good results. PC-1 captures the vast majority of the variance in MagdB8 and Corr8 (or CorrPower8). In fact, the interesting effect of the orientation of urban streets on MagF (an effect that does not seem to be as manifest in the CorrF raster) seems to be suppressed in PC-1 (and enhanced in PC-2). To identify an area as "Urban" should not be sensitive to street orientation; thus, PC-1 appeared to be a superior raster to either MagdB8 or Corr8 alone. PC-2 appeared to contain the effects of street orientation and softness (volume scattering nature) of the ground objects.



In late discussions between Calgis and JPL, it is clear that the original CorrF raster (and its derivative rasters, Corr8 or CorrPower8) contains three independent effects. According to Dr. Scott Hensley (JPL),

$$\text{CorrF} = \text{CorrGF} * \text{CorrSNF} * \text{CorrSFCF}$$

CorrGF represents the effects of poor geometry on CorrF (which changes systematically over the scene in the range direction). CorrSNF represents the signal-to-noise effects which are known during original processing (related somewhat to MagF, but affected also by absolute slant range; the effect of which has been removed during raw signal processing). CorrSFCF represents the effect of the nature of the scene object itself. A "soft" object will have a low value of CorrSFCF; a "hard" object will have a high value of CorrSFCF.

Calgis recommends that JPL provide in their standard TOPSAR products a supplemental correlation raster that has systematic effects removed. JPL reported (section 2.1.4.4) that they had used the Automap algorithm to produce land cover classifications (urban, water, trees, and other). This was based on Cor SFCF, Mag F, and Dem F. The Automap algorithm was not provided to DOC, therefore, this aspect of technology transfer was not performed.

#### 2.2.4.4.3 Aggregation of TOPSAR Rasters to Landsat TM Resolution

Calgis explored the notion of fusing a TOPSAR-derived raster (PC-1 from before) with Landsat TM by aggregating 25 5-m TOPSAR PC-1 values into one 10m raster (having the same size as a TM raster cell). Two rasters were produced by this aggregation process. One represented the expected value (average); the other, the deviation from the expected value. In general, neither aggregated raster appears to have much value. The expected-value raster, having the poor resolution of TM raster cells did not relate to FMMP. In general, PC-1 is high for urban areas, low for water areas, and medium for other landscape elements. While Calgis expected the deviation measure (standard deviation) to relate better to urban residential patterns, this was not the case. Calgis now believes that a more sophisticated measure of texture is needed (e.g., entropy). The standard deviation measure was high for randomly textured areas and for areas having strong edges (patterned texture). An effort is underway to identify other texture algorithms that might work for TOPSAR data.

#### 2.2.4.4.4 Proportional Indexing of Atmospherically-Corrected Landsat TM Rasters

In non-level terrain, the straight-forward use of TM data in a standard analysis approach (e.g., supervised maximum-likelihood estimation or unsupervised clustering followed by supervised labeling) runs into difficulties. All bands are brightened on sun-facing slopes and are darkened on slopes facing away from the sun. One approach to this problem is to use ratios of TM bands (after the effects of path radiance or haze have been removed by offsetting rasters by subtraction). Consider, for example, two TM rasters, A and B. If apath and bpath are the subtractive path-radiance offsets, then a simple ratio of these two bands would be:

$$\text{SRBA} = (B - \text{bpath}) / (A - \text{apath})$$

If  $(A - \text{apath})$  is close to zero, then SRBA becomes unstable high. Another "ratio" is called the Proportion Index of B and A, PIBA. The expression for this "ratio" is:

$$\text{PIBA} = (B - \text{bpath}) / (B - \text{bpath} + A - \text{apath})$$

If either  $(A - \text{apath})$  or  $(B - \text{bpath})$  are close to zero, PIBA is still well defined. In fact, the maximum value of PIBA is unity. Thus, to make an 8-bit unsigned integer raster from B and A, one simply needs to multiply the previous expression by 254. If both  $(A - \text{apath})$  and  $(B - \text{bpath})$  are zero, one can denote this undefined pixel condition by the null value, 255.

In the case of TM, PI43 (i.e., where  $B = \text{TM4}$  and  $A = \text{TM3}$ ) represents a measure of green vegetation amount (when large) and a measure of being non-vegetated (when low). PI31 represents a measure of vegetative yellowness; PI57 represents a measure of wetness. These PI measures are expected to work well on non-level terrain. They can be used to mask basic biophysical conditions as well (e.g., to separate green-vegetative areas from other with a threshold on PI43).

#### 2.2.4.4.5 Fusion of Landsat TM and SPOT Pan Rasters to TOPSAR at TOPSAR Resolution

In Year 1, the primary and successful method for merging TM and TOPSAR data was to use a method which has often been used with TM and SPOT Pan data. The methodology, widely used, is to start with three TM rasters assigned to red, green, and blue (RGB) primary colors in a display (e.g., R G B = TM5 TM4 TM3), an interesting combination which produces green vegetation as green. Another common use of RGB would be R G B = TM4 TM3 TM2, which causes green vegetation to look red (as in standard CIR photography). Any standard 3-color combination of TM bands has useful and recognizable colors, but poor (often insufficient) spatial resolution. This problem is addressed by using a high-resolution panchromatic band (e.g., 10m SPOT Pan) to modulate the intensity of colors. The procedure is to resample the TM rasters to 10m (nearest neighbor). Then, an RGB to Intensity Hue Saturation (IHS) transformation is made. After substitution of the high-resolution panchromatic raster cells (i.e., SPOT Pan) for the Intensity (I) raster, the data are transformed back to RGB for display. The result is a addition of spatial detail to the low-resolution TM data.

Calgis substituted the PC-1 raster (a 5m raster formed from MagF and CorrF) for the Intensity raster instead of using the SPOT Pan raster. While this fusion was useful, a better approach was to average the original TM intensity with the substituted (TOPSAR) intensity to preserve TM colors better for bright or dark TOPSAR objects.

## 2.2.5 Photogrammetric Data Processing

### 2.2.5.1 Aerial Photography

Calgis coordinated the acquisition of aerial photography for all experiment sites. The work included developing detailed flight plans, including specifications for photography acquisition, camera equipment to be used, scale of photography, location of flight lines, size and locations of ground control targets, photographic coverage requirements, flying conditions, and exposure and processing requirements. Calgis also provided assistance in configuring and installing a GPS system on board the aircraft for providing control, which allowed for a reduction in required ground control points. Calgis provided photogrammetric control via airborne and ground GPS data acquisition and processing for all flights.

Following is a summary of the aerial photography acquired at each site:

#### Antioch Hills:

##### (A) 1:6,000 Scale Photography

- Three strips containing 19 exposures were flown from an average altitude of 914m above mean terrain.

##### (B) 1:10,000 Scale Photography

- Five strips containing 36 exposures were flown from an average altitude of 1,524m above mean terrain.

##### (C) 1:20,000 Scale Photography

- Four strips containing 24 exposures were flown from an average altitude of 3,048m above mean terrain.

##### (D) 1:40,000 Scale Photography

- Four strips containing 38 exposures were flown from an average altitude of 6,096m above mean terrain.



Laurel Quad:

## (A) 1:40,000 Scale Photography

Two strips containing 10 exposures were flown from an average altitude of 6,096m above mean terrain.

## (B) 1:7,200 Scale Photography (SRI Swath)

One strip containing 9 exposures was flown from an average altitude of 1,280m above mean sea level. The photography was uncontrolled.

Iron Mountain:

## (A) 1:40,000 Scale Photography

Four strips containing 29 exposures were flown from an average altitude of 6,096m above mean terrain.

Gualala River:

## (A) 1:40,000 Scale Photography

Four strips containing 32 exposures were flown from an average altitude of 6,096m above mean sea level.

## 2.2.5.2 Aerial Triangulation

The scanned images of two overlapping aerial photographs can be used to create a stereo model on an ImageStation. Before any measurements can be made on this model, however, it must be brought to an exact scale and leveled. This requires at least three planimetric control points and five height control points for reliable orientation of the model in the object space. For large aerial photographic blocks, this need for the control for photogrammetric orientation of individual models is generally met through aerial triangulation which results in significant cost saving compared to conventional field surveying techniques. The aerial triangulation technique provides a means of extending the field surveyed control based entirely on photogrammetric data measurement and processing procedures as described below.

### 2.2.5.2.1 Image Selection and Mensuration

The strategy for the extension of control through aerial triangulation is based on the geometric linkage provided by the endlap between the successive photos in an aerial photographic strip and the linkage provided by the sidelap between adjacent photo strips. This requires a careful selection of pass points which fall in the triple-overlap area, and consequently, are common between adjacent models along the strip. Similarly, tie points which fall in the sidelap between adjacent strips must also be selected so as to locate at least one tie point in each model. The primary objective of the aerial triangulation is to establish the 3-dimensional coordinates of these selected pass points and the tie points. Besides meeting the overlap requirements, these points should be located on relatively level ground and where sufficient image detail is available for effective image correlation in overlapping images. With technical assistance provided by Calgis, this task was completed by DOC for all photo blocks of the Antioch Hills site.

The data acquisition procedure for aerial triangulation at the ImageStation consists of the measurement of the 2-dimensional image coordinates for all ground control, pass point and tie points in each photo image in which the points fall. The measurement involves the interior orientation of each photo and subsequently, the removal of y-parallaxes through stereoscopic measurement for each point of interest during the relative orientation procedure for each model. The procedure has been described in more detail in Section 3.1.3.1. The measurement of the image coordinates for all photo scales for the Antioch Hills area was completed by DOC, and the image coordinate data files were supplied to Calgis for processing.

#### 2.2.5.2.2 Bundle Adjustment

Calgis uses Interactive Simultaneous Bundle Block Adjustment (ISBBA) software for the aerial triangulation of photo blocks. ISBBA is proprietary software which has been commercially marketed by Calgis and is based on a rigorous mathematical model for the simultaneous least squares adjustment of the photogrammetric ray bundles for the entire block to the field surveyed control.

The input data for ISBBA consisted of the image coordinate data, the aerial camera calibration data and the ground control data. The image coordinate data used for processing were the image coordinates received from DOC which had already been transformed to the photo coordinate system but were not corrected for the systematic errors. Since it was agreed to output all DEM and other study data in California State Plan Coordinate system on NAD-83 datum, the ground control data used for bundle adjustment were transformed from the WGS-84 datum (latitude, longitude) to the NAD-83 datum (northing, easting). Since the primary photogrammetric data requirement was the production of DEM data for comparison with the corresponding radar DEM data, and in view of the fact that the existing USGS topographic quad sheets still display the contours representing orthometric heights based on the NGVD29, it was agreed to compute the photogrammetric elevations as orthometric heights on NGVD29. Consequently, the adjusted ellipsoidal heights for the control points resulting from GPS field surveys had to be transformed to orthometric heights.

The transformation of the ellipsoidal heights to the orthometric heights using any of the current geoidal models still carries uncertainties of up to 10 cm, and therefore, exceeded the control precision needed for this project. Consequently, this transformation was based on the known ellipsoidal and the orthometric heights at four of the existing control points which had been tied in the primary GPS network. Using the known geoidal height data at the four stations, a least squares fitting of a geoidal surface was made with the adjustment residuals less than 2 cm. This provided the locally applicable geoidal height model for the test site and was used to calculate the estimated geoidal heights from which the orthometric heights were reduced. The resulting orthometric height uncertainty between points located within proximity (the same stereo model) would be much less than 2 cm and is insignificant for the DEM heights derived from the 1:10,000 or 1:20,000 scale models used in the DEM analysis, discussed in section 3.1.3.2.

The procedure used for the block adjustment included the correction of the measured photo coordinates for the systematic errors due to lens distortion, earth curvature, and the atmospheric refraction. This was followed by the relative orientation and linking of the successive models in the strip resulting in the reduction of strip coordinates. Each strip, thus formed, is then scaled and leveled using the field control and/or the tie points from those adjacent strips which have already been scaled and leveled. This preliminary adjustment of the strips to the control is essential to detect errors made in control data or during the image coordinate mensuration. Some operator editing of the image coordinate data on the ImageStation was necessary where a pass or a tie point was located in a grassy meadow and was devoid of distinctive image detail, and had resulted in poor auto-correlation of the image.

The above procedure resulted in providing the initial estimate for the exterior orientation of all the photos and the spatial coordinates of all the pass and tie points for the block as input to the simultaneous bundle adjustment. Since the aerial camera had recently been calibrated, the self-calibration feature of ISBBA was not used for the processing of the different blocks. The summary of results of the aerial triangulation for the different scale blocks for the Antioch Hills site are shown in Table 2.2-1 below. The results were well within the industry standards, establishing the consistency of all geodetic and photogrammetric data.

Table 2.2-1: Results of Bundle Adjustment of Blocks

Photo Scale	Standard Error (meter)			
	Permissible in X,Y,Z	Actual		
		X	Y	Z
1:6,000	0.09	0.04	0.04	0.07
1:10,000	0.15	0.04	0.05	0.10
1:20,000	0.30	0.10	0.10	0.20
1:40,000	0.60	0.25	0.29	0.55

### 2.2.5.3 Digital Orthophoto Production from SAR DEM

An orthophoto generated from aerial photographic images is a widely used product for geographic information system and other planning applications. The orthophotos may be generated by an analogue or digital approach. The digital method was used in this project.

The digital rectification required for an image to generate an orthoimage may be accomplished in two ways. Using what is known as the anchor points method, a set of ground control points are collected at locations where the points are coincident on both the image and corresponding mapped positions. The image coordinates are modeled as functions of the map coordinates using the least squares method to fit some low order polynomials to the data. For each pixel on the orthoimage, the grey value is determined by locating the corresponding image position on the raw image followed by resampling. This method may be performed globally or locally.

The alternate approach known as the pixel by pixel method was adopted for this project. This is a more rigorous method and fits very well with the DEM generated from the IFSAR imagery which utilizes the DEM in the orthoimage generation. The correspondence between an image pixel and the conjugate ground element or a rectified photograph is related by the collinearity equations, which are defined as:

$$\begin{aligned}
 X &= f \frac{m_{11}(x-x_0) + m_{12}(y-y_0) + m_{13}(z-z_0)}{m_{31}(x-x_0) + m_{32}(y-y_0) + m_{33}(z-z_0)} \\
 Y &= f \frac{m_{21}(x-x_0) + m_{22}(y-y_0) + m_{23}(z-z_0)}{m_{31}(x-x_0) + m_{32}(y-y_0) + m_{33}(z-z_0)}
 \end{aligned}
 \tag{2.2.8}$$

where:

$X, Y$ :	image coordinates
$f$ :	camera focal length
$m_{11}, m_{12}, \dots, m_{33}$ :	elements of orientation matrix
$x_0, y_0, z_0$ :	perspective center coordinates
$x, y, z$ :	object space coordinates

Even the pixel by pixel method may be applied in two different ways. In the "top-down" approach, one starts from the image space and projects each pixel onto the object surface. This method is also called the direct or the Ray-Tracing method.

Using the alternate "down-top" method, also called the indirect method, one starts from the object space, and each ground element is projected onto the image space. The grey value of a ground element on the orthoimage is resampled using the projected location and its neighboring pixel values on the raw image as shown in Figure 2.2-5.

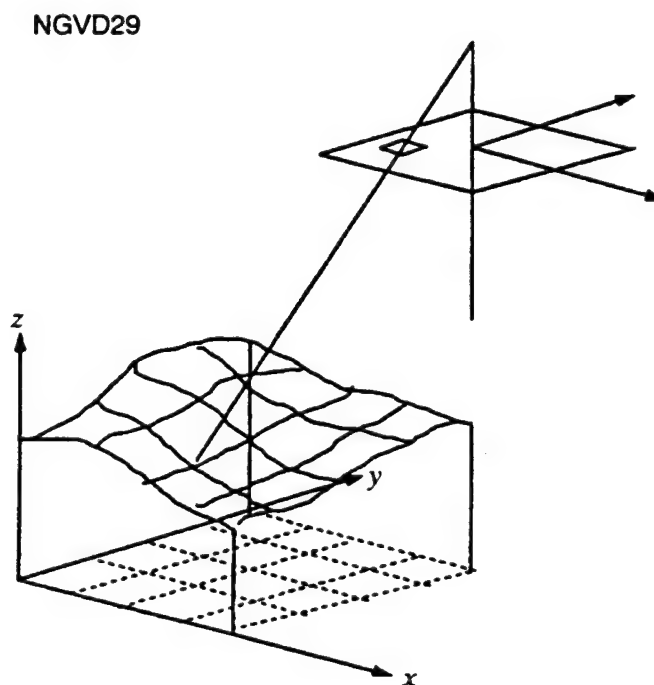


Figure 2.2-5: DEM projection model

With known photo orientation parameters, and the DEM, the major task of orthographic transformation is to determine the corresponding image point for each ground point. This can be achieved easily by applying the collinearity equations. The grey value of the ground element is achieved by resampling on the image plane.

The major disadvantage of this method is in handling those points on the ground which might be hidden on the photo, and, will produce wrong grey values.

The indirect method was chosen to develop orthoimages from IFSAR DEM because this method is more rigorous, and a better quality image is produced with less computational effort.

### 3.1 NON-VEGETATED HILLSLOPE DEM AND SLOPE HAZARDS EXPERIMENT

#### 3.1.1 ABSTRACT

DOC evaluated the utility of DEMs acquired by JPL's TOPSAR instrument for analysis of earthquake-induced slope hazards in open, sparsely vegetated terrain in the hills near Antioch, California. Radar-derived DEMs were compared with photogrammetrically-derived DEMs for production efficiency, accuracy, resolution, and completeness of coverage. Ground resolution of TOPSAR radar DEMs is 5 m with a root-mean-square height error of about 4.5 m, estimated after removing outliers using 3-sigma criteria. JPL has demonstrated that greater accuracy in terrain height estimates can be obtained with improved system calibration. Accuracy and resolution of TOPSAR DEMs are superior to USGS Level 1 DEMs, and can be immediately used to improve the assessment of seismic hazards.

#### 3.1.2 INTRODUCTION

##### 3.1.2.1 Purpose

The purpose of this experiment is to determine the effectiveness of using radar technology in mapping landslide hazards in open, sparsely vegetated terrain. Such conditions are generally considered "ideal" for mapping the locations of existing landslides using aerial photography or other remote sensing tools, and are conditions under which accurate digital terrain models of the ground surface can be generated. A subsequent experiment at the Laurel Quad Site will investigate the effectiveness of radar for landslide hazard mapping under the more difficult conditions of rugged, heavily vegetated terrain (see Section 3.3).

Under provisions of the Seismic Hazard Mapping Act of 1990 (Public Resources Code) DOC is mandated to designate seismic hazard zones that bound areas susceptible to slope failure during earthquakes. These zones are used by local government to indicate where special seismic investigations are required prior to issuance of a building permit. The zones are based on a comprehensive evaluation of hazard that considers the level of expected shaking from future earthquakes, the geologic material and its strength or resistance to seismic shaking, and other factors such as steepness of slope and slope form. Program goals are to designate zones for millions of hectares of land over the next few years, a formidable task under the best of circumstances. To achieve such a goal will require the application of remote sensing and GIS.

Utility of radar imagery in the assessment of earthquake hazards, particularly preferential shadow enhancement of topographic structures and all-weather capability, was recognized nearly 20 years ago (Glass and Slemmons, 1978). Various investigators have since demonstrated the utility of GIS and remote sensing in slope hazard analysis (Mora and Vahrson, 1994; Navarro and Wohl, 1994; Gao, 1993; Carrara et al., 1991; Rengers et al., 1992). Many of these studies have employed multivariate terrain classifiers to map slope hazards, while other approaches have been more direct in application of slope stability analysis employing either static (Keaton, 1990) or dynamic (Newmark, 1965; Wilson and Kieffer, 1983; and Wiezorek et al., 1985) models. Nearly all these approaches require quantitative estimates of slope parameters (aspect, gradient, curvature, etc.), which are derived from DEMs and can strongly influence the hazard estimate of a hillslope.

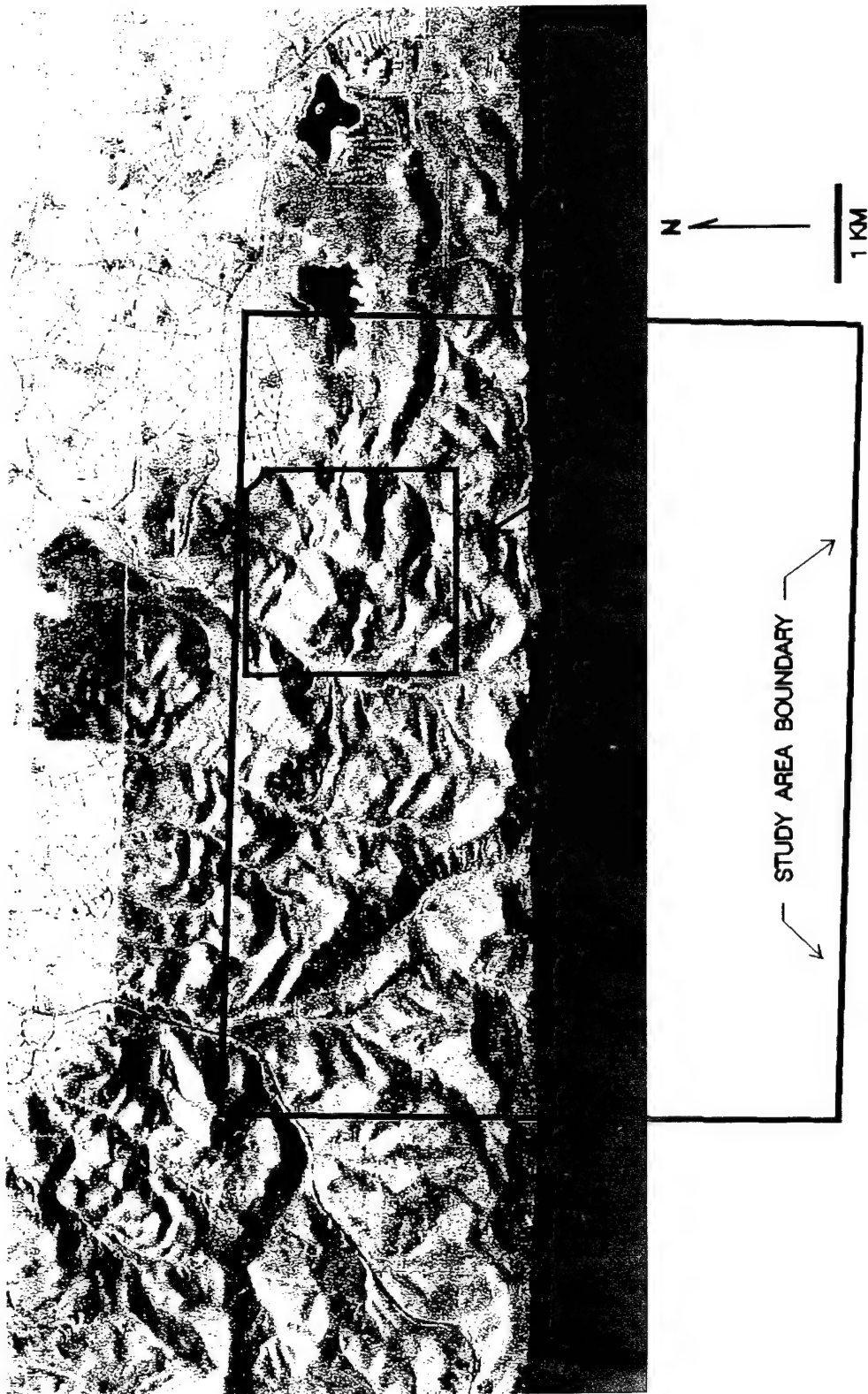


**Figure 3.1-1:** Location of the main study area and the digital elevation model (DEM) test area for the Antioch Hills seismic hazard experiment in relation to the ANT270 radar image. Note the southern edge of the radar swath does not cover the whole study area.





**Figure 3.1-2:** Oblique view of a portion of the study area that shows the character of the terrain. Note the presence of landslides in the figure.



Errors in DEMs have recently been studied by a number of investigators (Brown and Bara, 1994; Adkins and Merry, 1994; Issacson and Rippel, 1990), and in particular, the effects of such errors on the accuracy of spatial derivatives such as slope, aspect and curvature (Bolstad and Stowe, 1994; Chang and Tsai, 1994). Level 1 USGS DEMs have a reported target root-mean-square error (RMSE) of 7 m and a maximum tolerable error of 15m based on 20 randomly selected checkpoints (USGS, 1993). Li (1991), however, has pointed out the presence of systematic errors which make accuracy estimation problematic. These systematic errors are anisotropic and can be an artifact of the photogrammetric methods or interpolation techniques used in profiling USGS contour maps. Together, random and systematic errors in USGS DEMs limit the accuracy of derivative quantities.

In addition to errors resulting from uncertainty in elevation, are errors in slope estimates introduced by limited DEM resolution. Chang and Tsai (1991) demonstrated that estimates of slope gradient decrease with decreasing resolution, with differences as great as 7 degrees for a 2-fold decrease in resolution. This resulted in up to a 10% change of total area classified by slope category going from 20m to 40m spacing between posted elevations. Considering both accuracy and resolution, USGS DEMs are inadequate for large-scale mapping of slope hazards.

Sufficiently accurate DEMs can be generated by photogrammetric means, but they require lower altitude aerial surveys which cover less area, increasing production costs significantly. Even the best photogrammetrically derived DEMs have limited accuracy in forested regions where optical imaging captures canopy relief. So, a major issue facing large-scale mapping of seismic hazards is data deficiency. Available USGS DEMs lack the accuracy and resolution necessary to meet program requirements, and photogrammetrically derived DEMs, while accurate, are costly, time-consuming to produce, and likewise lack accuracy in forested terrain.

Radar-derived DEMs may provide a solution, however the accuracy and cost effectiveness must be demonstrated. This is the principal purpose of the seismic hazards element of the GeoSAR Project.

### 3.1.2.2 Objectives

The primary goal of this experiment is to demonstrate the efficiency and accuracy of radar-derived DEMs for use in mapping landslide hazards in open terrain. Radar products, including the DEMs, imagery, as well as other ancillary data, are analyzed and evaluated to determine their utility as a routine tool in the State's seismic hazard mapping program. Three aspects on the use of radar for mapping landslide hazards are addressed:

- (1) Slope Hazard Assessment and Detection - The different DEMs and imagery are combined, tested, and evaluated as to the degree of utility with which these related source products can be used to a) characterize, identify, and map terrain geometry associated with the occurrence of hillslope failures, and b) to recognize particular terrain morphology for purposes of computer-assisted identification of hillslope failures;
- (2) Economic and Efficiency of DEM Construction - DEMs are constructed using the present state-of-the-practice in photogrammetry and radar technologies. Time, cost of effort, and products are compared to determine what efficiencies or drawbacks, savings or added costs, and what accuracy or precision differences may exist between the two approaches; and,
- (3) Utility of Radar-DEMs for Orthophoto Map Construction - A radar DEM is combined with optical imagery to produce an orthophotograph. This objective includes comparing, and evaluating the quality of optical-based orthophotographic maps from both radar and photogrammetric source DEMs.

### 3.1.2.3 Site Description

The Antioch Hills study area is centered about 65km east-northeast of San Francisco in the Northern Diablo Range, north-central Contra Costa County, California. It is a rectangular area of about 39 square kilometers, and lies south of the cities of Pittsburg and Antioch, northeast of Mount Diablo and east of the city of Clayton (Figure 1.4-2). The main study area, hereafter referred to as the "study area," occupies a portion of two USGS 7.5-minute topographic quadrangles: the northwest quarter of the Antioch South and the northeast quarter of the Clayton quadrangles. Within the northern portion of the study area, there is a "test area" delineated by the subarea boundary shown in Figure 3.1-1. It is within the test area where the detailed comparison presented in this report is made between photogrammetric- and radar-derived DEMs. The study area covers a much larger area, and provides a broad variety of readily exposed terrain and landslide features for which automatic detection methods can be tested in the future (Figure 3.1-2).

The study area contains almost all the Black Diamond Mines Regional Preserve and part of the Contra Loma Regional Park, both operated by the East Bay Regional Park District. These parks make up nearly half of the study area. The balance of the lands is privately owned and used primarily for cattle grazing.

Geology of the Antioch Hills study area is described in Dibblee (1980a and b), Crane (1994a and b), and Graymer, Jones, and Brabb (1994). Soil information was derived from Welch (1977). The study area is underlain by clastic sedimentary rocks with interbedded tuffs, colluvium, older and younger alluvium, and landslide debris. The sedimentary rocks consist of 28 named formations of Cretaceous to Pliocene age. These formations consist of 1) coarse-grained rocks, mostly sandstone with some conglomerate, 2) fine-grained rocks, mostly shale with less siltstone and claystone, and 3) units which contain interbedded coarse- and fine-grained rocks. When these formations are grouped together by texture, they generally form an alternating sequence of coarse-grained and fine-grained rocks. The tuffs form two thin beds in the northern portion of the study area. The rocks in the area have been tilted into a north-northeast facing monocline and generally strike east-west or northwest-southeast and dip to the north or northeast. Dips generally range from about 20 to 50 degrees.

Most of the hillslopes, with the exception of the very steep escarpments, are covered by a thin but varying thickness of surficial deposits. The coarse-grained formations are generally overlain by sandy and loamy, slightly expansive residual and colluvial soils while the fine-grained rocks are overlain by clayey, highly expansive residual and colluvial soils. Landslide scars and deposits mantle many of the slopes, and are discussed in more detail in section 3.1.3.1.

North of an east-west line through the Nortonville and Somersville town sites, about the northern half of the study area, the sedimentary rocks have been eroded into a topography consisting of long, sub parallel, generally north-south trending ridges and valleys that are perpendicular to the strike of the formations with shorter generally east-west trending spur ridges that are generally parallel to the strike of the formations and diverge obliquely from the longer, main ridges. Generally, the sandstone units underlie the spur ridges and knobs while the shale units underlie the saddles and drainages on the perpendicular-to-strike ridges. These topographic features occur along strike laterally across the long ridges and from one ridge to the next. Locally, there are steep to very steep, sandstone escarpments. These conditions have resulted in a topography with about equal areas of, but a complex arrangement of dip-slopes, anti-dip slopes, and perpendicular-to-dip slopes. Vegetation in this area is almost entirely grassland with widely scattered oaks and is generally unfaulted. The DEM test area is here.

In the southern half of the study area, the topography changes to a series of long, sub-parallel, generally east-west trending ridges and valleys that are parallel to the strike of the formations with shorter generally north-south trending spur ridges that are generally perpendicular to strike and diverge obliquely from the longer, main ridges. Generally, the sandstone units underlie the upper portions and crests of the parallel-to-strike ridges. Vegetation on the sandstone ridges consists of grassland with isolated dense stands of oak, laurel and buckeye or dense coyote brush and chemise. These ridges are asymmetrical, with moderately steep to steep, north-facing dip-slopes underlain by sandstone, and south-facing, steep to very steep, anti-dip slopes or near vertical, anti-dip escarpments where the sandstone units overlie shale units. The shale units generally underlie the valley floors, the lower portions of the valley flanking slopes where they form moderately steep to steep, dip and anti-dip slopes, and below the sandstone escarpments where they form steep, anti-dip slopes. Vegetation in the shale valleys is grassland with scattered oaks. This area is crossed by a number of generally east-west and north-south trending strike-slip faults.

### 3.1.3 USER EXPERIMENT

#### 3.1.3.1 Methodology

In order to investigate the potential uses of an advanced IFSAR mapping system like JPL's TOPSAR, a key element in the experiments completed during Year 1 of GeoSAR was to establish the geometric accuracy of the radar-generated DEM data. The only "true" situation in the context of mapping is the terrain surface itself, and since the condition of "absolute accuracy" cannot be attained by measurement, the accuracy of DEM data can only be assessed by comparisons with measurements made to a known and much higher order of accuracy. Thus, when defining accuracy, in most cases this is strictly the relative rather than the absolute accuracy.

The evaluation of radar products for slope hazard mapping is based on a comparison of two approaches of data collection for DEMs: 1) soft copy photogrammetry (SCP), and 2) IFSAR. SCP supplemented with air-photo interpretation and field mapping is used to acquire ground truth, and is considered the baseline against which IFSAR products are evaluated.

Four scales of aerial photography were acquired: 1:40,000, 1:20,000, 1:10,000, and 1:6,000 (see Section 2.2.5.1). The smallest scale photography (1:40,000) is equivalent to that obtained from the National Aerial Photography Program (NAPP) of the USGS, for which the accuracy and efficiency in determining horizontal location and elevation has been evaluated (Light, 1993), and for which coverage for California is widely available. The largest scale photography (1:6,000) is used to characterize the detailed geomorphology of landslides for the purpose of quantifying criteria for automated detection. The remaining two intermediate scale air photo sets are the principal products for comparison with radar. The 1:20,000-scale photography is believed to be roughly equivalent to the attainable accuracy from IFSAR, while the 1:10,000-scale photography is considered ground truth for this study.

Flying height for the 1:10,000-scale photography was approximately 1,800 m. The precision of photogrammetrically derived spot heights from this coverage is about 0.2 m (about 1/10,000 of the flying height, Wolf, 1983). While Fryer et al. (1994) indicate that undetectable systematic errors could cause variations up to a factor of five in height precision from one area of a photo to another, the procedures we employed in the DEM collection process attempt to minimize this possibility. DOC used DEMs derived from the independently flown and processed 1:10,000- and 1:20,000-scale photos to demonstrate the accuracy of the photogrammetric terrain models. This is discussed in more detail in a subsequent section. For DOC's purposes the results from large-scale SCP (1:10,000 or larger) are taken as "ground truth" in this study, and will be referred to as "ground-truth DEMs."

### 3.1.3.1.1 Landslide Inventory

DOC prepared a landslide inventory to provide "ground truth" for the study area using conventional air-photo interpretation and field mapping. This is a highly effective method of conducting detailed landslide mapping in grasslands or areas which lack extensive tree cover, and is probably the most common approach employed by geologists. Because the study area is primarily grassland, it was anticipated this method would identify most, if not all, of the landslides in the study area. The purpose of this inventory is to prepare a reliable baseline study of the landslide distribution from which a radar-derived inventory can eventually be compared and evaluated.

#### 3.1.3.1.1.1 Landslide Inventory Methodology

The inventory was conducted by interpretation of stereo-paired aerial photographs of the site using a mirror stereoscope. Two sets of aerial photographs were used. The interpretation was mostly conducted on approximately 1:24,000-scale, black and white photographs taken in 1994. A second set of black and white photographs taken in 1950 with an approximate scale of 1:19,600 were used in areas where the interpretation from the 1994 photographs was unclear or ambiguous. While it is important to interpret landslides from aerial photographs of different vintages to observe changes in development, vegetation cover, and size and distribution of landslides, few differences for any of these parameters were noted between the two sets of photographs. Using these photographs, and the magnification provided by the mirror stereoscope, landslides as small as 10m in length or width were identified.

Landslides were mapped by identifying the characteristic geomorphology and tonal features produced by slope failures on the aerial photographs. During the aerial photograph interpretation, an interpretation was also made of the topography of the corresponding area on the USGS 7.5-minute topographic quadrangle map to identify the characteristic geomorphology produced by slope failures. Using this method, the identification of the landslides was based on the simultaneous interpretation of the geomorphology by both the visible features on the photographs and the topography from the maps.

Each identified landslide was classified by type, recency of movement and confidence of interpretation using the system described in Wieczorek (1984). The landslide outline was then transferred by hand to the USGS 7.5-minute topographic quadrangle using measurements taken from the photographs and fitting the landslide to the topography. The majority of mapped debris flows was taken from Ellen and Wieczorek (1988) and generally represents those failures that occurred in the study area during the storms of January 3-5, 1982. Approximately 80 hours were required for one geologist to complete the aerial photographic interpretation of the study area.

Field mapping was conducted (1) to confirm the interpretation from the aerial photographs, (2) identify landslides which may have occurred since the photographs were taken, (3) check for landslides in the local dense stands of trees and brush which may have not been identified on the photographs, and, (4) evaluate the geologic, hydrologic and soil conditions associated with the landslides.

#### 3.1.3.1.1.2 Results of Landslide Inventory

The results of the landslide inventory, and comparison with the geologic map, indicate that landslides range from generally uncommon to very common throughout the study area and that their distribution, size, and type are controlled by the bedrock geology (Figure 3.1-3). As with the topography, the landslide distribution, size, and type, differ in the northern portion of the study area from that in the southern portion.

In the northern portion of the study area, landslides are common to very common. Landslides range from small (fewer than 4 hectares) to large (many tens of hectares) and this area has the highest concentration of large landslides in the study area. Small to large single and coalescing earthflows

were mapped throughout much of this area. They occur in the greatest volume and most frequently in the shale units and occupy many of the strike-parallel drainages or valleys underlain by shale. Examples of these landslides are northeast of Kirker Creek, northwest of Kirker Pass Road, west of Nortonville, and at Nortonville and Somersville. A few moderate-sized to large slumps were mapped in areas underlain primarily by shale, such as on the western flank of the ridge west of Sidney Flat and immediately to the northeast of Sidney Flat. Several of the larger landslides have retrograded or expanded into areas underlain by sandstone units, such as the large earthflows in the area north of Nortonville, and east-southeast of Sidney Flat.

Several large slumps and slump-earthflows were mapped in the areas underlain by sandstone west of Kirker Creek, on the eastern flank of Markley Canyon north of Somersville, and on the eastern flank of the ridge east of Markley Canyon.

Local areas of shallow debris-slide and rockfall/slide slopes were mapped on the south-facing sandstone escarpment north of Nortonville, and north and east of Somersville. At the base of these slopes, there are coalescing landslide debris fans adjacent to earthflows.

In the southern portion of the study area, landslide occurrences range from uncommon to very common and there is a stronger correlation between geology and landslide distribution than in the northern portion. The southern portion also lacks the high concentration of large landslides that occur in the northern portion.

Small to moderately sized earthflows are very common throughout most of the strike-parallel valleys underlain by shale, and often extend up the valley flanks to the overlying sandstone units on the dip-slopes of ridges or escarpments on the anti-dip side. Where present, the overlying, near vertical sandstone escarpments form rockfall/slide, debris-slide slopes which shed debris onto the earthflows formed on the valley flanks underlain by shale. Examples of these slope failures are in the valley below Stewartville and the overlying southern flank of the ridge above, and the large, coalescing earthflow north of Irish Canyon. This earthflow is by far the largest landslide in the southern portion of the study area.

Landslides are uncommon or rare on large areas of the southern portion of the study area on the north-facing, sandstone dip-slopes. Examples of this are the ridges south of Nortonville and Somersville, the next ridge to the south, and the ridge south and east of Sand Creek. Slope failures in these areas are generally single very small debris slides, debris flows and larger areas of rockfall/slide-debris slide-slopes on the south-facing escarpments.

#### 3.1.3.1.2 Soft Copy Photogrammetry

Photogrammetric DEMs used as ground truth for the GeoSAR project were produced by DOC with the help of Calgis using an Intergraph ImageStation Photogrammetric workstation and an Intergraph/Zeiss Photoscan 1 high-resolution flatbed scanner. Intergraph ImageStation software applications used to digitally convert and process aerial photographs include: 1) Photoscan for analog to digital conversion, 2) Digital Orientation (ISDO) for image restitution, and 3) DTM (digital terrain model) Collection (ISDC) for both manual feature collection and automatic Match T collection of elevation points. MicroStation Feature Collection (MSFC) and Terrain Modeler (MSM) were used for final editing and DEM production. See Figure 3.1-4 for a generalized workflow.

Diapositives (228 X 228 mm) for all four flight scales of photography were scanned at 15-micron resolution. The resulting digital raster image files were compressed using JPEG format with a Q factor of 25. Transmissivity values were adjusted for each image, as needed, to optimize image contrast for subsequent Match T pixel correlation. Using ISPN, a full set of averaged binary overviews was created for each image to speed up image display times and decrease memory requirements.





**Figure 3.1-3:** Landslide inventory map produced for the study area. The topographic base includes portions of the USGS 7.5-minute Clayton (1980) and Antioch South (1980) quadrangles

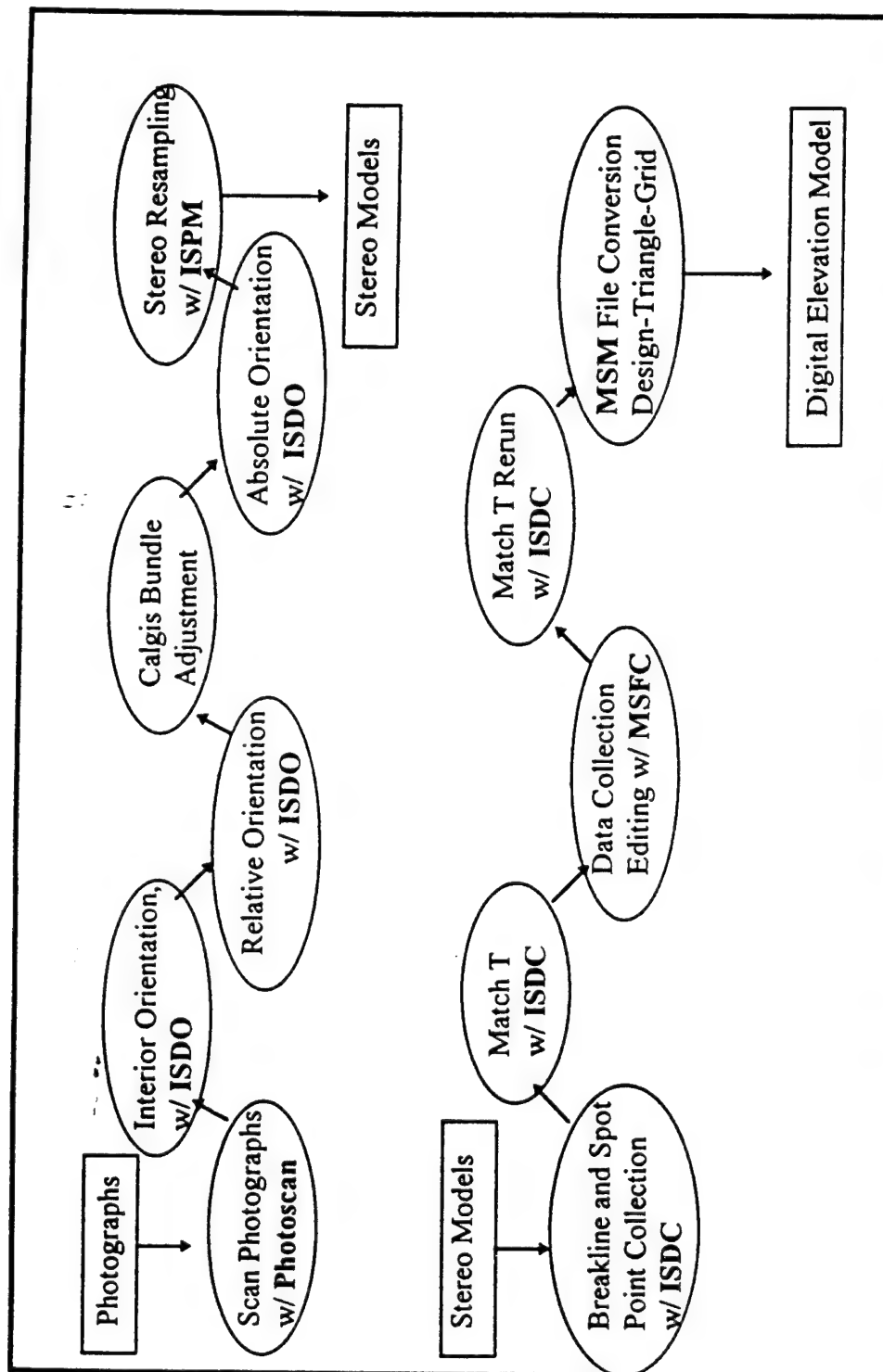


**Figure 3.1-4:** Generalized workflow for producing photogrammetric DEMs using the Intergraph soft copy photogrammetry system (after Intergraph, 1994).



**Year 1**  
**Research and Development Status Report**  
**for**  
**GeoSAR**  
**A Radar Based Terrain Mapping Project**

*Contributors*

CALIFORNIA  
DEPARTMENT OF CONSERVATION

Integrated GeoData Management Unit  
Robert Yoha

Seismic Hazards Evaluation and Zonation Project  
Charles Real  
Rick Wilson  
Tim McCrink  
Emily Oatney  
Wayne Hayden  
Chris Wills

Farmland Mapping and Monitoring Program  
Molly Penberth

Timber Harvest Review Project  
Tom Spittler  
Mary Ann McKittrick

Office of Mine Reclamation  
Kit Custis

JET PROPULSION LABORATORY

Dr. Scott Hensley  
Dr. Jeff Klein  
Dr. Frank Webb  
Dr. Theiry Michel  
Dr. Ernesto Rodriguez  
Dr. Bijan Houshmand  
Dr. Thomas Thompson

CALGIS

Gerald Dildine  
Dr. Mushtaq Hussain  
Dr. Riad Munjy  
Dr. Jack Paris  
Jeffrey Seib  
Chris Bohain

#### 3.1.3.1.2.1 Stereo Models

Interior Orientation (ISDO) converts the fiducial based-system into a 2-dimensional raster coordinate system. Using calibrated photo coordinate data for the fiducial points (USGS, 1991), the transformation relationship between the row and column system used for the scanned image and its corresponding photo coordinate system was established. The image principal point origin, calculated from the eight photo fiducial points, serves as a reference for subsequent mathematical solutions. An affine model transformation was employed in this process to correct for nonuniform deformation along the orthogonal coordinate axes, including any emulsion deformation that occurs during the photographic process.

Relative Orientation (ISDO) spatially ties the relative position and attitude of two overlapping images along a given flight line together and clears the y-parallax. This effectively brings overlapping images into the same viewing plane as a stereo model. The process entails selecting nine pass points per image, including three points down the center of each individual image where the neighboring images on both sides also overlap by 10 to 20%. Pass points were selected in areas having gentle slopes and high intensity contrast for best possible pixel correlation between images. Automatic correlation capabilities of Relative Orientation quickly match pixels using a least squares refinement. In the case of low image contrast, this technique sometimes fails, and manual parallax clearing is required. During this orientation process, corrections for systematic errors due to earth curvature and atmospheric refraction were also applied to the measured image coordinates for 1:20,000- and 1:40,000-scale photography.

Absolute Orientation (ISDO) incorporates aerial triangulated California NAD-83 State Plane pass point coordinates, as calculated by Calgis through a bundle adjustment (see Section 2.2.5.2.2), to essentially tie the stereo models to the ground. Two adjusted stereo models from the 1:10,000-scale photography and one from the 1:20,000-scale photography were chosen for Absolute Orientation and further model processing because they represent an area covered by the radar swath and the landslide survey.

Epipolar stereo resampling is an individual pixel warping process used to improve stereo viewing and feature collection for DEM generation. Additionally, it arranges all conjugate pixels to lie in corresponding epipolar planes. This resampling process was applied to the three previously mentioned stereo models using a cubic convolution interpolation, which provides better image enhancement than bilinear or nearest neighbor interpolations.

#### 3.1.3.1.2.2 Data Collection and DEM Building Process

Feature data, including digital breakline and spot point data, were collected using MSFC for the two 1:10,000-scale stereo models. This information delineates nearly all unique geomorphic features in the study area, such as ridges, drainages, and landslides. To improve speed and accuracy, all 1:10,000-scale feature data were transferred to the 1:20,000-scale model. Elevation points were automatically generated using Match T (ISDO) over a uniform grid having 5 and 10m spacing for the 1:10,000- and 1:20,000-scale stereo models, respectively. The 10m sample interval is consistent with the lower resolution of the 1:20,000-scale model. Match T is a process which matches identical features and filters the resulting data points to create a precise DEM (see Intergraph, 1994, for mathematical model).

DEMs were created from the Match T results using MSM. Line and point features were converted into triangles using Delauney triangulation. A bilinear interpolation method was used over nearest neighbor or bicubic interpolations to convert the triangles to a grid file having 5m postings because it is less computer intensive and yields nearly indistinguishable results. The global origins of the photogrammetric DEMs were registered to that of the radar DEM, prior to final grid conversion, so that

the grid nodes were co-registered planimetrically. This procedure eliminated the need for introducing further interpolation when comparing the radar and photogrammetric DEMs. The two 1:10,000-scale photogrammetric DEMs were merged along their overlapping boundary using a simple grid averaging technique.

Initial difference grids between the two photogrammetric models revealed areas where pixel correlation was inhibited, particularly at the model edges and in areas with low contrast. Apparent floating or buried points in such areas were replaced with additional breaklines and spot points. A Match T repeat was conducted on the edited feature file and final DEMs were created from the edited Match T files.

### 3.1.3.2 Analysis

#### 3.1.3.2.1 Background Data

The ground-truth DEM, derived from the 1:10,000-scale aerial photos, and the 1:20,000-scale photogrammetric DEM are used to analyze the relative accuracy and potential application of the radar DEM to seismic hazard mapping. The analysis procedure is based on comparing, visually and statistically, height differences between radar and ground-truth DEMs. DOC did most of the grid-file manipulation in this section, and both DOC and Calgis performed the statistical analysis on the data. The following data were used in the analysis:

- 1:10,000-scale photogrammetric DEM (Figure 3.1-5)
- 1:20,000-scale photogrammetric DEM
- ANT270 radar DEM (Figure 3.1-6)
- ANT90 radar DEM (Figure 3.1-7)
- 1:10,000-scale and 1:20,000-scale (Figure 3.1-8) photographic images
- ANT270 radar image (Figure 3.1-9)

A slope gradient map and a slope aspect map were made from the ground-truth DEM using Intergraph's MSM software (Figures 3.1-10 and 3.1-11). Slope gradient and aspect are determined from the orientation of surface normal vectors computed for each grid location. Four quadrilateral grid nodes are used in the computation. Both maps are grid files having the same origin and planimetric spacing as the ground-truth DEM.

The ANT270 radar data were flown with a southward look direction and the ANT90 radar data were flown with a northward look direction. The DEM test area lies in the far range of the ANT270 radar data (depression angle = 26°) and the near range of the ANT90 radar data (depression angle = 56°). Because the actual flight lines were displaced to the north of the planned flight lines, several key ground control points to the south were missed and could not be used for system calibration (see Section 2.1.2). This problem is avoidable and correctable by adding supplemental ground control. Additional ground control was not available in time for first year's analysis, consequently DOC and Calgis analyses are limited to analyzing the partially calibrated TOPSAR images and DEMs as stand-alone products in a cartographic projection. In Section 3.1.3.4, JPL demonstrates that after removal of systematic biases, height errors are consistent with the expected performance of the TOPSAR instrument.

The procedure for comparing radar and photogrammetric DEMs is based largely on the examination of height differences in two ways: 1) mapping them to permit visual inspection for possible spatial trends, and 2) statistical analysis. Using the differences in height (residuals) of the measured grid and the reference grid, several statistical parameters were calculated which included the Algebraic Mean (AM) which takes into account the sign of the residuals, and therefore, tends to zero if there are similar

magnitudes of positive and negative values; the Absolute Mean (ME) the mean error of all residuals ignoring their sign and thereby reflecting the range or the distribution of the residuals, so that 50% of the residuals values lie in the range  $-ME$  to  $+ME$ ; Root-Mean-Square Error (RMSE) which obviates the problem of having positive and negative residual values, and assuming that the algebraic mean is zero, and that there is a normal distribution, then 68.3% (approximately two-thirds) of the residual values will fall in the range  $-RMSE$  to  $+RMSE$ ; Standard Deviation (S or sigma) or deviation from the mean which is a commonly used statistical parameter which, for normal distribution, reflects that the residuals are symmetrical about AM and 68.3% of the residual values lie between  $-S$  to  $+S$ , and 99.7% of the values fall between  $-3S$  to  $+3S$ . This value of  $+3S$  is often accepted as the "maximum value" and often used as the criterion for rejection of those residual values which deviate more than  $3S$  from the mean value. If the data are free of any systematic biases (i.e., AM is equal to zero), then  $RMS = S$ .

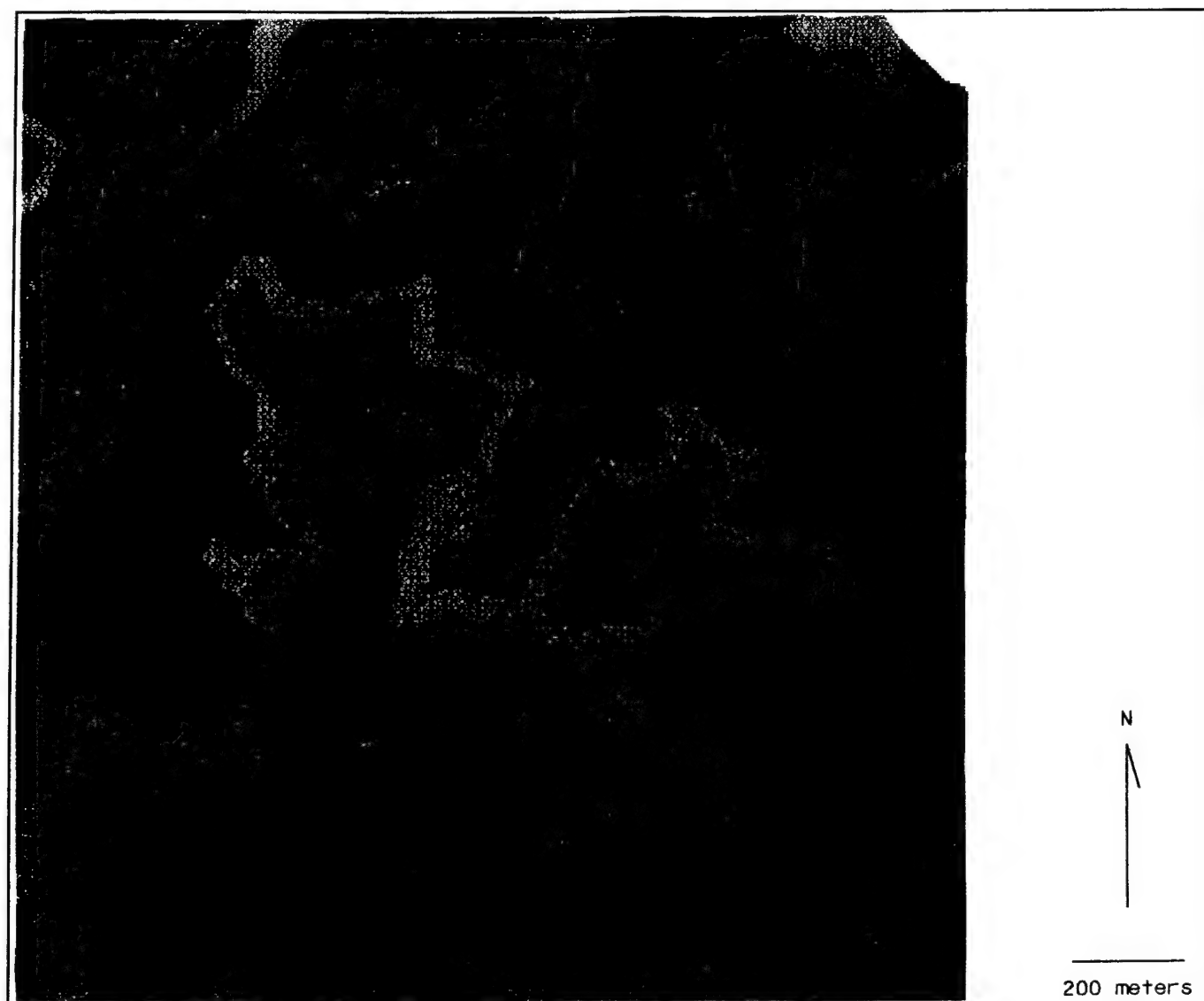


**Figure 3.1-5:** Isopleth of the 1:10,000-scale photogrammetric DEM, also referred to as the ground-truth DEM, of the test area.

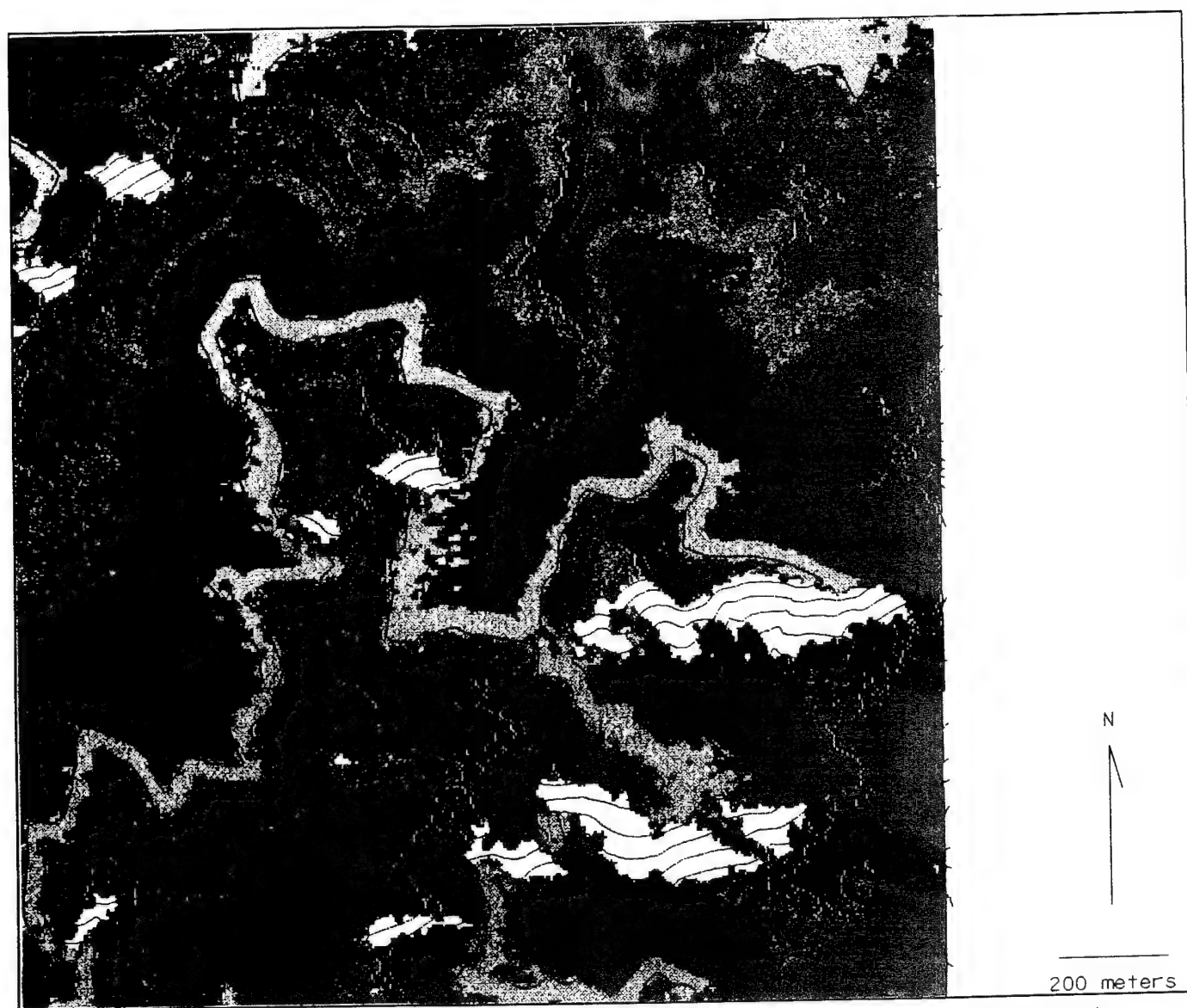


**Figure 3.1-6:** Isopleth of the ANT270 radar DEM of the test area. Note the roughness of the contours caused by noise in the elevation data, and the void areas where data 'drop-outs' occur.

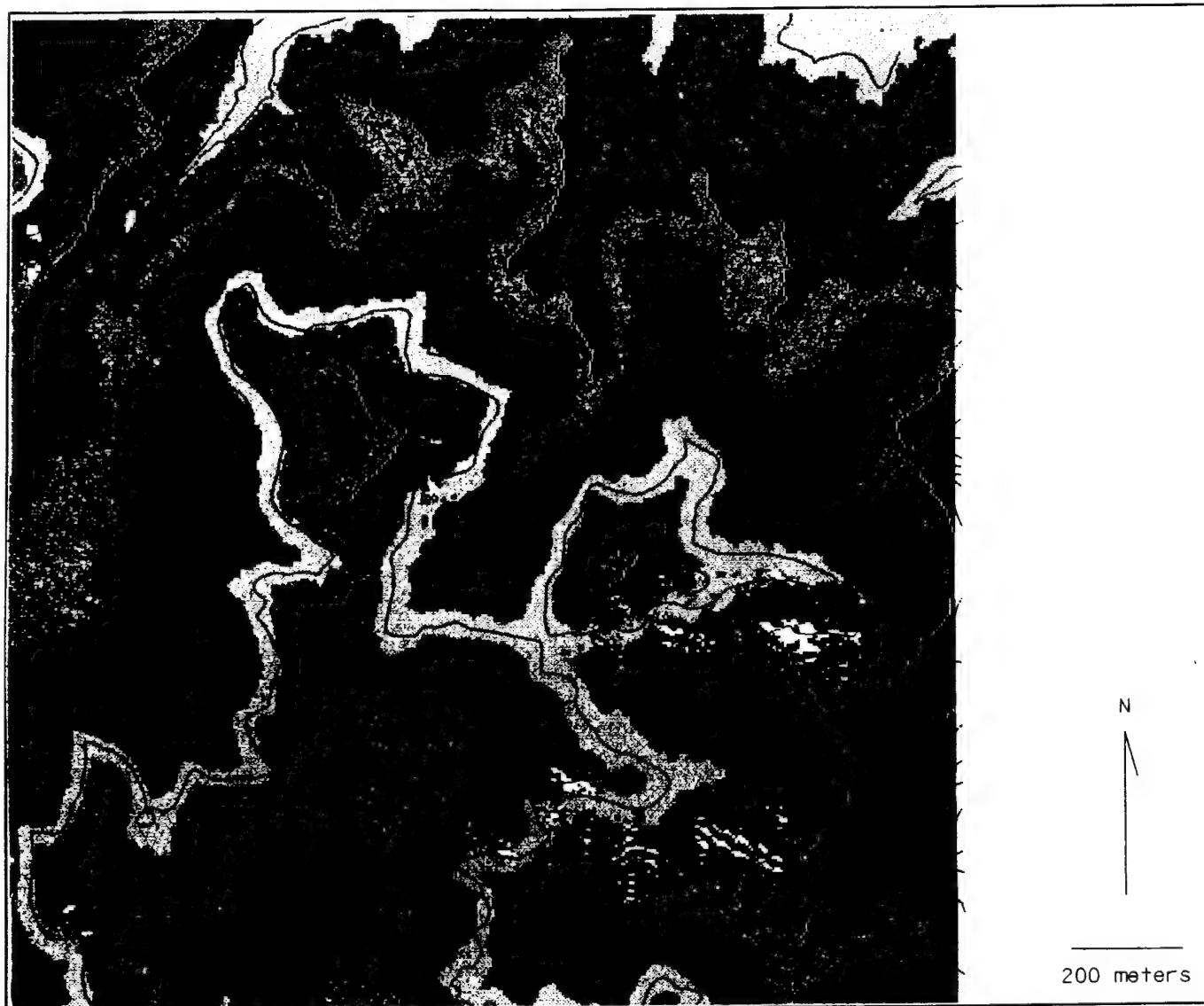


**Figure 3.1-7:** Isopleth of the ANT90 radar DEM of the test area. Note the void areas where "data drop-outs" occur. This radar DEM exhibits less noise than the ANT270 radar DEM shown in Figure 3.1-6.

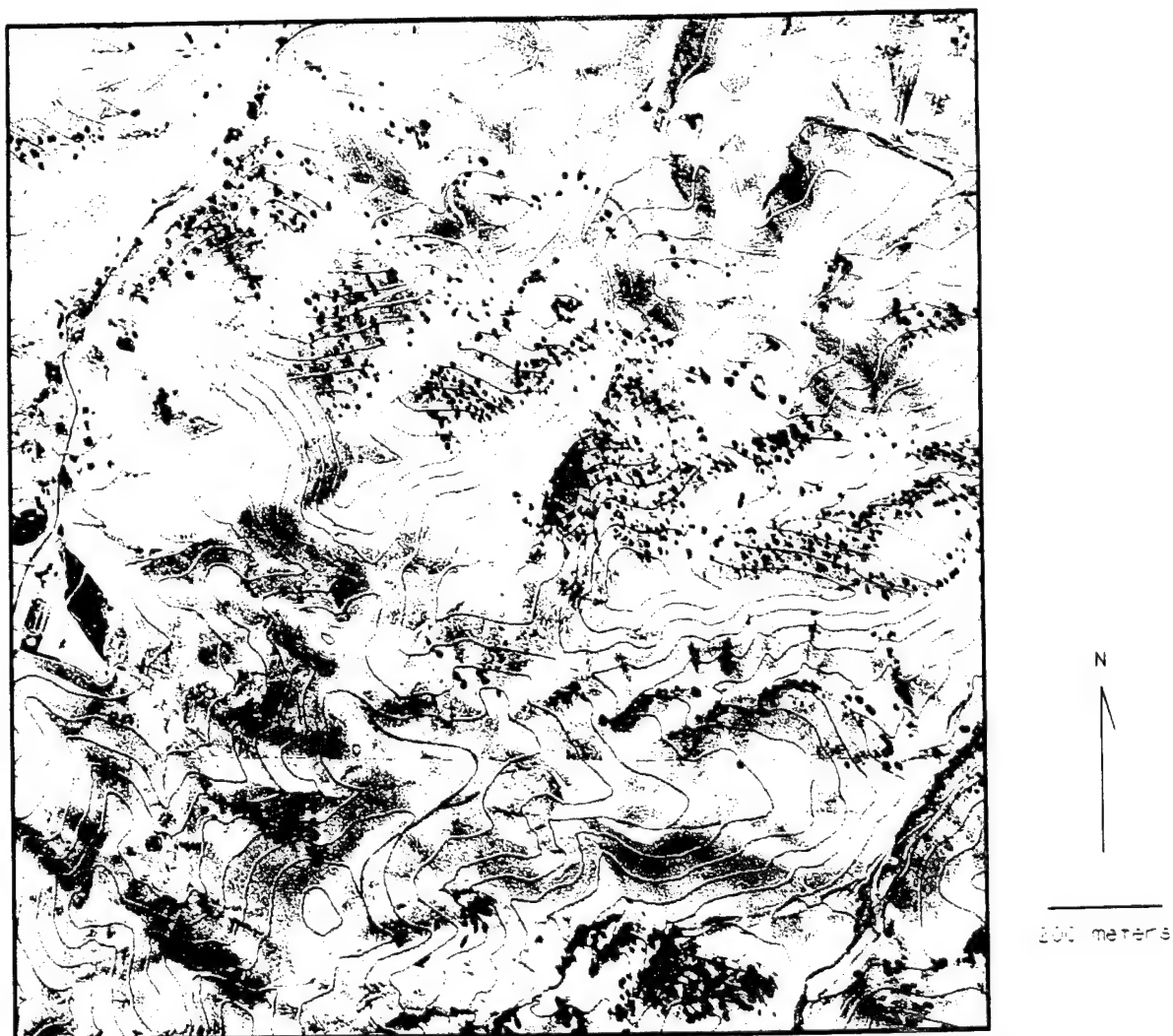


**Figure 3.1-8:** The 1:20,000-scale photographic image of the test area. The image is overlain by 20m contours from the ground-truth DEM.



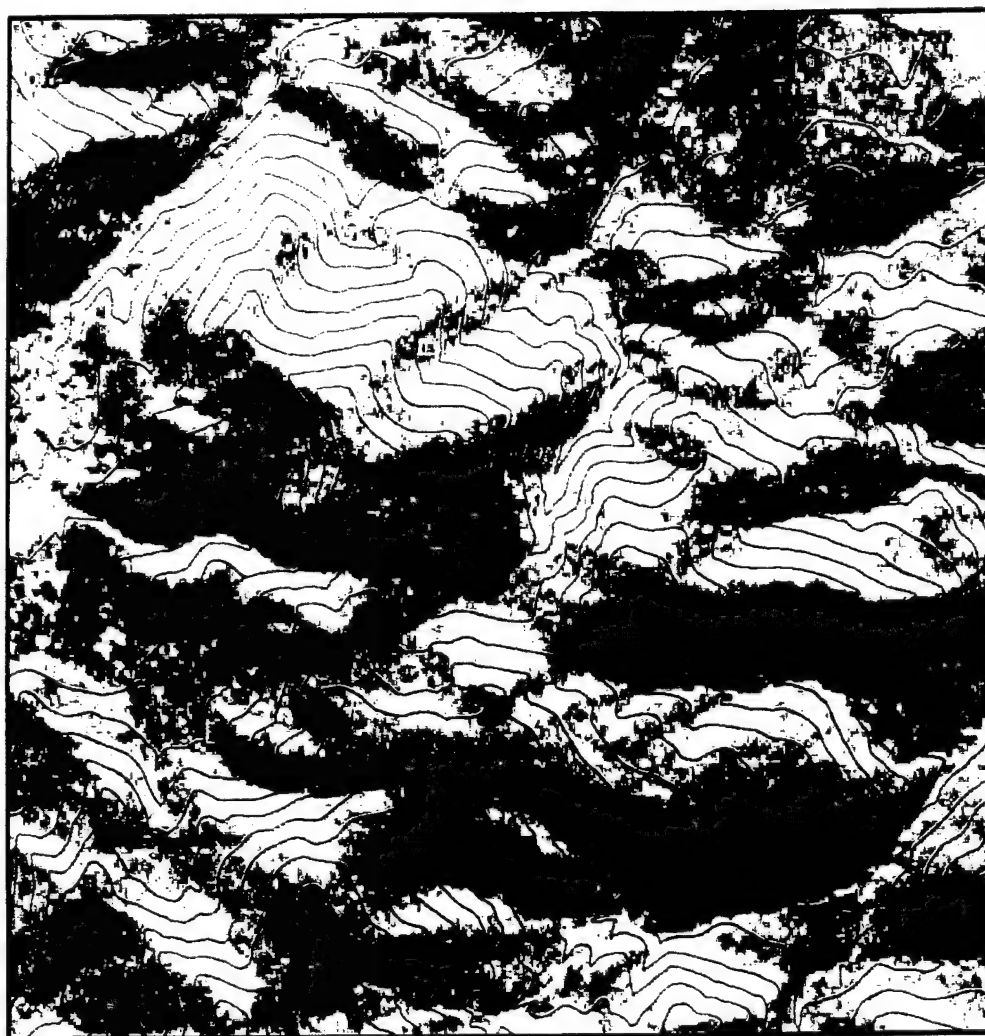


**Figure 3.1-9:** The ANT270 radar image for the test area. Note the data drop-outs on the south-facing slopes. The image is overlain by 20m contours from the ground-truth DEM.

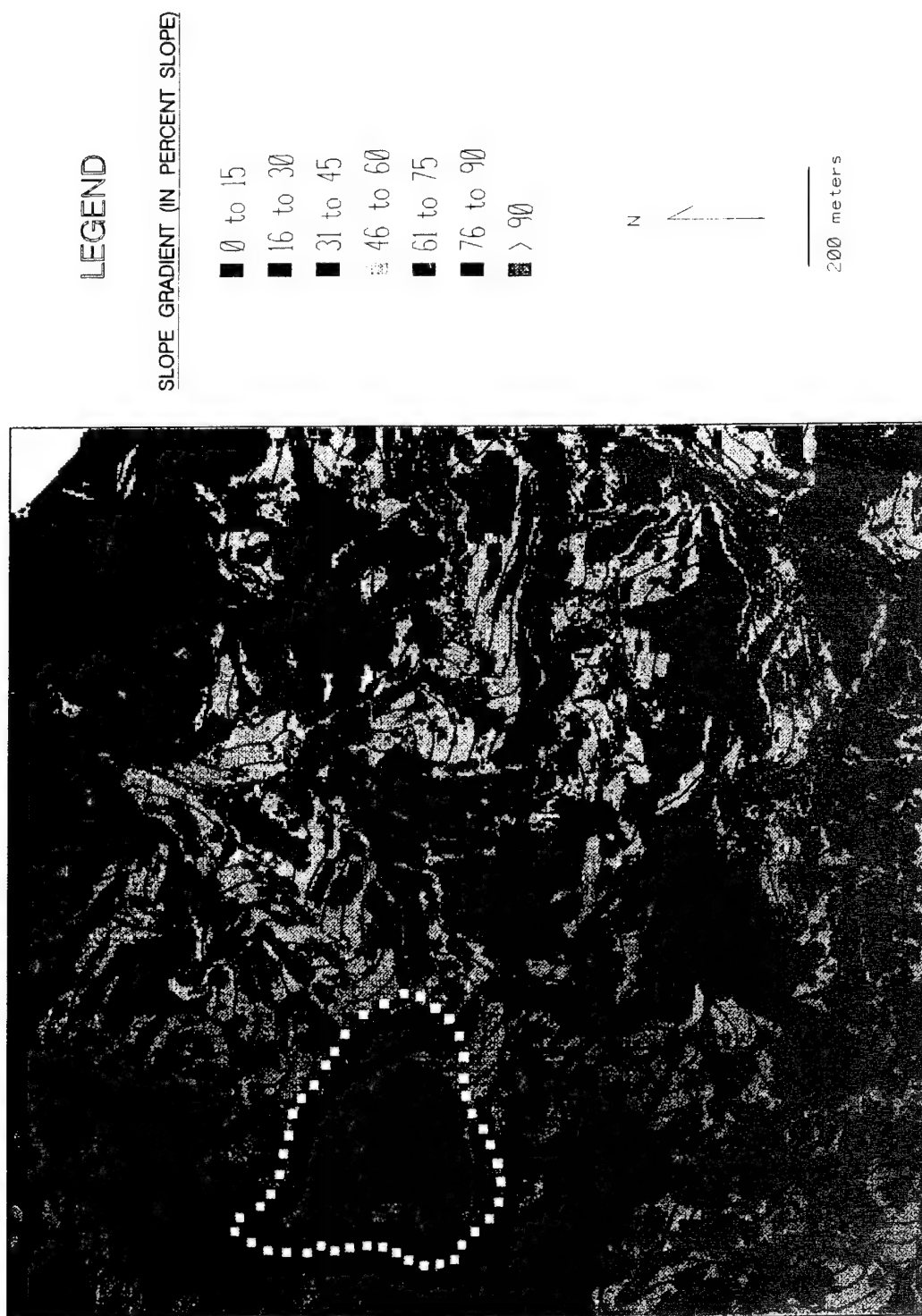


**Figure 3.1-10:** Ground-truth slope gradient map of the test area. Note the landslide outlined in the west-central portion of the map and the slope features exhibited, as discussed in the text. The map is overlain by 20m contours from the ground-truth DEM.

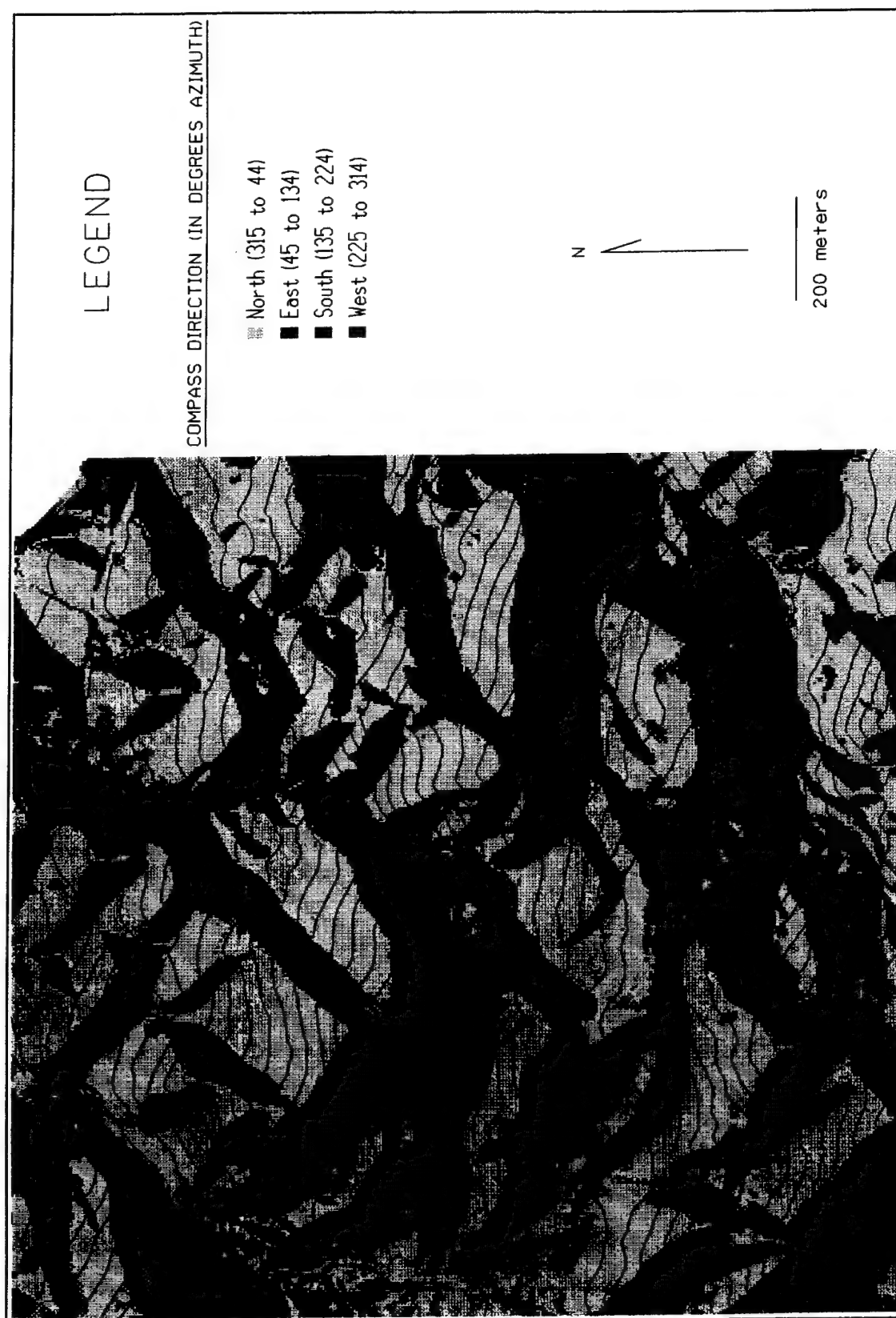


**Figure 3.1-11:** Ground-truth slope aspect map of the test area. The map is overlain by 20m contours from the ground-truth DEM.

A computer program was specially developed to calculate the above statistics. All those residuals which deviated from the mean by more than  $3S$  were rejected and another iteration for the computed statistics was performed. The updated residuals were again tested for the above rejection criterion, and if any additional grid points had to be rejected, the computation was repeated for another iteration. This iterative computation was ended when no more grid points had to be rejected. Rejected points were mapped to confirm systematic error and to justify exclusion.

#### 3.1.3.2.2 Comparison

Several visual and statistical comparisons were performed on the data. These are summarized as seven separate tests as follows:

**TEST 1 - Relative Accuracy of the Ground Truth DEM:** To better understand the relative accuracy of the ground-truth DEM (1:10,000-scale photogrammetric DEM), it was subtracted from the 1:20,000-scale photogrammetric DEM to produce a height difference grid. Grid coordinates and spacing are identical for these DEMs, and the magnitude of the height differences serves as a measure of the stability of each photogrammetric model as well as a baseline for later comparisons with radar DEM height differences. The locations of the largest height differences were used to reexamine the adequacy of breaklines in the DEM collection process. Modifications were made as necessary, and the DEM collection process repeated until the best possible ground-truth DEM was obtained. Statistical analysis of the resulting height difference grid was performed by DOC and Calgis. DOC's area of analysis is slightly smaller than that of Calgis; it was cropped before the analysis for figure presentation purposes. DOC's height differences are statistically summarized by maximum error, minimum error, AM, RMSE, S, and percentage of points rejected during the iterative process. Calgis' statistical analysis includes the same information, along with the ME, as well as varying the original grid interval from 5 m to 25 m in steps of 10 m; the analysis of these different intervals simulates what effects data thinning would have on the analysis.

**TEST 2: Planimetric Accuracy of Radar Data:** The errors in comparative height values between two DEM grids are affected by the planimetric error in what is regarded as the "same terrain point." The U.S. National Map Accuracy Standards allow the points being tested to be moved within the range for permissible planimetric error, before deriving the height discrepancies. Accordingly, it was necessary to establish the planimetric accuracy of the radar DEM. Ideally, such a test requires that several trihedral radar targets be located evenly in the radar image coverage, the accurate ground positions of which are surveyed. A comparison between the known ground position and the radar image position then provides a reliable estimate of the planimetric radar mapping accuracy. Since no such extra targets had been located during the radar flights, the test had to be carried out between same ground features that can be identified with confidence, both in a photogrammetric model and the radar image. The only features that would lend themselves to such an identification were the major highway and road intersections in the urbanized areas. No such points could be identified in the hilly test site. Calgis carried out this test by extracting positional data from 1:20,000-scale photogrammetric models.

**TEST 3 - Spatial Accuracy of the Radar DEM:** The relative 3-dimensional accuracy of the radar DEMs was tested by comparing them to the photogrammetric DEMs using the same methodologies established in TEST 1. Height difference grids were created between the radar DEMs and the photogrammetric DEMs, as well as between the two radar DEMs, and statistical analyses on the data were performed. In an effort to help recognize patterns in the distribution of errors in the data, Calgis divided the height difference grids into quarters along the cardinal directions (Quarter 1: NW; Quarter 2: SE; Quarter 3:

NE; Quarter 4: SW), and calculated the same statistical parameters as in TEST 1 separately for each quarter. DOC's analysis was limited to a comparison between the 1:10,000-scale photogrammetric DEM and the ANT270 radar DEM because the planar coordinates for the ANT90 radar DEM co-registered to the other DEMs, although included in Calgis analysis, were not available in time for DOC's analysis. Data dropouts in the radar DEMs were designated as null values and were not included in the analysis by Calgis. The same objective was achieved by DOC by ignoring elevations below a value of 59 m, which corresponds to the lowest elevation in the ground-truth DEM.

**TEST 4 - Accuracy of the Radar DEM as a Function of Topography:** To examine the correlation between height errors in the radar DEM and terrain conditions, elevation contours for the ground-truth DEM were overlain on the height error map for visual comparison. Also, the ground-truth DEM was classified by slope gradient (in increments of 15%) and aspect (north, south, east, and west directions), and then intersected with the radar height error grid in order to group height errors by slope gradient and aspect. Summary statistics were calculated by DOC for each data group and analyzed for trends in slope gradient and aspect, with particular attention given to the look direction and depression angle of the radar.

**TEST 5 - Accuracy and Utility of Slope Gradient Maps Generated from the Radar DEMs:** Slope gradient maps were generated from the ANT90 and ANT270 radar DEMs using the same methods described for the ground-truth slope gradient map. These maps were generated for increments of 15% slope, and were visually compared by DOC to the ground-truth slope gradient map for relative accuracy and suitability for use in landslide analysis and recognition.

**TEST 6 - Usefulness of Radar Image for Hazards Mapping:** To evaluate the utility of the radar image for landslide mapping, a visual analysis of the radar imagery was performed by DOC in a manner similar to that done for the air-photo landslide inventory described previously. The attributes of radar imagery were compared and contrasted with those of aerial photography in terms of their value to seismic hazard evaluation.

**TEST 7 - Use of Radar DEM in Orthophotograph Generation:** To test the suitability of using radar derived DEMs to orthorectify aerial photos, orthophotographs were generated by DOC using Intergraph's softcopy photogrammetry software (ISPN). The ground-truth and ANT270 radar DEMs were each used to orthorectify the same original digital photographic image (1:10,000 scale). The resulting orthophotographs were then visually compared for overall image quality.

### 3.1.3.3 Results

**TEST 1 - Relative Accuracy of the Ground Truth DEM:** Figure 3.1-12 shows height differences (errors) between the ground-truth DEM and the 1:20,000-scale photogrammetric DEM, as mapped by DOC. Most of the error is assumed to be in the 1:20,000-scale DEM as a result of its lower resolution. Positive and negative errors are presented in two-meter color-coded intervals and are overlain by ground-truth elevation contours for reference. Positive errors represent "floating" elevation points that lie above the ground-truth surface, while negative errors represent "buried" elevation points that fall below the ground-truth surface.

DOC's first run of this process revealed errors on the order of 5-10 m in isolated areas. Possible causes for some of these high difference values may be related to: 1) areas of high reflectance and low contrast on the aerial photographs, specifically for the 1:20,000-

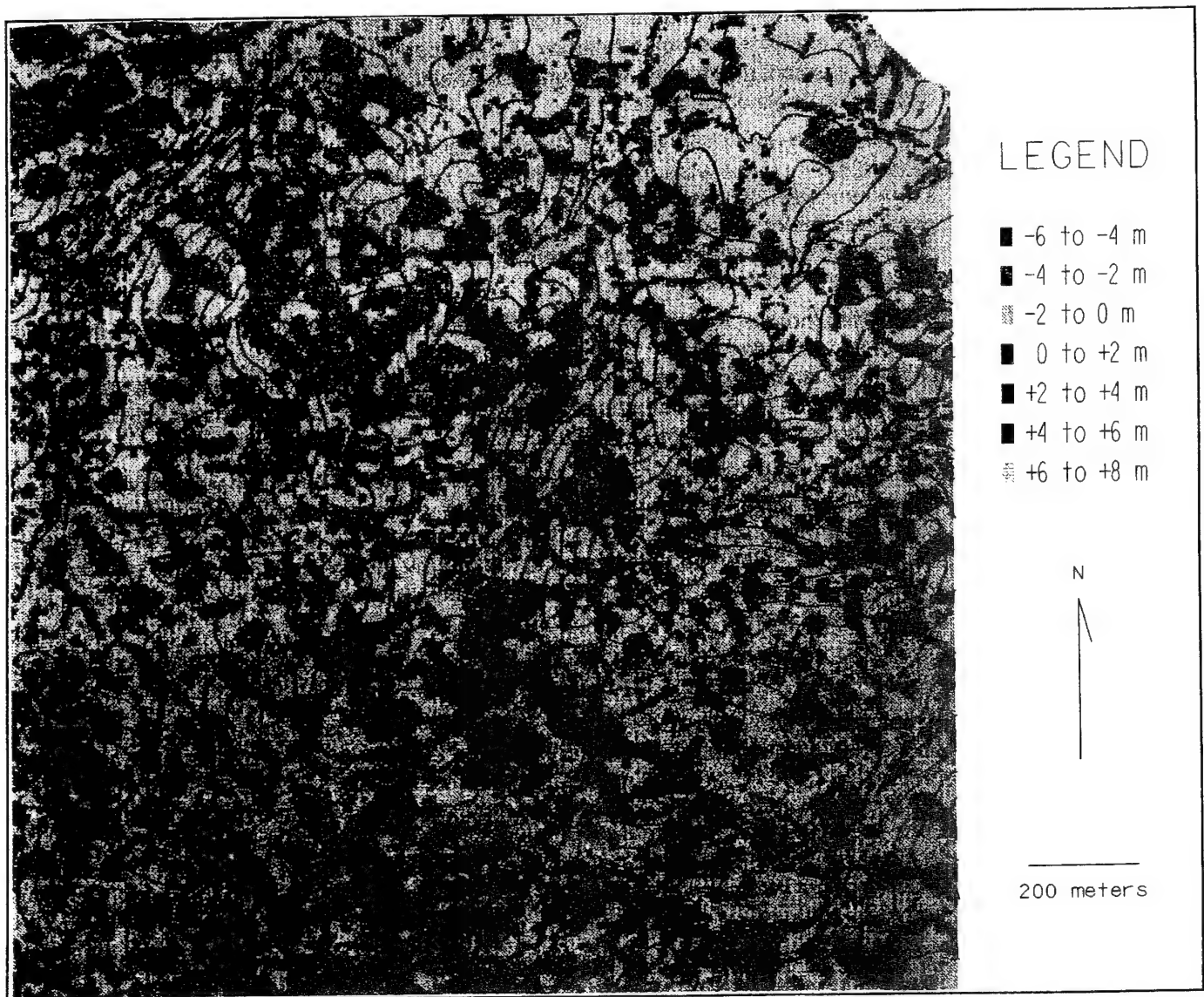


**Figure 3.1-12:** Height difference map for the 1:20,000-scale photogrammetric and ground-truth DEMs. The map is overlain by 20m contours from the ground-truth DEM.



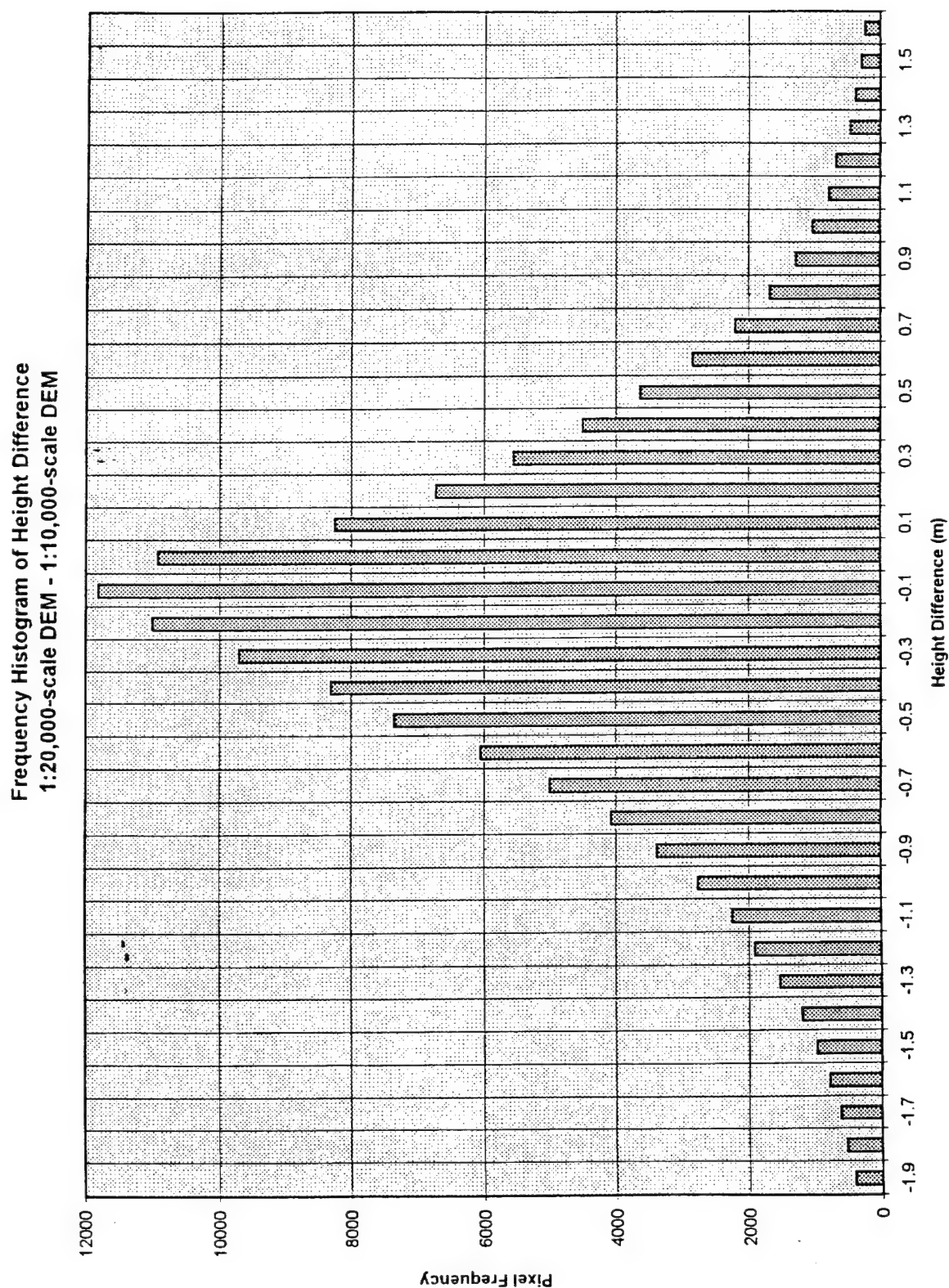


**Figure 3.1-13:** Frequency histogram of height differences between the 1:20,000-scale photogrammetric and ground-truth DEMs. Data are grouped into 0.1m intervals.



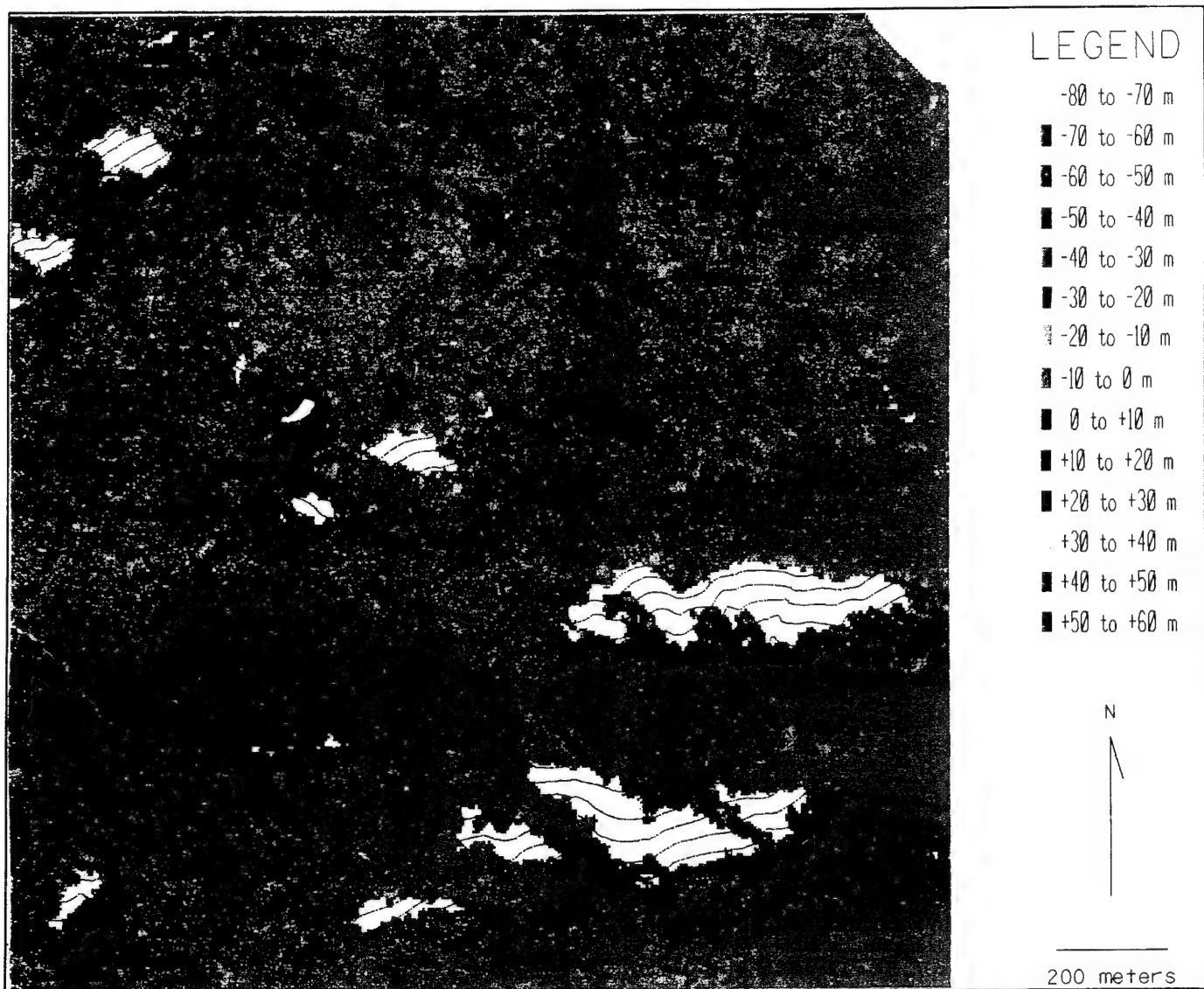


**Figure 3.1-14:** Height difference map for the ANT270 radar and ground-truth DEMs. The map is overlain by 20m contours from the ground-truth DEM.

Frequency Histogram of Height Difference  
270 Series Radar DEM - 1:10,000-scale Photogrammetric DEM

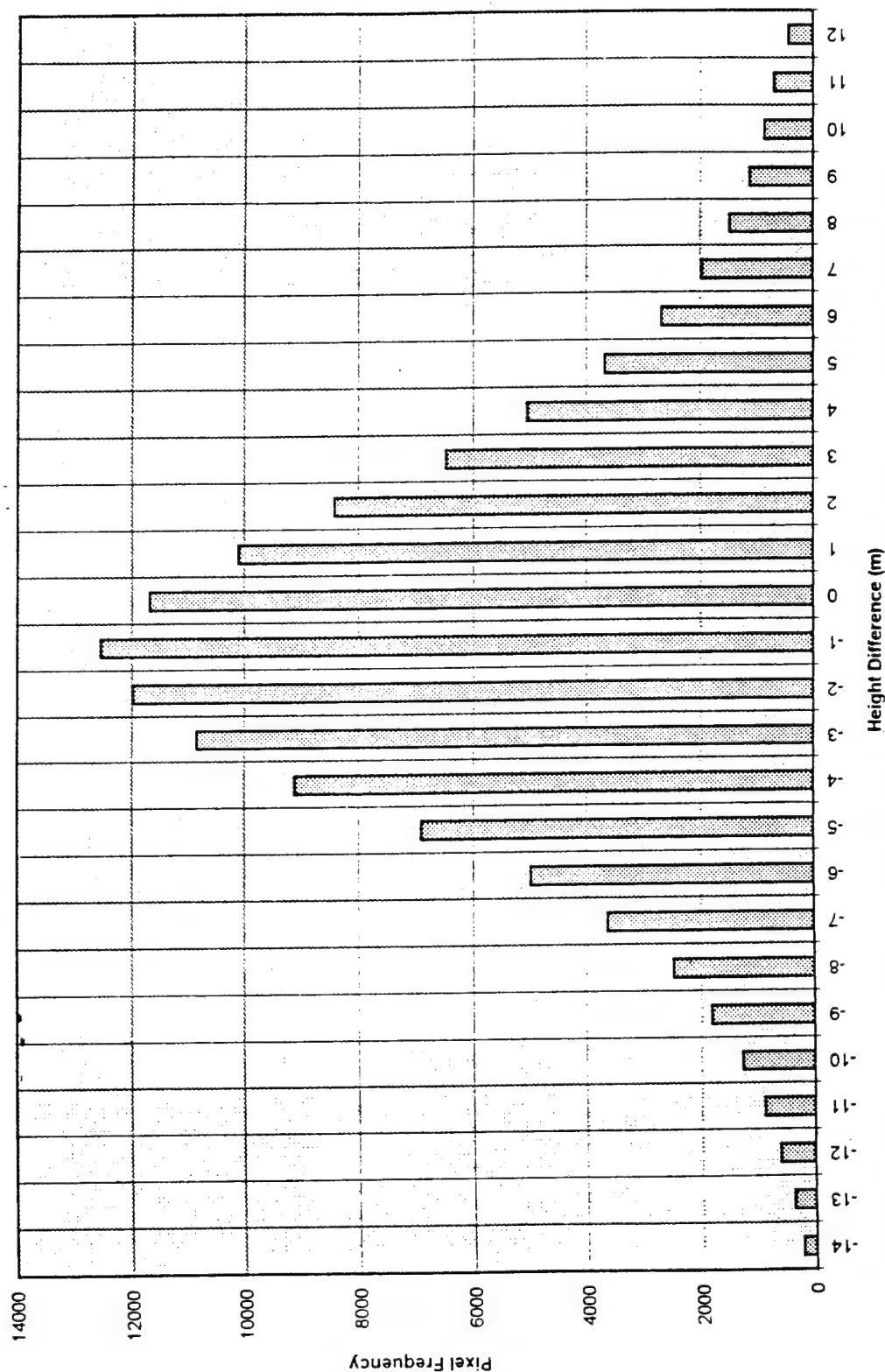


Figure 3.1-15: Frequency histogram of height differences between the ANT270 radar and ground-truth DEMs. Data are grouped into 0.1m intervals.

scale photographs, which can make correlation in the Match T process difficult, 2) distortion along edges of the original stereo models causing errors in the Match T correlations, 3) apparent differences between the two models merged for the 1:10,000-scale photogrammetric DEM along the matching edge where they overlap, or, 4) an insufficient number of breaklines in the DEM collection process to account for abrupt changes in topography such as reversals in dip direction. Editing consisted of analyzing the areas where large errors occur, adding additional breaklines where needed, and replacement of outliers with manually collected points.

Once editing was completed and Match T DEM production was repeated, height differences were recomputed and statistically analyzed by both DOC and Calgis (Table 3.1-1). DOC's data are presented as a frequency histogram in Figure 3.1-13, having height errors grouped into 0.1 m intervals. After three iterations by DOC, the range in height error decreased about 71% while RMSE reduced from 0.69 m to 0.59 m with a point rejection of only 2.4%. Similar results were found by Calgis: an RMSE of 0.57 m and a point rejection of 2.8%. Calgis also determined that there was no difference in errors by varying the grid interval in the analysis.

2:

**Table 3.1-1:** Statistical analyses by DOC and Calgis of height differences between the two photogrammetric DEMs [(O) = original data, (3) = number of iterations of data, NA = not analyzed or not available].

Grid Int	No. of Grids	Max. Error	Min. Error	AM	ME	RMS	S	%Pts Rejected
DOC Analysis = Reference Grid: 1:10,000 Photo				Measured Grid: 1:20,000 Photo				
5 m (O)	133,990	6.3	-5.8	-0.16	NA	0.69	0.67	0
5 m (3)	130,917	1.6	-1.9	-0.15	NA	0.59	0.58	2.3
Calgis Analysis = Reference Grid: 1:10,000 Photo				Measured Grid: 1:20,000 Photo				
5 m	NA	6.3	-5.8	-0.11	0.44	0.57	0.56	2.8
15 m	NA	6.3	-4.7	-0.11	0.44	0.58	0.56	2.8
25 m	NA	4.5	-5.0	-0.11	0.44	0.57	0.56	2.6

**TEST 2 - Planimetric Analysis of Radar Data:** A total of 18 road intersection points were selected by Calgis in the ANT270 image and their X (easting), Y (northing), and Z (height) were digitized from the radar image. Similar X, Y, and Z coordinates were then read from absolutely oriented models at 1:20,000-scale photography. The precision of the photogrammetric coordinate data is estimated as 0.3m. The difference in coordinates was calculated as ANT270 minus 1:20,000-scale photography for the 18 test points and the mean difference value was +2.0m in X, +2.6m in Y, and +3.2m in Z, with standard deviation of 2.07m, 1.97m, and 2.28m, respectively. The maximum difference in X was 6.7m, 5.1m in Y, and 9.2m in Z. The planimetric accuracy of radar imagery, at least in the open urbanized tested landscape, therefore, corresponds to about one-half the 5m pixel size used. This positional error would satisfy the positional National Map Accuracy Standard for a map at 1:5,000 scale.

TEST 3 - Spatial Accuracy of the Radar DEM: Height differences (errors) between the ANT270 DEM and the ground-truth DEM are mapped by DOC in Figure 3.1-14. As in the TEST 1, positive errors represent areas of elevation in the radar DEM that are floating above the ground-truth DEM while negative values represent buried elevation points. Note that the color-coded interval for the elevation difference is 10m, five times larger than height differences between the two photogrammetric DEMs. The void areas in the map represent data drop-outs in the radar. Figure 3.1-15 is a frequency histogram of these data.

Results from the statistical analysis by Calgis and DOC for this test are shown in Table 3.1-2. The measured and the reference grids have been identified in each case. It is again emphasized that all the DEM grids used in this analysis had been co-registered to the same planimetric position at 5m posting.

**Table 3.1-2:** Statistical analyses by DOC and Calgis of height difference between the photogrammetric DEMs and the TOPSAR DEMs [(O) = original data, (6) = number of iterations of data, NA = not analyzed or not available].

Grid Int.	No. of Grids	Max. Error	Min. Error	AM	ME	RMS	S	%Pts Rejected
DOC Analysis = Reference Grid: 1:10,000 Photo				Measured Grid: ANT270 Radar				
5 m (O)	127,549	51.8	-239.8	-1.8	NA	12	12	0
5 m (6)	122,325	12.2	-14.1	-1.0	NA	4.5	4.4	4.1
Calgis Analysis = Reference Grid: 1:10,000 Photo				Measured Grid: ANT270 Radar				
5 m	124,403	13.5	-13.5	-0.9	3.4	4.6	4.5	4.1
Calgis Analysis = Reference Grid: 1:10,000 Photo				Measured Grid: ANT90 Radar				
5 m	124,311	11.0	-11.0	-6.1	6.5	7.1	3.7	23.4
Calgis Analysis = Reference Grid: 1:20,000 Photo				Measured Grid: ANT270 Radar				
5 m	128,852	13.8	-13.8	-0.9	3.7	4.7	4.6	4.0
15 m	134,153	13.8	-13.7	-0.9	3.6	4.7	4.6	3.9
25 m	134,591	13.8	-13.7	-0.9	3.7	4.7	4.6	4.1
Qtr. 1	133,807	13.4	-13.4	-0.6	3.5	4.5	4.4	3.7
Qtr. 2	130,387	14.9	-14.9	-1.4	4.0	5.1	4.9	6.9
Qtr. 3	134,774	13.0	-13.0	-0.5	3.4	4.3	4.3	2.6
Qtr. 4	134,380	13.9	-13.9	-1.4	3.8	4.8	4.6	3.2
Calgis Analysis = Reference Grid: 1:20,000 Photo				Measured Grid: ANT90 Radar				
5 m	134,071	11.2	-11.2	-6.1	6.5	7.1	3.7	21.7
15 m	134,076	11.1	-11.2	-6.1	6.5	7.1	3.7	22.0
25 m	134,114	10.4	-10.9	-6.0	6.4	7.0	3.6	23.6
Qtr. 1	134,088	11.8	-11.8	-5.6	6.2	6.9	3.9	6.5
Qtr. 2	133,633	14.7	-14.8	-7.5	8.1	8.9	4.9	11.8
Qtr. 3	134,134	8.4	-8.5	-5.0	5.3	5.7	2.8	33.3
Qtr. 4	134,117	8.2	-8.2	-5.3	5.6	5.9	2.7	62.4
Calgis Analysis = Reference Grid: ANT90 Radar				Measured Grid: ANT270 Radar				
5 m	128,544	15.4	-15.4	6.3	7.2	8.2	5.1	8.7
Qtr. 1	133,122	14.7	-14.7	5.4	6.3	7.3	4.9	5.9
Qtr. 2	130,011	18.4	-18.4	7.0	8.2	9.3	6.1	9.9
Qtr. 3	134,068	13.4	-13.4	6.0	6.6	7.4	4.5	8.7
Qtr. 4	133,721	15.8	-15.8	7.2	7.9	8.9	5.2	9.8



Figure 3.1-16: Map of height differences rejected in the statistical analysis of the ANT 90 DEM/  
1:20,000-scale photogrammetric DEM comparison.

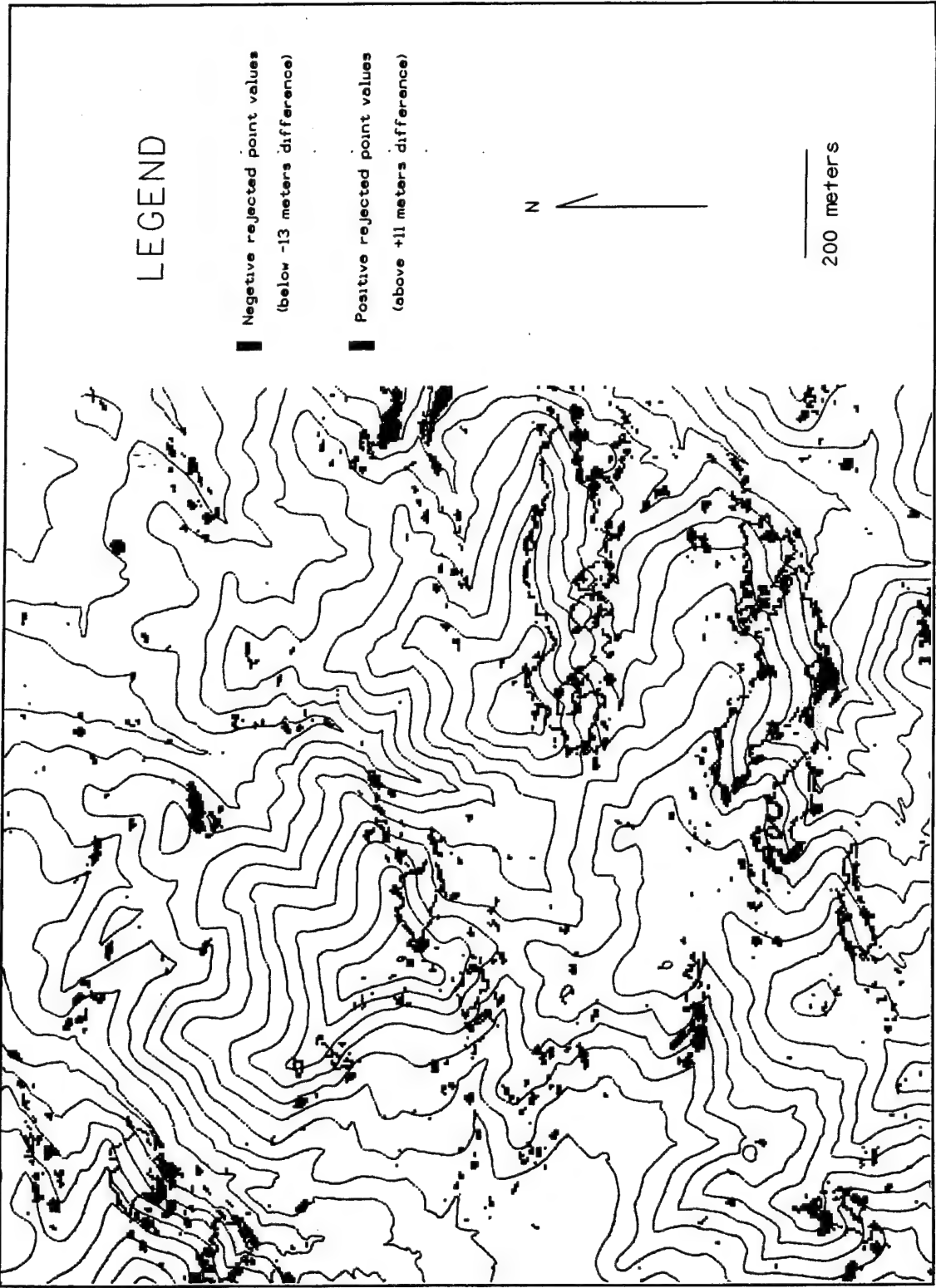


Figure 3.1-17: Map of the height differences rejected in the statistical analysis of the ANT270 radar DEM/ ground-truth DEM comparison. The map is overlain by 20m contours from the ground-truth DEM.



A comparison made by Calgis between the ANT270 and the ANT90 DEM grids shows a positive algebraic mean,  $AM = 6.3$  m,  $ME = 7.2$  m,  $RMSE = 7.2$  m, and  $S = 5.1$  m. These statistics clearly indicate a systematic bias between the two height data sets which, perhaps, cannot be attributed entirely to the look direction. Some local variation due to the look direction was expected because the test area falls in the near range for the ANT270 flight, while it falls in the far range for the ANT90 radar flight. Some variation in the statistical parameters is indeed noticeable, as for example, the RMSE value changes by about 2 m while processing the northern and the southern half of the test area, accompanied by a change of about 4% in the number of points rejected.

The comparison of the ANT90 radar DEM with the 1:20,000-scale photogrammetric DEM height data shows a mean value of - 6.1 m which is a clear indication of the presence of a systematic bias in the radar data. This conclusion is further supported by a variation of about 3.4 m between the RMSE and the standard deviation values. This bias practically overrides any small variation due to the sampling interval or processing of different quarters of the test site. More precise calibration of the TOPSAR system is required to eliminate systematic biases.

The comparison of the ANT270 DEM with 1:20,000-scale photogrammetric DEM provides the best measure for the potential use of TOPSAR DEM data. The mean error of 0.9 m shows an absence of any significant bias in the data, which is further confirmed by the close agreement between the RMSE value of 4.6 m with the standard deviation of 4.5 m. These statistical values remain unchanged even for a sampling interval of 25 m, and are consistent for all quarter subsets of the test area.

DOC's statistics for the data shown in Figure 3.1-14 and 3.1-15 closely resemble the results from Calgis' analysis of the ground-truth DEM to ANT270 radar DEM comparison. After six iterations the range in height error decreased about 91% while the RMSE decreased from 12 m to 4.5 m with a point rejection of 4.1%.

To test the validity of removing points from the data set, the statistically rejected points are displayed for two height difference analyses; Figure 3.1-16 shows Calgis' comparison between the 1:20,000-scale photogrammetric DEM and the ANT90 radar DEM, and Figure 3.1-17 shows DOC's comparison between the ground-truth DEM and the ANT270 radar DEM. Figure 3.1-16 indicates the large number of points rejected are primarily due to the systematic bias in the ANT90 radar data, and are not considered to provide any meaningful correlation with terrain topography. Figure 3.1-17 shows that for the ANT270 DEM, the majority of the rejected points with high negative values occur along the edge of void areas, and other rejected points occur on south-facing slopes and within steep canyons.



**TEST 4 - Accuracy of the Radar DEM as a Function of Topography:** DOC shows in Tables 3.1-3 and 3.1-4 the statistical results from grouping radar height errors in the ANT270 radar DEM into slope gradient and aspect categories using the ground-truth gradient and aspect grids. There are seven slope gradient categories in increments of 15%, and four aspect categories representing the four compass directions. The distribution of points in each category indicates the data are suitable for slope gradient and aspect analysis.

**Table 3.1-3:** Statistical analysis of height difference between the ANT270 and the ground-truth (1:10,000-scale photographic) DEMs based on slope gradient categories.

DOC Analysis = Reference Grid: 1:10,000 Photo				Measured Grid: ANT270 Radar			
	No. of Grids	Max. Error	Min. Error	AM	RMS	S	% Pts. Rejection
<b>0 - 15 %</b>							
Original Data	10,478	37.7	-197.7	-1.1	5.5	5.4	0
Fourth Iteration	10,379	11.8	-13.9	-1.1	4.4	4.3	0.94
<b>16 - 30 %</b>							
Original Data	25,672	45.6	-201.4	-1.0	6.3	6.2	0
Fourth Iteration	25,131	11.4	-13.4	-1.0	4.3	4.1	2.1
<b>31 - 45 %</b>							
Original Data	37,449	47.3	-197.4	-1.5	8.7	8.5	0
Sixth Iteration	36,224	11.6	-14.1	-1.2	4.4	4.3	3.3
<b>46 - 60 %</b>							
Original Data	33,034	51.8	-215.2	-2.3	14	14	0
Eighth Iteration	31,131	12.0	-14.0	-1.0	4.4	4.3	5.8
<b>61 - 75 %</b>							
Original Data	15,494	48.4	-220.8	-2.6	17	17	0
Sixth Iteration	14,558	13.5	-14.9	-0.70	4.8	4.7	6.0
<b>76 - 90 %</b>							
Original Data	3,962	45.0	-218.0	-3.4	24	24	0
Ninth Iteration	3,624	16.4	-14.7	0.85	5.2	5.2	8.5
<b>&gt; 90 %</b>							
Original Data	1,568	48.7	-239.8	-2.6	26	26	0
Eighth Iteration	1,410	20.9	-16.3	2.3	6.6	6.2	10

Based on the grouping of height error by slope gradient (Table 3.1-3), the original data set shows a positive progression in RMSE of 5.5 m for 0% to 15% slopes, to 26 m for slope gradients over 90%. This indicates a strong correlation between height errors and slope gradient. After several iterations, the range in RMSE reduced to 4.4 m for slope gradients between 0% and 15% and 6.6 m for slope gradients over 90%. Although the final RMSE values are much lower than the original values, and their correlation with slope gradient are not as substantial, height errors still show an increase with slope gradient.

Table 3.1-4 shows height error statistics grouped by slope aspect categories. North-facing slopes, which face the incident radar beam, have the highest accuracy (RMSE = 3.4 m) and south-facing slopes have the highest error (RMSE = 7.9 m). The comparably higher errors for south-facing slopes may be related to the same physical causes as the abundant data drop-outs on these slopes. Despite this, it appears that slopes shadowed from the incident radar beam, south-facing slopes in this case, will have higher elevation errors than other slopes, especially when using radar data in the far range of the ground swath.

**Table 3.1-4:** Statistical analysis of height difference between the ANT270 and the ground-truth (1:10,000-scale photographic) DEMs based on slope aspect categories.

DOC Analysis = Reference Grid: 1:10,000 Photo			Measured Grid: ANT270 Radar				% Pts. Rejected
	No. of Grids	Max. Error	Min. Error	AM	RMS	S	
<b>North Facing Slopes</b>							
Original Data	47,730	42.2	-114.6	-1.2	3.9	3.7	0
Fourth Iteration	46,908	8.0	-10.7	-1.3	3.4	3.1	1.7
<b>South Facing Slopes</b>							
Original Data	15,000	51.8	-239.8	-6.9	30	30	0
Ninth Iteration	13,427	24.1	-23.2	0.47	7.9	7.9	10
<b>East Facing Data</b>							
Original Data	34,393	48.4	-220.8	-2.1	9.2	8.9	0
Sixth Iteration	33,386	12.7	-16.4	-1.9	5.2	4.8	2.9
<b>West Facing Slopes</b>							
Original Data	30,426	37.9	-187.1	0.22	6.5	6.4	0
Fourth Iteration	29,905	13.9	-13.4	0.27	4.5	4.5	1.7

#### TEST 5 - Accuracy and Utility of Slope Gradient Maps Generated from the Radar DEMs:

Slope gradient maps were produced by DOC using the same method as applied to the ground-truth DEM. Of the two slope gradient maps generated from the radar DEMs, the ANT90 (Figure 3.1-18) is the most presentable. The ANT270 slope gradient map shows little coherency, which is probably due to the sensitivity of the computational method to height error. The ANT270 radar DEM contains a higher level of random noise as can be seen by comparing Figures 3.1-6 and 3.1-7.

Insights can be obtained from a visual comparison of the ground-truth slope map (Figure 3.1-10) and the radar slope map (Figure 3.1-18). Correlation appears to be better in flatter areas as seen in the western and northeastern portions of the project site. The color bands representing slope intervals appear to be less continuous for the radar slope map. Because of drop-outs in the radar data, slope calculations were not possible for some of the south-facing slopes.

Gross landslide features are noticeable in the radar slope gradient map. A large landslide, which has been mapped in the west-central portion of the test area, is recognizable on the ground-truth slope map by: (1) its steep, west-facing arcuate head-scarp, (2) its hummocky central bench portion, and (3) its oversteepened lower toe. Some of these

same features can be seen in the radar slope gradient map although with less continuity. This indicates that the slope gradient method used in this study, though sensitive to height error, still yields radar slope gradient maps that show potential for use in landslide feature recognition.

TEST 6 - Usefulness of Radar Image for Hazards Mapping: During DEM construction, three stereo photographic models were created, two at a scale of 1:10,000 and one at 1:20,000 (Figure 3.1-8). Photographic image quality is dependent on variables such as the flying height, the photo scanning resolution, the type of ground cover, and, the sun intensity and illumination angle. Although these variables were considered during the flight planning stage, only the flight height and the scanning resolution can be manipulated. Ideal physical conditions for landslide recognition include springtime ground conditions with darker grasses, and a shallow sun angle to show subtle relief. Because the aerial photographs were taken in August 1994, ground conditions were not optimal. However, because of the high resolution of the photography and of the scanned images (15 microns), features on the ground, particularly landslide features, are well defined and can be mapped digitally.

- 2. The radar image does not present an accurate account of surface features (Figure 3.1-9). It has an overall low contrast level and appears grainy. However, radar provides its own illumination and the image was thus acquired independent of sun intensity, sun angle, and weather conditions. Typically, an illumination direction and angle can be selected that will accentuate the terrain and the associated landslide features. However, as is seen in the radar image, sometimes data loss occurs on shadowed slopes in the far range and on steep slopes in the near range due to layover.

TEST 7 - Use of Radar DEM in Orthophotograph Generation: Figures 3.1-19 and 3.1-20 represent portions of the orthophotographs rectified by DOC using the ground-truth DEM and the ANT270 radar DEM, respectively. An urban area adjacent to the project area was selected to show how they compare using known linear features. The orthophotograph rectified by the ground-truth DEM appears to be accurate planimetrically. In contrast, the radar rectified orthophotograph undulates, distorting obvious linear-trending features. Clearly, height (and or planimetric) errors in the current radar data set prohibit its use for this purpose.

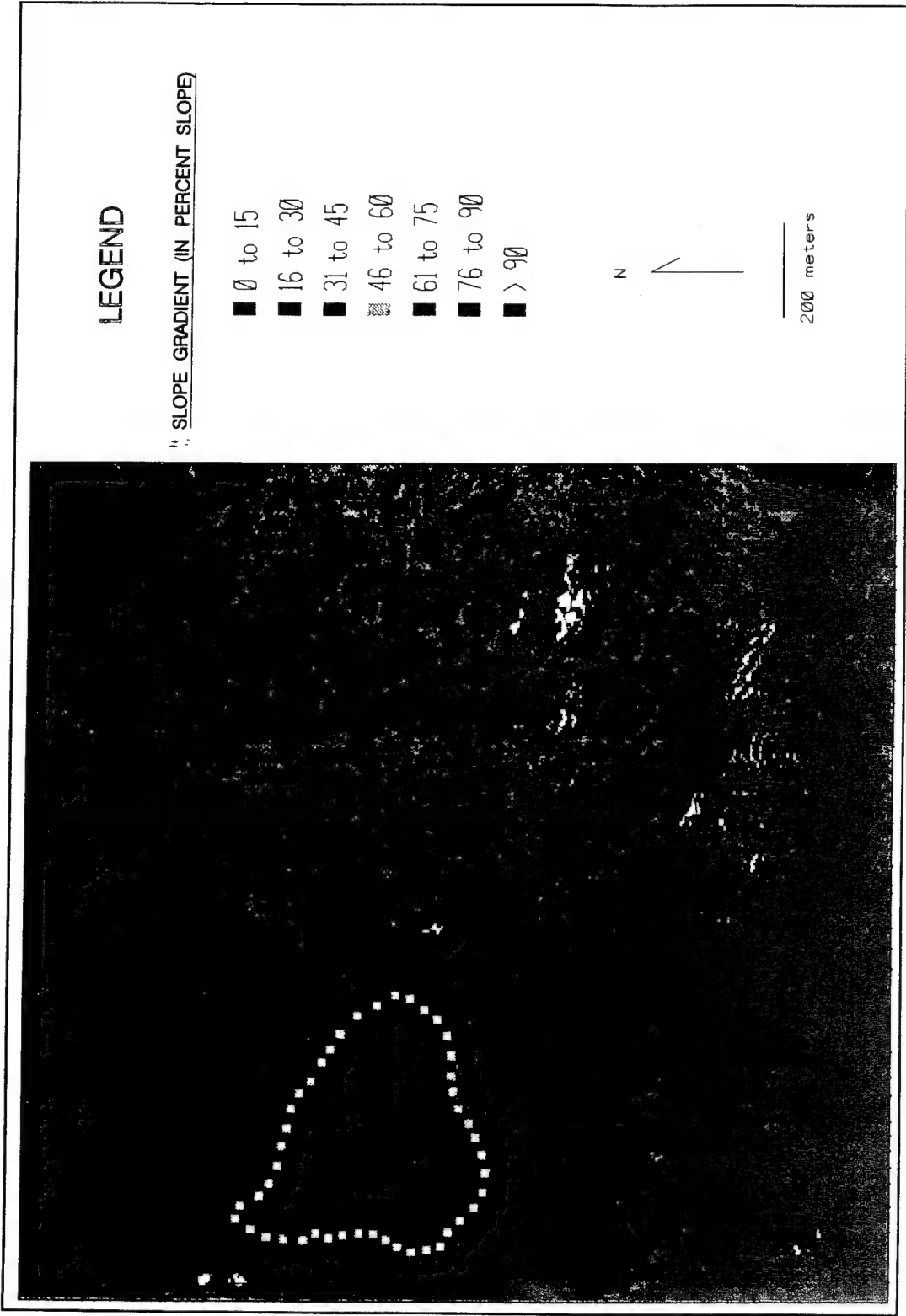


**Figure 3.1-18:** Slope gradient map of the ANT90 DEM. A landslide outlined in the west-central portion of the map displays similar slope features as the ground-truth slope map (Figure 3.1-10). The map is overlain by 20m contours from the ground-truth DEM.



100 m

**Figure 3.1-19:** Orthophotograph rectified using the ground-truth DEM showing urban features located northeast of the test area.

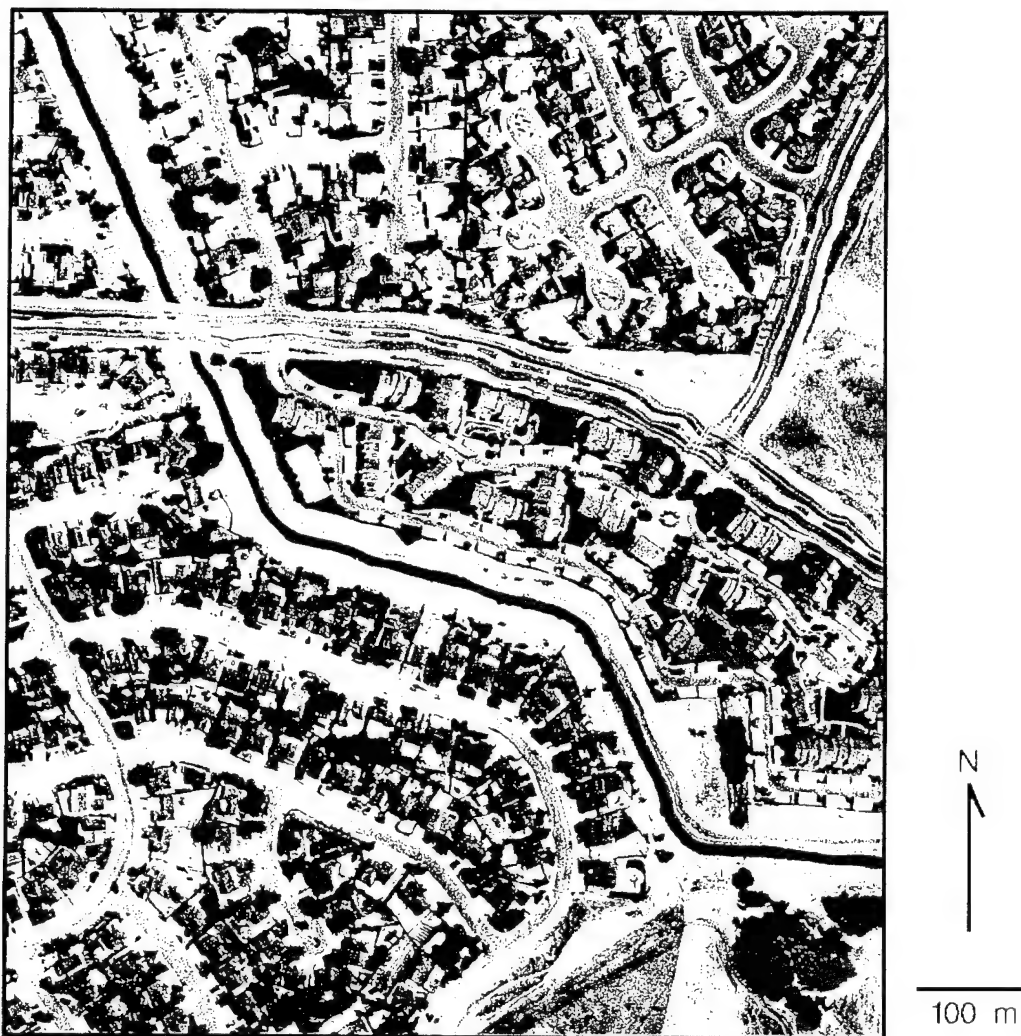


**Figure 3.1-20:** Orthophotograph rectified using the ANT270 DEM showing the same urban area as Figure 3.1-19. Note the undulating nature of the linear features caused by noise in the radar DEM.

### 3.1.3.4 Analysis of Radar Data with Systematic Bias Removed

A primary purpose of the DOC's study is to determine the accuracy of JPL's TOPSAR DEMs as a stand-alone terrain data acquisition product. Because sufficient ground control was not available for this analysis, systematic errors developed in the DEMs that could only be corrected by using additional precise, spatially accurate ground-truth data. The only data of this type available were photogrammetrically derived DEMs, the same type of DEM that is used for comparison in the primary study. For this reason, DOC and Calgis chose to maintain continuity in the study and only evaluate the partially-calibrated TOPSAR data. In this section JPL demonstrates that after removing systematic bias, the TOPSAR instrument is performing as expected and that more complete calibration should improve the absolute accuracy of TOPSAR data.

In JPL's analysis, two types of comparisons with the reference DEM were performed. First, the TOPSAR DEMs were coregistered with the reference DEMs using coordinate information output directly from the radar processor and the coordinate information provided with the reference DEM. This is similar to the approach used by DOC and Calgis and does not account for any position biases, scales, or rotations between the two data sets. In a second approach, the DEMs were coregistered using an automatic tie pointing program that cross correlated the height values to obtain a spatially distributed set of tie points. An affine transformation was least-square-fitted to the tie points where only rotation about the three axes, scales along the two axes in the plane, skew in the plane, and translation terms were allowed. In both cases the reference DEM was interpolated to the TOPSAR data so that the more accurate data set was interpolated.

JPL analyzed a slightly different region than that of DOC and Calgis using a 1:40,000-scale photogrammetrically derived DEM provided by Calgis as reference (see Table 2.2-1). Figures 3.1-21 and 3.1-22 show portions of the TOPSAR DEM containing the area of the reference DEM for ANT270 and ANT90 data sets, respectively. The image intensity is the SAR image intensity and the elevation of each pixel is mapped to a color wheel where each revolution of the color wheel represents a height change of 100m. In the ANT270 the radar near range is at the top of the image and far range at the bottom, this is reversed in the ANT90 image.

Figures 3.1-23 and 3.1-24 show height difference maps obtained by JPL between the reference DEM and the unadjusted TOPSAR ANT270 and ANT90 data sets, respectively. This was done using the same approach as DOC and Calgis, except that the photogrammetric DEM was transformed to the JPL radar mapping coordinate system. The image intensity is from the radar backscatter and the height difference is the color where one cycle of color represents 50m of height change. Examination of these images shows that in both cases the ANT90 and the ANT270 have slight misregistration errors causing the systematic component of observed height errors. Figures 3.1-25 and 3.1-26 contain histograms of the height errors for the uncorrected ANT270 and the ANT90 data sets, respectively. The large mean offset in both cases is primarily a result of different vertical datums being used in the TOPSAR DEMs (WGS-84) and reference DEMs (NGVD-29). In the Antioch Hills region this offset between the datums is approximately -31.0 m leaving a mean offset of 1.26m for ANT270 and -4.65m for ANT90. The remaining mean offset is due to the residual 0.05° slope that was not removed during the calibration process. The RMS height error for the ANT270 height difference is 6.23m and 5.89m for the ANT90 height difference which is larger than is expected from the TOPSAR sensor parameters. Further indication of an offset between the DEMs can be seen from Figures 3.1-27 and 3.1-28 which contain plots of the RMS height error as a function of terrain slope for the ANT270 height difference and the ANT90 height difference, respectively. The RMS height error increases as a function of slope. This is expected when a planimetric offset between two DEMs exists; the expected variation is a function of the tangent of the terrain slope.



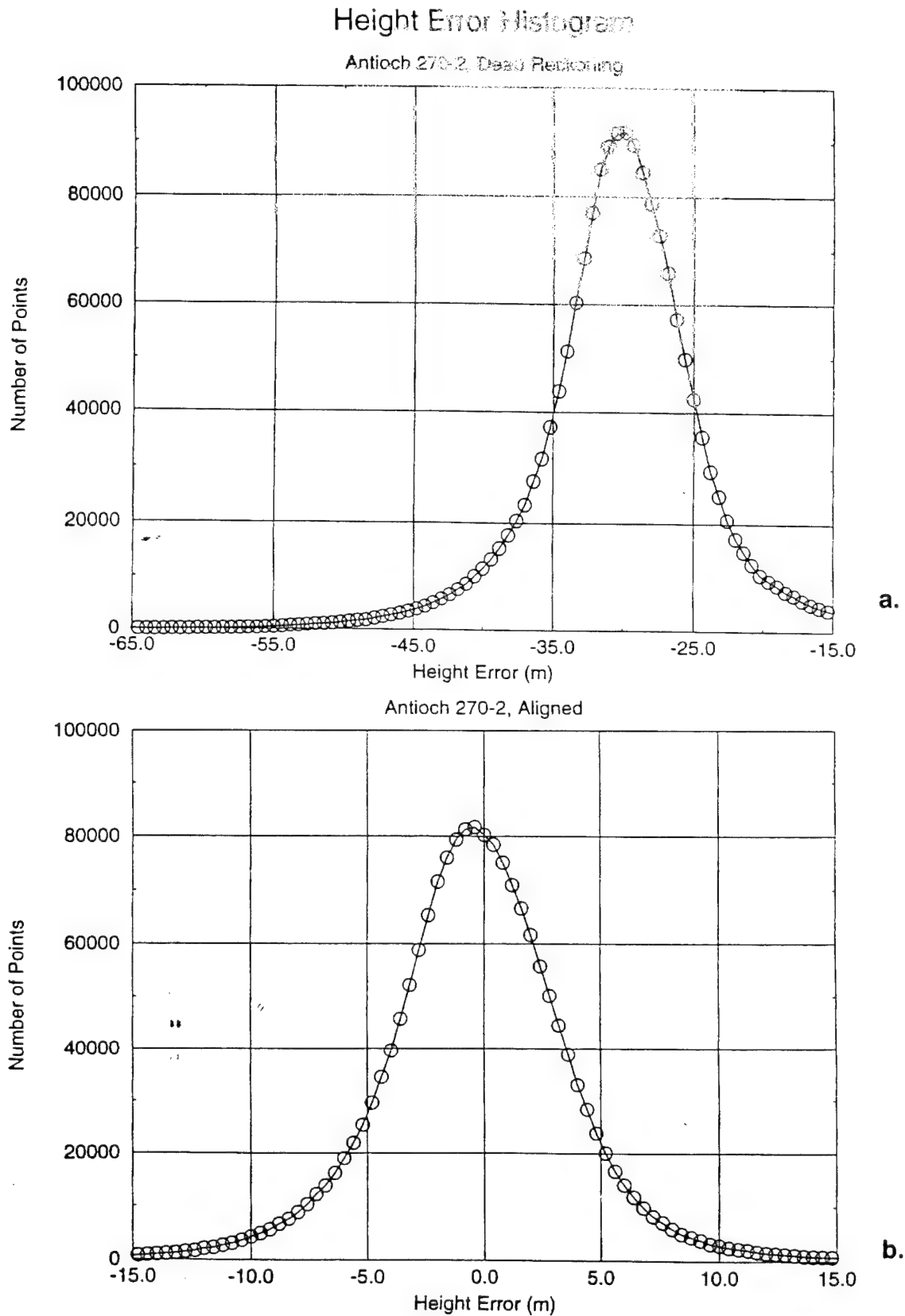
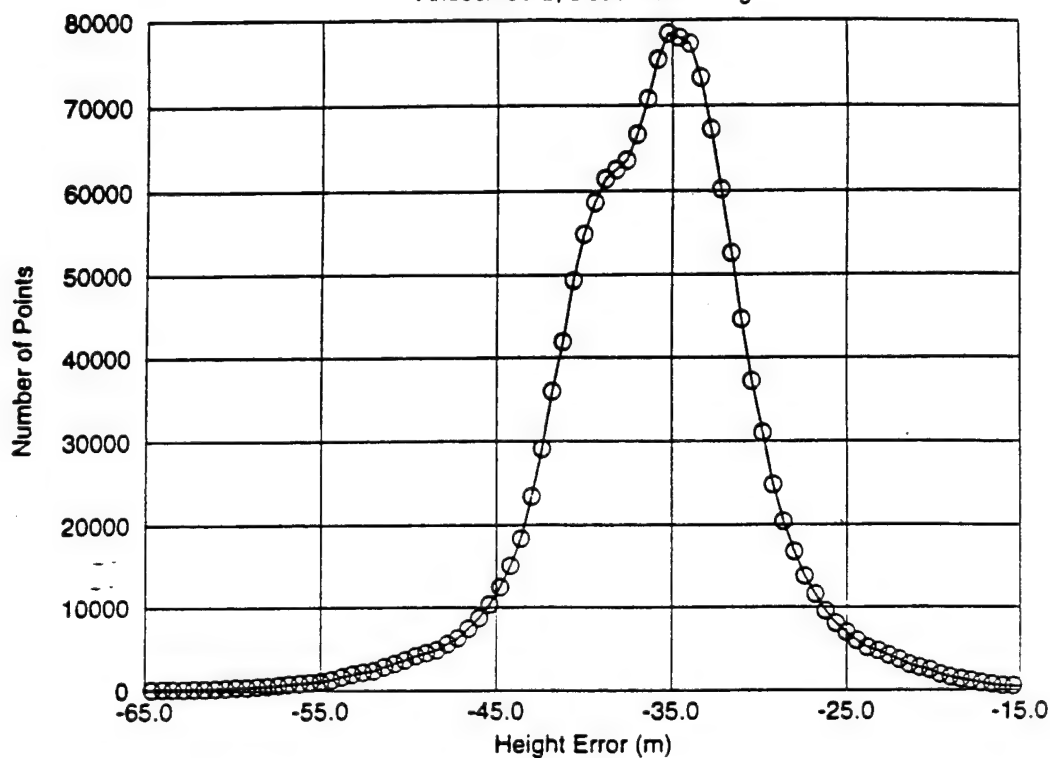


Figure 3.1-25: (a) Height error histogram for ANT270-2 using dead-reckoning. (b) Height error histogram for ANT270-2 after precise alignment.

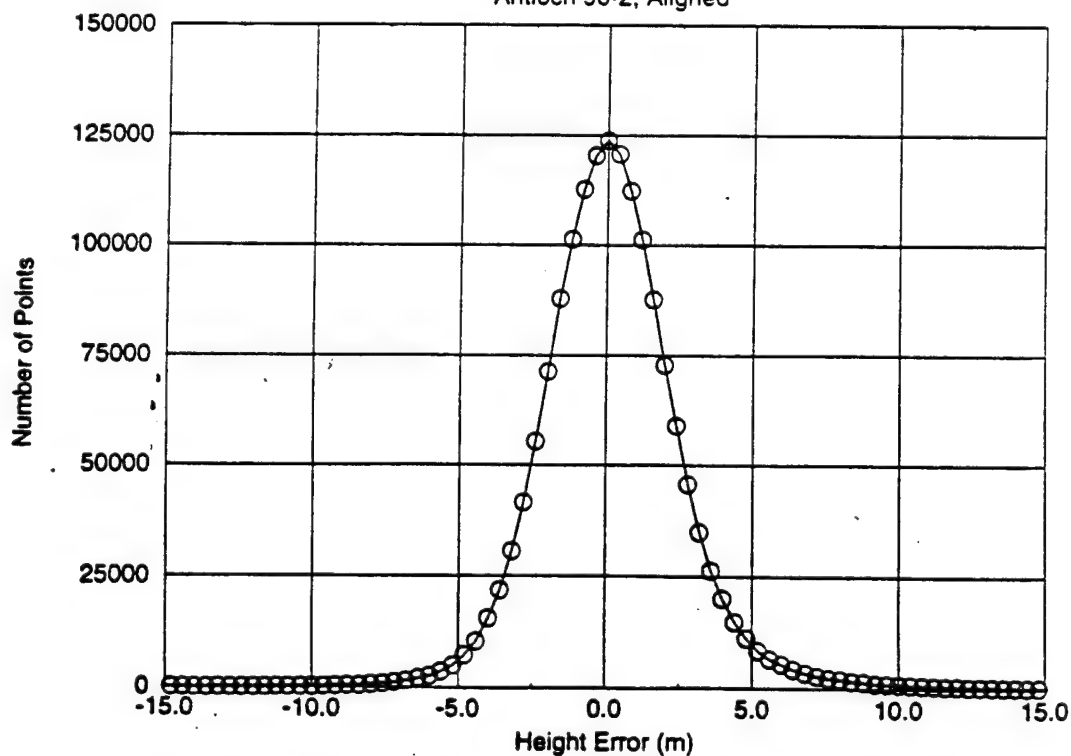
## Height Error Histogram

Antioch 90-2, Dead Reckoning



a.

Antioch 90-2, Aligned



b.

**Figure 3.1-26:** (a) Height error histogram for ANT90-2 using dead-reckoning.  
(b) Height error histogram for ANT90-2 after precise alignment.

## Height Error Std. Deviation vs. Slope

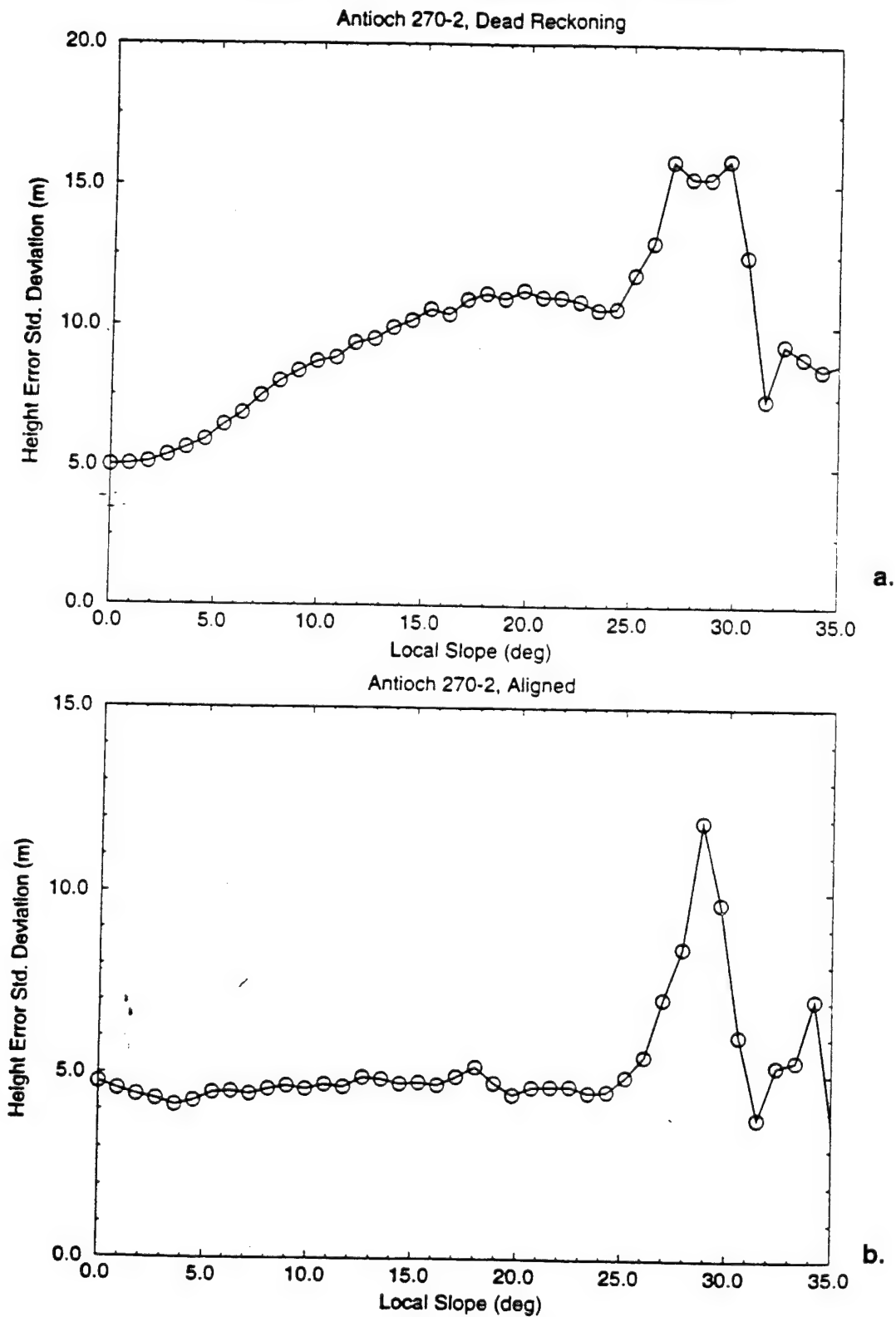


Figure 3.1-27: (a) RMS height error vs slope for ANT270-2 using dead-reckoning.  
(b) RMS height error vs slope for ANT270-2 after precise alignment.

## Height Error Std. Deviation vs. Slope

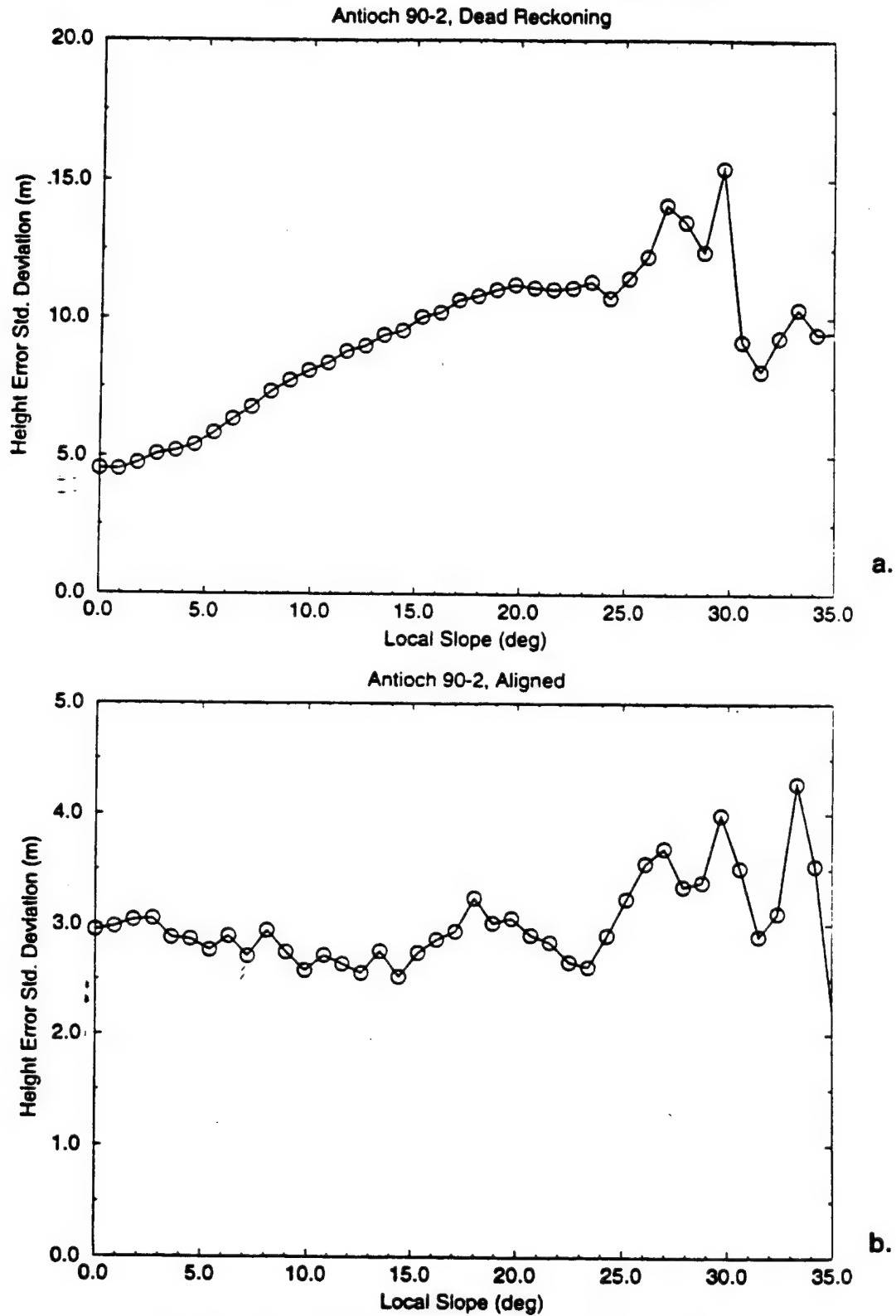
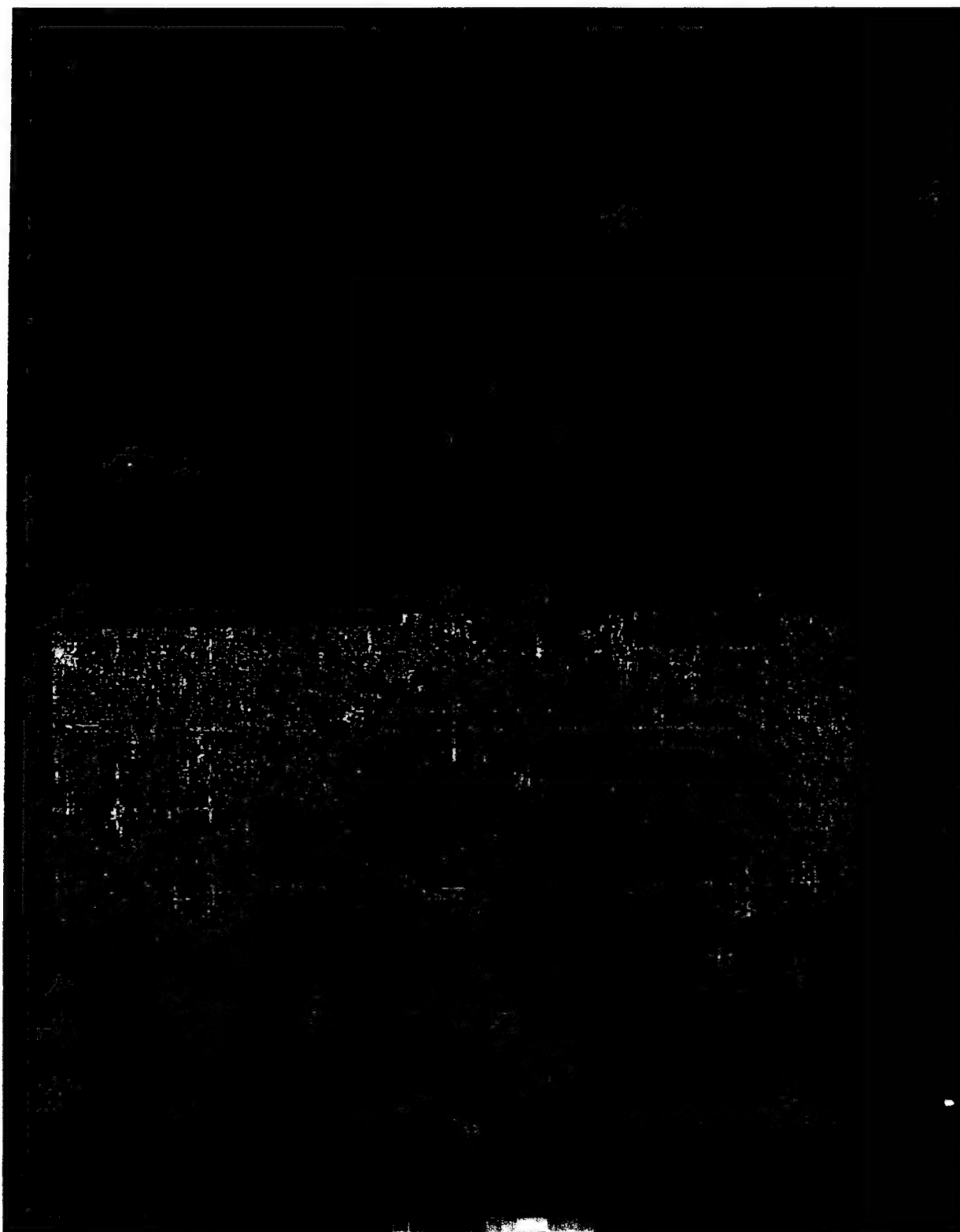


Figure 3.1-28: (a) RMS height error vs slope for ANT90-2 using dead-reckoning. (b) RMS height error vs slope for ANT90-2 after precise alignment.

Figures 3.1-29 and 3.1-30 show height difference maps between the TOPSAR DEMs for the ANT270 and ANT90 data, respectively, where an affine transformation derived from tie pointing the ANT270 and ANT90 DEMs with the reference DEMs has been used to align the data sets. The RMS height error for the ANT270 height difference is 4.5 m and for the ANT90 height difference is 3.0 m. These numbers are in agreement with expected TOPSAR height accuracy for data in the far and near ranges, respectively. Histograms of the height errors are shown in Figures 3.1-25 and 3.1-26. Note that the height error histograms are more symmetric for both sets of TOPSAR data after the offset has been removed. Additional evidence that the data have been correctly coregistered is seen in Figures 3.1-27 and 3.1-28 showing the RMS height error vs. slope for ANT270 and ANT90, respectively. Here the RMS height errors are approximately constant with slope indicating there are no residual offsets between the TOPSAR data sets and the reference DEM.

A more sensitive indication of how well the system is performing can be obtained by computing a predicted local error map using the correlation data and the DEM, and comparing it with local RMS height error derived from the TOPSAR DEM and the reference DEM. Figures 3.1-31 and 3.1-32 show the predicted local RMS height error derived from the correlation data for ANT270 and ANT90, respectively, using Equations 4 and 5 in Section 2.1.3. In these figures, the local predicted height error is shown in color with blue being 0-1.5 m RMS height error and yellow being 5 m RMS height errors. Notice that in general the predicted height errors are greater in the north of ANT90 and south of ANT270 which is the far range in both images. This is a result of reduced signal-to-noise in the far range which increases the height error. Also note that roads are clearly visible in both images where reduced correlation has increased the local height errors. To see how the local predicted height errors compare with actual local statistical height errors a 5 x 5 box centered around each point in the TOPSAR DEM and the standard deviation of the height differences with the reference DEM was computed. Figures 3.1-33 and 3.1-34 show the measured local RMS height errors for ANT270 and ANT90, respectively. The agreement between the predicted and actual observed local height errors, after eliminating all systematic errors, indicates the TOPSAR is performing as expected.

The JPL analysis shows that the primary source of errors was a half pixel offset between the reference DEM and the TOPSAR DEMs in the along track and cross track directions, and the 0.05° residual slope not removed in the calibration process. Predicted RMS height errors very closely match the observed errors indicating the TOPSAR system was operating nominally. Using the Antioch Hills reference DEM coupled with the kinematic GPS points should allow a more complete calibration of the TOPSAR radar that will eliminate most of the errors found with the uncorrected data. Because TOPSAR uses nearest neighbor interpolation to regrid the interferometric heights to a regular grid, residual half pixel offsets may not be eliminated, however for most slope hazard applications 2.5m planimetric accuracy will suffice.



**Figure 3.1-29:** Height difference map of the ANT270-2 TOPSAR DEM and the reference photogrammetric DEM after a precise alignment. Height differences are shown in color with one cycle of color representing 50m of height error change. North is at the top of the image which is approximately 10 by 12km.

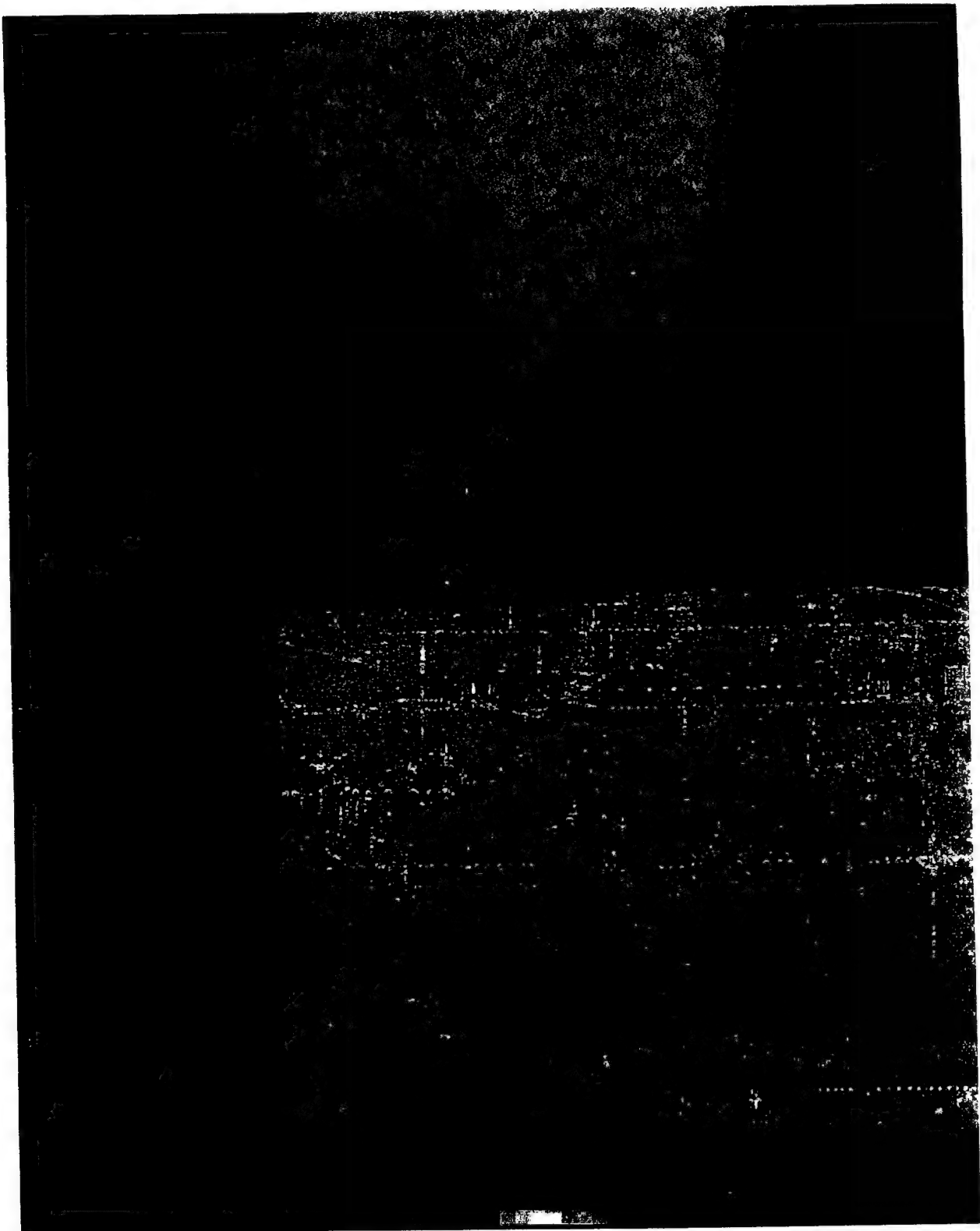


**Figure 3.1-30:** Height difference map of the ANT90-2 TOPSAR DEM and the reference photogrammetric DEM after a precise alignment. Height differences are shown in color with one cycle of color representing 50m of height error change. North is at the top of the image which is approximately 10 by 12km.



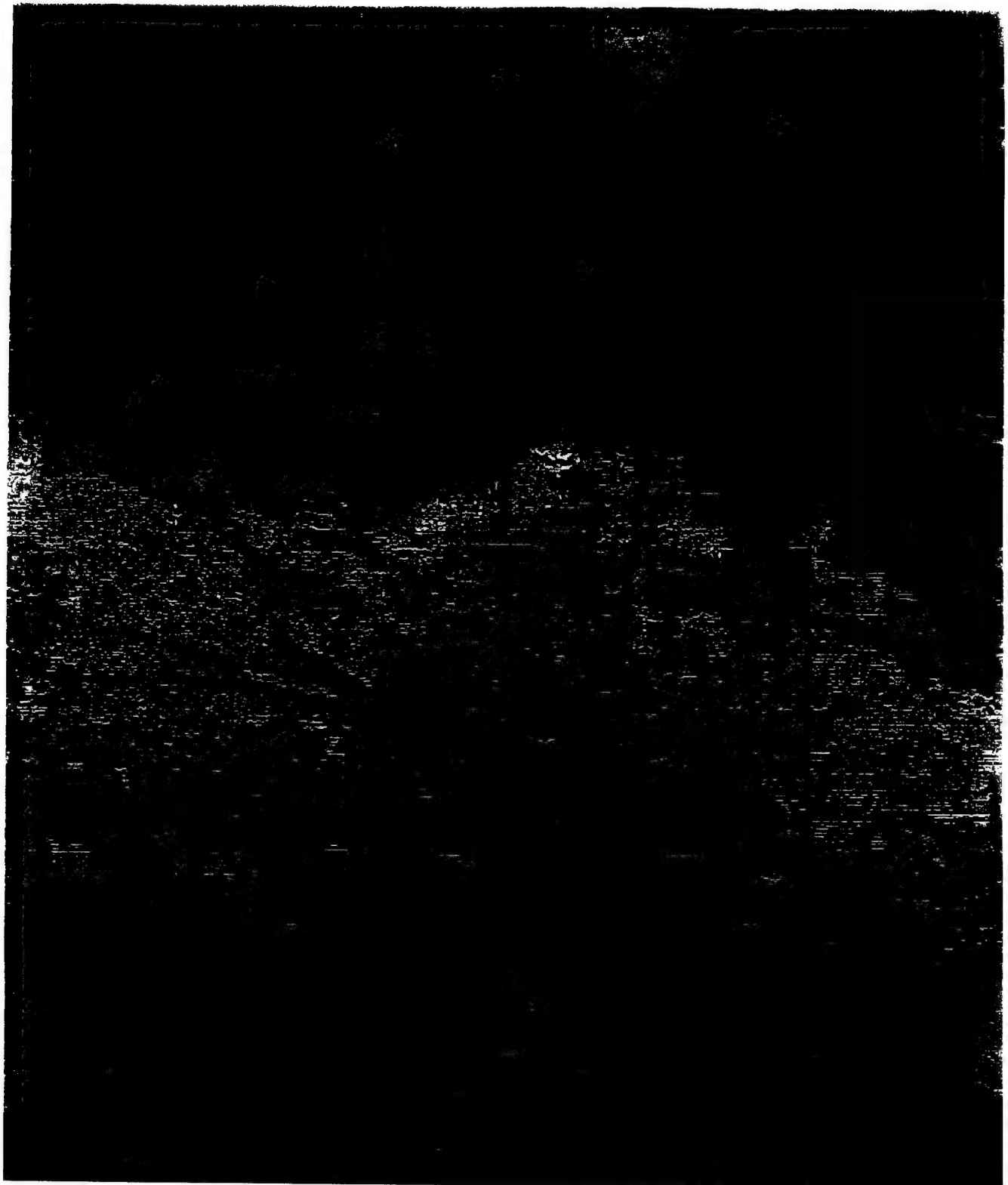


**Figure 3.1-31:** Predicted local statistical height errors derived from the correlation map for ANT270-2.  
Blue represents about 1 m RMS height error while yellow represents about 5m RMS height error.  
North is at the top of the image which is approximately 10 by 12km.

In summary, the scale of terrain features of interest in mapping seismic ground-failure hazards falls in the range of microrelief as defined by Ditzel (1989). When compiling inventories of existing hazards using air photos and imagery, we seek to identify ground failures having dimensions as small as 15m on a side. The term "identify" as used here means to enable classification of landslide type. To do so requires that features less than 15m be detectable within the slide mass. For visual identification this requires the use of 1:20,000-scale imagery or larger (Rengers et al. 1992). In order to adequately quantify the topographic habitat, we must be able to compute slope gradient and aspect to within 5 degrees with a resolution of 15m. This requires a locational precision of about 1-2m horizontal and vertical, and a DEM resolution of about 5m. Because the end user of hazard zones will be comparing zone boundaries with parcel boundaries, absolute location accuracy should be at least 5m.

### 3.1.4.2 Discussion

#### 3.1.4.2.1 Radar Imagery

An evaluation was conducted on the utility of preparing a landslide inventory by interpretation of the radar images of the study area. Three images were interpreted. Because only the northern portion of the study area was imaged the evaluation is restricted to that area. The first two images were at a scale of approximately 1:7,900 with one having a look direction to the south and one to the north. These two images provided a radar image of slopes of all aspects. The third image was of the northwest quarter of the study area at a scale of 1:4,000 with the digitized aerial photograph landslide inventory overlain. Resolution (pixel size) on all the images was 5m.

Interpretation of the three images indicates that the radar images would be useful in identifying some of the large (several tens of hectares) earthflows and slumps. The hummocky topography characteristic of earthflows can be identified by a 'speckled' reflectance pattern on the images, essentially, a mixture of light and dark pixels, adjacent to the even tones of smooth, unfailed slopes. Bulging toe areas can also be identified. Examples of these are the earthflows northeast of Kirker Creek and southeast of Sidney Flat. Slumps can be identified by their characteristic topography of bowl or amphitheater shaped crowns, steep headscarps, backturned blocks and bulging toes. Examples of these are the large slump immediately northeast of Sidney Flat, and west of Nortonville.

While the radar images interpreted in this evaluation were adequate to identify some of the large landslides they had several drawbacks. The boundaries of the larger landslide were often very diffuse and difficult to identify in detail. Landslides smaller than about a few tens of hectares could not be identified, even with the landslide boundaries overlain on the image or by comparison with the aerial photograph interpretation. The reflectance pattern simply showed a drainage or swale indistinguishable from others without landslides. Debris-flows, soil creep or gullies could not be identified. This problem may be the result of noise in the radar image which obscures the reflectance shown on the image and reduces the contrast between the pixels.

The south-facing (oriented toward or away from the radar signal) near vertical escarpments, such as those west of Nortonville, had reflectance patterns that were generally represented by dropouts or oversaturated areas where the topography could not be interpreted, other than it was very steep. The topography of steep areas with other orientations, such as immediately above and northeast of Kirker Creek, could be interpreted but the landslides mapped there by aerial photograph interpretation were too small to be identified on the radar image.

In summary, the radar image evaluated would be useful in identifying the larger landslides but is not adequate to sharply define the landslide boundaries or identify small landslides or other slope failures. These images are not suitable to prepare an accurate, detailed landslide inventory and landslide mapping based on the interpretation of these images would be incomplete. Although high quality stereo aerial photographs are far more suitable to prepare a detailed landslide inventory, there are conditions where preferential shadow enhancement and all-weather capabilities of radar imagery would prove valuable.

#### 3.1.4.2.2 Radar DEMs

The first conclusion that can be drawn from the results of this study is the reliability of the photogrammetric DEM grid which has been used as reference for testing the radar DEM data. The precision of the photogrammetrically generated elevations is inversely proportional to the photo scale used. Therefore, the DEM data from 1:10,000-scale photography offers the most precise and reliable height data. These results clearly show the absence of any systematic biases between the two photo height grids. Since the bundle adjustment of the two photo scale blocks was based on different set of ground control data, the absence of any systematic error is a convincing proof of the internal consistency of the GPS geodetic control network, and the robustness of the digital photogrammetric procedures used for generating DEM grid data. As expected, the comparative analysis does not show any significant change when the grid interval is changed from 5 m to 25m.

The major source of error in the radar DEMs results from the lack of complete calibration. As the flight line was inadvertently displaced to the north, the southern extent of the radar coverage did not reach the southern series of surveyed ground control points. This has introduced a half-pixel planimetric offset and a  $0.05^\circ$  residual slope not removed in the calibration process, which will limit the degree of correlation between the radar DEMs and photogrammetric DEMs. Planimetric errors will cause errors in height estimates that increase proportionally with slope gradient, which may partly explain the trend shown in Table 3.1-3. Although the radar could be corrected by a more complete calibration using a photogrammetric DEM, this would have defeated the purpose of independently comparing the radar DEM to the ground-truth DEM. Regardless, navigational flight errors are avoidable and more extensive ground control will permit more comprehensive calibration for future data acquisition.

Data voids or drop-outs occur in both sets of radar data. They are caused by layover in the near range and by shadowing in the far range, and are inherent to radar data collection over steep terrain. The large negative height errors located along the edges of the drop-out areas are the result of edge effects caused by the interpolation process applied while transforming the data into a cartographic projection. This problem was subsequently corrected by Calgis. It may be possible to reduce the area affected by data drop-outs by flying overlapping or cross coverages; however, this would increase the flight time and volume of data to process and may not be cost effective.

Thermal variations along the transmission path of the radar, introduces random errors in height estimates that cannot be completely eliminated. Thermal noise is more severe in the far range as demonstrated in the ANT270 radar products (Figures 3.1-6, 3.1-20, and 3.1-33). Such error may represent the ultimate noise floor for radar-derived DEMs.

As discussed in Section 2.1.2, much of the error observed in the radar data evaluated in this experiment is largely predictable and can be reduced significantly. When large errors in the radar DEMs are discarded, the RMSE is about 4.5m. A separate data set in a different area of the Antioch Hills Test Site was corrected for ground registration and yielded slightly better precision (3.0 to 4.5 m RMSE) without removing any data points (see Section 3.1.3.4).

In summary, independent analyses of the TOPSAR data were performed by DOC, Calgis, and JPL. All three investigations arrived at similar results, however a number of small differences were observed. DOC and Calgis are primarily interested in the accuracy of the TOPSAR data relative to the National Map Accuracy Standards, and hence performed the comparison in a planimetric reference frame. According to JPL, the mean height error and larger than predicted RMS height errors between the reference DEMs and the TOPSAR data sets are due to the  $0.05^\circ$  slope in the TOPSAR data and the half pixel of misregistration between the data sets. The large slope dependent height errors observed in DOC analysis will be greatly reduced with adequate ground control coverage for the TOPSAR data as shown by the JPL analysis. The larger RMS height error in the ANT270

compared to the ANT90 is mainly a result of the comparison region being in the far range of the TOPSAR swath for the ANT270 data. The increase can be produced directly from the correlation data as shown in the JPL analysis.

Although future improvements in the data acquisition system will further increase the accuracy of radar DEMs, the data analyzed here are much better than that currently available for California. RMSE is a factor of 2-3 less, while the resolution is a factor of 6 better (36 times the density of information) than what is currently available from the USGS. Based on the National Map Accuracy Standards, a standard deviation of 4.5m in the radar DEM data would make it suitable for use for maps with a 15 to 20m contour interval (American Society of Photogrammetry, 1980). While further improvements may ultimately permit attaining the target goal of 1 to 2m accuracy, which will fully meet the desired standards for the State's seismic hazard mapping efforts, current capabilities of IFSAR-derived DEMs can be immediately used to improve the evaluation of seismic hazards.

#### 3.1.4.2.3 Recommendations for Further Work

Based on the evaluation of the initial radar data set, IFSAR clearly demonstrates the potential for rapid production of accurate DEMs over non-vegetated areas. A second flight is planned to acquire high-quality data over Antioch Hills, with adequate ground control. That data should not contain the registration errors inherent in the present data series, and will be evaluated according to the National Map Accuracy Standards perspective.

Additional work to be completed for the Antioch Hills experiment includes: 1) a comparison of the radar-derived DEM with a 1:40,000-scale photogrammetrically-derived DEM, and 2) generating a DEM from the USGS contour plates covering the study area in the Antioch Hills, and comparing it to the radar- and photogrammetrically-derived DEMs. Results indicate that the accuracy of radar-derived DEMs used in this study does not meet the quality of the 1:20,000-scale photogrammetric DEM, and may be closer to the accuracy of DEMs derived from 1:40,000-scale aerial photography. This needs to be evaluated because of the greater cost efficiency against which the radar method must then be compared. The second objective represents an economical alternative method of acquiring improved DEMs over what are currently available. It remains to be demonstrated how much better radar-derived DEMs are than those developed from original USGS topographic surveys using GIS technology.

A potentially valuable future research topic is the development of an automated landslide detection algorithm. Considering the markedly distinct geomorphology of slope failures, which typically contrasts with the surrounding undisturbed terrain, and the ability of radar DEMs to quantify these characteristics, there exists the possibility of training the computer to recognize landslide features. Such a capability could significantly expedite the landslide inventory process, quickly leading the analyst to candidate landslide features while allowing the analyst to make the final judgment call. With the extensive calibration that has been completed during the first year of the GeoSAR program, the Antioch Hills Test Site would be the ideal laboratory for such an experiment.

### 3.2 ANTIOCH HILLS, LAND USE AND LAND COVER EXPERIMENT, FARMLAND MAPPING PROGRAM

#### 3.2.1 Abstract

Data from the May 1994 JPL C-band interferometric radar flight of Antioch, California was evaluated for mapping of agricultural, urban, and native land cover classes. Radar magnitude, correlation, and DEM products were used alone and in combination with TM multispectral and SPOT panchromatic data, for specific application to the classification requirements of FMMP, and for general land use mapping potential. The 17,126 hectare study area lies at the rapidly urbanizing eastern edge of the San Francisco Bay area and contains delta agriculture, extensive marshlands, and grassland habitats. A 1994 ground truth map for the area was compiled with traditional air photo and field reconnaissance methods.

Precision point placement tests indicated that the radar imagery had higher spatial accuracy than the rectified TM and SPOT data; the satellite data was then resampled to the 5m radar data. Image enhancement routines included magnitude and correlation normalization, pixel substitution, principal components analysis, and IHS/RGB transformations. IHS-enhanced TM images (432 combination) using radar and other data types as intensity were compared for clarity in a 'heads up' digitizing test; radar enhancements improved the ability to discern among dry vegetation types and urban construction zones but decreased agricultural category differentiation. Automated classification tests were conducted on radar alone, TM alone, and radar/TM combinations using the training and classification algorithms resident within in-house software. In most tests, five major land cover classes were clustered from 18 spectral classes. Comparisons between the control land use and automated classifier results were inconclusive as to which band combinations were most accurate for automated land use mapping. Inherent differences between desired land use classes and spectral land cover classes will require further work to refine classification methods for better clustering results.

#### 3.2.2 Introduction

##### 3.2.2.1 Purpose

FMMP was established in 1982 to develop and maintain data on agricultural land use conversion in California and to provide this data in map and statistical formats to decision makers, planners, and the public. Map categories include a qualitative set of agricultural classes based on modern soil surveys, as well as grazing, urban, water, and miscellaneous categories. The project covers 17.3 million hectares as of 1994, with new regions being added to the FMMP database as modern soil surveys become available. Land use covering 1762 1:24,000 USGS quad sheets is updated every 2 years.

The FMMP currently uses a map updating system that consists of aerial photo interpretation and field verification at 1:24,000; digitizing and linework clean up; and production of new maps for public review at 1:100,000. Linework and database operations are carried out on Intergraph workstations, resulting in farmland maps and conversion statistics for each of 47 counties in the survey area, as well as regional and projectwide summaries.

Because of the need for current and widespread air photo coverage, FMMP has relied on purchased high altitude color infrared (CIR) photography of California's Central Valley from NASA-Ames and rented photography at various formats and scales from private sector air photo vendors in the major urban areas. Current photo coverage is limited in many rural areas of interest to FMMP. The uncertainty of coverage, inconsistency of data sources, and extensive labor involved in manual photo interpretation are of concern for quality control and cost reasons.

Improvements to FMMP's current workflow which would further automate data collection and analysis utilizing remote sensing technologies are being investigated. For DOC's GeoSAR study, the Antioch site in Contra Costa County was selected due to the pace of urban development witnessed at the agricultural fringe. Urban acreage in the county increased by 12% between 1984 and 1992, predominantly from land that formerly supported irrigated agriculture and grazing (DOC, 1994).

The purpose of this experiment is to evaluate the use of radar products, alone and in combination with commercially available sensor data, (1) for FMMP's land use classification and change detection requirements, (2) for GeoSAR's potential to improve the land use classification accuracy of commercially available multispectral data, and (3) for the potential to automate FMMP procedures and upgrade products currently produced using traditional air photo interpretation and field mapping methods.

### 3.2.2.2 Objective

Year 1 objectives for this experiment included the procurement, registration, enhancement, and initial classification of GeoSAR data and commercial satellite imagery as appropriate to FMMP's mapping system. The expertise of study participants and capabilities of the available image processing software were the bases for determining the most promising approaches to land use classification using GeoSAR data. Year 1 output objectives included initial classification map and image products, as well as a preliminary analysis of the applicability of GeoSAR products to FMMP's workflow.

Objectives for Year 2 and beyond include more detailed analyses of classification accuracy using these data, refining classification algorithms, change detection analysis, and conducting initial analyses in other regions of California of interest to FMMP.

### 3.2.2.3 Site Description

The Antioch study area is located at the eastern edge of the San Francisco Bay and is an active interface between urban development, agriculture, and native land cover. The area totals 17,126 hectares or about 1.1 times the size of a 1:24,000 USGS quad. Agricultural uses include deciduous orchards and vineyards, field crops (wheat, corn, milo, sorghum, asparagus), irrigated pastures, idle fields, and one dryland grain field. Urban lands include a wide array of industrial, commercial and residential uses, developed parklands, and rural residential lands (mixed use parcels of .6 to 4 hectares). Hillside and formerly agricultural areas are being prepared for development with levelling and excavation equipment. Extensive natural areas are devoted to grasslands, wetlands, and permanent water bodies. Figure 3.2-1, 1994 Land Use Classes, shows actual land use at the time of data acquisition in late spring of 1994.



### 3.2.3 User Experiment

#### 3.2.3.1 Methodology

FMMP's Year 1 GeoSAR analysis was designed to follow standard remote sensing procedures for compilation of land use data in order to compare the results using raster-based methods with those of traditional photographic-based mapping processes. Because FMMP's agricultural mapping categories are a composite of current land use (irrigated versus non-irrigated) and qualitative soil ranking (highest quality soils are considered Prime, etc.), a set of more direct agricultural land cover categories (field crops, pastures, etc.) were used for this study. The urban category groups most industrial, commercial, and residential uses; while large vacant parcels and parks are categorized separately (see Figure 3.2-1).

Ground truth data representing the desired land use categories for the planned 6-quad area were compiled current to the radar flyover date of May 27, 1994. A number of different data sources, as described in section 3.2.3.2, was used in the compilation. The boundaries of FMMP's study area were modified after radar data were received to take advantage of coverage east of the planned study area that substantially increased the agricultural acreage which could be analyzed. Ground truth information was amended and the land use data was digitized into a UTM zone 10, NAD 27 seed file, which is the standard FMMP file format.

Following the radar flight, photographic and satellite data that would be used for comparison was obtained. Dates of satellite acquisition, cloud cover, and digital data quality determined which imagery was obtained. Data procured included SPOT Image Panchromatic data (June 18, 1994), Landsat Thematic Mapper data (July 1, 1994), and 1:40,000 black and white aerial photography flown by Calgis (August 10, 1994). Satellite data were obtained in rectified UTM format to facilitate registration processes.














Three layers of radar data were received for analysis: a brightness or magnitude image, a digital terrain elevation (DEM) raster, and a data reliability measure known as a correlation layer. The correlation layer is a function of signal to noise ratio, geometric factors and volume scattering. The initial data shipment (the 270 series data) was flown from east to west with a southerly look angle. Subsequently, magnitude and DEM data flown with a northerly look angle (90 series), as well as a file representing the results of JPL's automated classifier, were received. Radar data were received with 5m postings, while the SPOT and Landsat (TM) data were 10 and 25m, respectively. Data registration required resampling to a control image and uniform pixel size. Precision point placement tests of the satellite and radar magnitude data compared with a softcopy stereo image produced from the low altitude photos revealed that TM data had a registration offset of two or more 25m pixels, while the radar data was within 1 to 2 5-m pixels. Thus, TM and SPOT were resampled to the radar data using a series of control points with an affine transformation and nearest neighbor routine.

As a result of the resampling using radar data as the control, the TM and SPOT data were shifted to the radar's coordinates (State Plane California zone 3, NAD 83). Secondary coordinate system parameters in the imagery headers and in the ground truth design file had to be adjusted to allow for registration using WGS 84 coordinates as a translator. The 90 series radar, as initially received, was also slightly offset from the 270 series. Image to image registration, using the 270 series as control, was conducted with resampling parameters as described above. Later versions of the Calgis conversion routine from the JPL format allowed for this resampling to occur as a single step process.

Two characteristics of the radar data needed to be modified to facilitate image processing. Since the image classification software used does not accommodate the radar's floating point data, conversion to 8-bit unsigned data was necessary. In addition, the radar magnitude data were highly skewed toward the lowest values (see Section 3.2.3.3). A routine which accomplishes the 8-bit



## 1994 LAND USE CLASSES, ANTIOCH HILLS AREA

-  **Urban Land**  
Land occupied by structures with a building density of at least 1 unit to 1.5 acres or approximately 6 structures to a 10-acre parcel.
-  **Urban Construction and Levelling**  
Land on which pads have been graded and construction of roads and buildings have begun.
-  **Urban Parks and Greenspace**  
Golf courses, developed parks and cemeteries.
-  **Rural Residential**  
Land occupied by structures with a building density of at least 1 unit to 10 acres.
-  **Orchard and Vineyard Crops**
-  **Annual Field and Truck Crops**
-  **Irrigated Pasture**
-  **Non-irrigated Grain Crops**
-  **Idle Farmland**
-  **Urban Vacant Land**  
Barren or disturbed lands within or adjacent to urban land.
-  **Grasslands**
-  **Marsh and Tidal Lands**
-  **Water**  
Open water areas, water courses, and man-made water holding structures.

0 500 1000 2000 Meters



California Department of Conservation  
Farmland Mapping and Monitoring Program  
GeoSAR Study

Figure 3.2-1: 1994 Land use compiled using aerial photograph, agricultural commissioner records, and field reconnaissance.

conversion as well as normalizing the magnitude data was developed by Calgis. For initial testing, correlation and DTE data were converted to 8-bit using the routine resident in the software.

Image enhancement routines included removal of atmospheric haze, histogram stretches, and intensity-hue-saturation (IHS) transformations of the TM data, as well as principal components (PC) analysis of the radar data. Selective merging of 90 and 270 series data was used to decrease the number of null or oversaturated pixels. Notable results of these techniques for improved visual analysis of the data are described in section 3.2.3.3.

Land use classification was approached using two methods, one focusing on human analysis of enhanced images and the second on automated analyses of spectral data with in-house software. The enhanced image clarity or "heads up" digitizing test compared four IHS-enhanced image permutations as the data sources for a trained photo interpreter mapping the desired categories. The number of misclassified and unknown hectares would be used as a relative rating of image enhancement.

The automated classification trials consisted of systematic application of the training and classification algorithms contained within the software to radar layers alone, radar combined with TM, and TM imagery alone. A large number of initial trials, varying the parameters of each training method, were used on the radar data layers alone with a minimum distance classifier; those which yielded poor visual results were discarded. The best set of parameters for each training method were then applied to the six TM layers alone and the nine combined bands of TM and radar; again using the minimum distance classifier. The most satisfactory training sets were then tested on a maximum likelihood classifier and hybrid classifiers within the software. The relative number of misclassified and unclassified pixels compared with the control land use vectors were used to rate the results.

### 3.2.3.2 Field Evaluation

Prior to the May 27, 1994 radar flight, land use within the planned 6-quad study area was compiled at 1:24,000 by updating and modifying FMMP's 1992 Important Farmland maps. Supplemental data sources included 1992 field notations regarding areas with expected change and in-house photo coverage from August 1993 and February 1994. Ground surveys occurred on May 26 and 27, 1994, focusing on areas of land use change expected from these prior information sources as well as site visits to each agricultural field in the study area.

Upon receipt of the 270 series radar data and the August 10, 1994 air photos, flight index maps were drawn up which revealed that the southern portion of the planned study area was missed. However, radar coverage extended east into an area which contained a better mix of land uses, particularly more irrigated agriculture, than the original area. The boundaries of FMMP's study area were shifted to take advantage of this opportunity.

Gathering ground truth for the modified study area was complicated, however, due to the fact that by the time the radar coverage shift was mapped out, the 1994 growing season was over and wet ground limited access to agricultural areas. Thus, parcel by parcel research on 1994 crop patterns as contained within county agricultural commissioner's records was conducted. This first required compilation of a list of grower names from local agriculture officials, which included individual land owners, agricultural corporations, and lessees. Files based on grower names were then examined for maps and field data on the crops grown in 1994.

After the land use data was gathered, digitizing at 1:24,000 occurred and a database representing all categories present on the map was developed for production of acreage calculations. The study area totalled 17,126 hectares in Contra Costa and southern Sacramento counties. Figure 3.2-1, 1994 Land Use Classes, depicts the ground truth with base map information.

### 3.2.3.3 Results

The Antioch land use experiment was designed primarily to test GeoSAR image products, the magnitude and correlation layers, for usefulness in determining land cover types. Other components of the GeoSAR study focused on spatial accuracy testing of these products. Likewise, image processing conducted by JPL prior to release of the data is discussed elsewhere in this report. Hence, post-delivery image enhancement and classification methods and their results are discussed in this section.

#### 3.2.3.3.1 Image Enhancement

Contrast adjustments, histogram manipulations, elimination of atmospheric interference, data substitution and other adjustments are commonly made to raster imagery in order to improve its clarity and remove undesirable influences. Enhancements to both TM and radar images were conducted for this experiment, and are discussed in this section and in section 2.2.4.

##### 1. Data substitution

Both the 90 and 270 series of radar data contained a percentage of null and oversaturated pixels which prevent any type of analysis. In most instances, these unusable pixels were located in the radar shadow of hilly areas or were associated with highly reflective hard targets in the industrial area along the waterfront. In addition, the 90 series data did not cover 9.34% of the study area at its the northern edge. Table 3.2-1, Antioch Land Use Study, Radar Magnitude Substitution Effects, shows the number and percent of null and missing pixels in each of the data sets.

**Table 3.2-1: Antioch Land Use Study, Radar Magnitude Substitution Effects**

	90 series(1)	270 series	"90270 maximum"
# null pixels (bin 0)	897,312	163,610	55,625
# oversaturated pixels (bin 255)	66,247	102,963	66,247
Total unclassified pixels	963,559	266,573	121,872
% unclassified pixels	14.05%	3.88%	1.77%

Total 5m pixels in study area      6,853,224

(1) 90 series data did not cover northern margin of study area. This gap accounted for 9.34% of total study area.

A 2-step data substitution was performed which decreased the proportion of unclassified pixels to 1.78% from a high of 14.06% in the 90 series data. First, the large number of oversaturated pixels (bin 255) in the 270 series data were reassigned to bin 0, and second, the 90 and 270 data were compared and the higher of the two corresponding pixel values (maximum analysis) was used in forming a new image. A test of image averaging as opposed to selection of maximum values was also conducted, but the resultant image was concentrated in the lower bin values and was unacceptable for further analysis. The '90270 maximum' image was then used in the classification tests which followed.

## 2. Intensity-Hue-Saturation (IHS) transformations

Three imagery layers are commonly combined to form color or RGB images for highlighting desired features. The color values produced by portraying three bands together can alternatively be described in terms of hue or wavelength, saturation or purity, and intensity or brightness/dullness. An RGB image can be converted into IHS values and each of these can be stretched or replaced with other data; then inserted back into an RGB format (Mather, 1994). While normal histogram stretching of the intensity layer can increase contrast in a TM image, substitution of data such as SPOT or radar for intensity may provide even greater image detail for subsequent analysis.

In this experiment, radar was used in the form of PC1 (270 series data) as the intensity band in a 'heads up' digitizing test of image clarity. Three other combinations substituted the following data layers for intensity: (1) the unaltered TM intensity, (2) a mathematical average of PC1 and the TM intensity, and (3) the SPOT panchromatic layer. The clarity of each image would be tested by having a trained photointerpreter categorize the Antioch study area into the desired land use classes and digitize linework representing the known and unknown portions of each of the four images. Each set of linework would then be compared to the ground truth for errors and degree of uncertainty.

The RGB combination used in this experiment includes TM bands 4, 3, and 2 assigned as red, green, and blue, respectively. Growing vegetation absorbs blue and red light (bands 1 and 2) to provide energy for photosynthesis, while it reflects both green and near infrared portions (bands 3 and 4) of the spectrum (Sabins, 1987). The 432 TM combination creates an image which emulates the CIR photography used by FMMP, in which growing vegetation appears bright red. While other TM combinations could also be used for land cover mapping, interpreter familiarity with this spectral combination would help to eliminate uncertainties due merely to the changed spectral characteristics of otherwise familiar signatures.

The IHS-enhanced Imagery Comparison, Table 3.2-2, indicates that all of the images reasonably distinguished the Urban Land and Water classes, with differences of between 0.83 and 7.45% from

**Table 3.2-2: IHS Enhanced Imagery Comparison**

Category	Control Hectares	TM 432 Hectares % error	PC1 enhanced Hectares % error	Average PC1 & TM Hectares % error	SPOT enhanced Hectares % error
Urban grouping	5,516	5,892 6.82%	5,524 0.14%	5,459 -1.04%	5,665 2.70%
Urban Land	5,056	5,197 2.78%	5,098 0.83%	4,905 -2.99%	4,811 -4.86%
Urban Construction	268	388 44.49%	146 -45.55%	222 -17.19%	440 63.95%
Urban Parks	63	44 -30.13%	53 -15.38%	54 -14.10%	56 -10.90%
Rural Residential	128	264 105.68%	226 76.03%	277 116.09%	358 179.18%
Agriculture grouping	2,909	1,573 -45.92%	1,296 -55.45%	1,139 -60.85%	1,974 -32.16%
Orchard & vineyard	765	0 -100.00%	0 -100.00%	0 -100.00%	237 -69.05%
Annual field & truck crops	1,309	1,061 -18.92%	2,626 -18.83%	771 -41.08%	1,095 -16.35%
Irrigated pasture	836	512 -38.74%	233 -72.06%	368 -55.98%	642 -23.15%
Dry vegetation grouping	3,289	2,390 -27.32%	3,166 -3.74%	3,382 2.84%	2,721 -17.26%
Urban Vacant	1,064	577 -45.80%	2,420 -7.95%	1,018 -4.30%	947 -10.95%
Non-irrigated grain	112	0 -100.00%	0 -100.00%	0 -100.00%	0 -100.00%
Idle farmland	540	126 -76.72%	0 -100.00%	667 23.35%	109 -79.79%
Grasslands	1,572	1,688 7.36%	2,187 39.07%	1,697 7.95%	1,664 5.87%
Marsh & tidal land	1,733	1,855 7.05%	1,857 7.19%	1,820 4.60%	2,006 15.74%
Water	3,679	3,665 -0.36%	3,492 -5.06%	3,600 -2.12%	3,405 -7.45%
Unknown	0	1,749	1,790	1,733	1,355
<b>Total</b>	<b>17,126</b>	<b>17,126</b>	<b>17,126</b>	<b>17,126</b>	<b>17,126</b>
<b>Study area, % unknown</b>		<b>10.22%</b>	<b>10.45%</b>	<b>10.12%</b>	<b>7.92%</b>

the control acreages. Agricultural differentiation, however, was poor in all the images. None of the enhancements allowed detection of the non-irrigated grain field, and only the SPOT-enhanced image enabled discrimination of certain orchards and vineyards as such in the study site. The proportion of unclassifiable pixels ranged from 7.92% for the SPOT enhancement to 10.45% for the PC1 enhancement. These pixels would, in practice, be field checked by the analyst to determine which would be the proper category.

The radar-enhanced products, particularly the enhancement which used the average value of PC1 and TM intensity, produced better results than SPOT in the dry vegetation grouping, Water, Marsh, and Urban Land categories. The PC1/TM average had the best visual discrimination between Urban Construction areas and other categories of all the permutations. This is an important indicator of changing land use considered critical to FMMP's workflow.

In all four images, three categories were consistently overmapped: Rural Residential, Grasslands, and Marsh and tidal lands. Seven categories were undermapped in all images: Urban Parks, Urban Vacant, Non-irrigated grain, Water, and the three irrigated agriculture classes. Some of these discrepancies may be explained by image resolution and time of data acquisition. Tidal influence may account for some of the differences in the Water and Marsh categories from image to image. The lack of detail in the images led to misclassification of dry vegetation types and irrigated land into the Grasslands category. The reflectivity of the soil as well as the pixel resolution are likely to have impacted the ability to detect vineyards in the study area. Since the commercial imagery acquisition dates were June 18 and July 1, trees and vines were completely leafed out such that this should not have affected the results.

Analysts rated the PC1 image as the most difficult to work with, as contrast and colors were harsh. Three land use classes – Orchard/vineyard, Non-irrigated grain, and Idle farmlands – were not discernible in the PC1-enhanced image. The averaging with TM intensity helped to mute this harshness and also brought back some of the subtleties to improve mapping capabilities in categories such as Urban Construction.

#### 3.2.3.3.2 Automated Image Classification

Automated classification attempts to categorize each image pixel into land cover classes based on spectral response patterns present in each band used for analysis (Mather, 1994). It consists of two primary steps: training and classification. In the first step, subunits of the study area are chosen for statistical analysis and grouped in various ways to obtain the best class differentiation possible. This is accomplished either by using ground control information as a means of determining spectral response patterns (supervised training) or by allowing the software to aggregate data into appropriate spectral associations (unsupervised training). Once the patterns for each category have been determined for the subunits, each pixel in the image is classified based on how closely its spectral response matches that of the training data. The classification algorithms also use a number of different measures to determine in which category to place a given pixel.

For this experiment, the Antioch study area was classified using the suite of training algorithms available in the in-house software, to determine which methods yielded the best result with the radar data. These algorithms each use different parameters to aggregate or split data to arrive at



unsupervised training set results. Supervised methods, using the control land use design file, were also tested. A brief description of each is contained in Table 3.2-3, Training Algorithms Used in Automated Classification, Antioch Land Use Experiment (Intergraph Corp., 1994).

**Table 3.2-3: Training Algorithms Used in Automated Classification, Antioch Land Use Experiment (1)**

Algorithm	Description
K-means	The sum of the squared distances (in all bands) from the pixel value to the mean pixel grey level value is used as an index. Algorithm attempts to minimize the index until within user-specified tolerance. Behavior is affected by the number of classes selected and choice of cluster centers.
Isodata	A cluster-seeking algorithm in which cluster centers are iteratively determined sample means. Clusters are lumped or split based on user-specified tolerances, including minimum cluster size.
Aggregate	A clustering algorithm which uses a threshold for determining either a natural or a preset number of clusters. Class mean is considered the cluster center and the threshold is a geometric radius. All pixels outside of threshold are discarded.
Competitive	A clustering algorithm which begins with a randomly selected mean for each band and a given number of clusters and iterations. A distance measure is applied and means of the closest clusters are updated; low count clusters eliminated with a threshold. This algorithm is designed around the neural network concept.
Supervised	Manual selection of classes and clustering units based on polygons drawn by the analyst or by region growing parameters.

(1) Descriptions excerpted from Modular GIS Environment/ImageStation Imager-3 User's Guide, Volume 2, Chapter 10, Intergraph Corporation.

Tests of training algorithms, all using the same classifier, were first conducted on three layers of radar data: the 90270 substitution magnitude, the 270 series correlation, and the 270 series DTE. Each method was used a number of times, varying parameters within the algorithm, in effort to improve the results. All of the early tests were rated on a visual comparison between them and the control design file and on the proportion of unclassified pixels.

Factors that were found to improve all of the unsupervised methods were: (1) the number of iterations the training routine was allowed to conduct, (2) the sampling percentage used for the training, and (3) the number of categories selected for discrimination. Generally speaking, the larger the number of each of these, the better the result; although this began to be offset by higher processing and analysis time. After multiple tests, the best balance was being achieved with settings of 30 iterations, 5% sample, and 18 clusters for discrimination. The aggregate algorithm was found unacceptable with the radar data due to the high proportion of the image (40 to 60%) that was left unclassified.

Following minimum distance classification, the 18 original classes determined with the three unsupervised methods were grouped into like categories, resulting in five master land cover classes: Urban, Agriculture, Dry vegetation, Marsh, and Water. In the supervised method, polygons were added to or dropped from the training set to reduce variability within a desired class, thereby achieving better differentiation. The same five master categories were sought for the supervised method as with clustering of the unsupervised data. All classmaps were then simplified with a 10x10 mode filter.

The best results of the four training methods were saved; then the same parameters were applied to the 6 TM bands alone and a combination of TM and radar (nine bands total). The classification maps (four training algorithms x three band combinations) were compared to one another and to the control land use. The acreage results for the best classification maps for each band combination, as well as those from the JPL automated classifier, are contained in Table 3.2-4, Automated Classifier Acreage Results.

Table 3.2-4: Automated Classifier Results

	Control air photo	Radar only				Radar & TM		TM only	
		JPL (1)		K-means		Isodata		Isodata	
Category	Hectares	Hectares	% error	Hectares	% error	Hectares	% error	Hectares	% error
Urban grouping	5,516	5,900	6.94%	4,954	-10.19%	3,893	-29.41%	4,059	-26.41%
Agriculture/vegetation	2,910	3,157	8.51%	3,750	28.87%	3,240	11.34%	3,298	13.33%
Dry grasses/bare soil	3,289	4,090	24.35%	3,922	19.25%	4,510	37.12%	5,326	61.95%
Marsh & tidal land	1,733	0	-100.00%	1,381	-20.31%	1,817	4.88%	706	-59.27%
Water	3,679	2,380	-35.29%	2,992	-18.66%	3,386	-7.96%	3,534	-3.92%
Unclassified	0	1,599		126		280		203	
Total	17,126	17,126		17,126		17,126		17,126	
Study area, % unclassified		9.33%		0.74%		1.63%		1.18%	

(1) JPL classification conducted on 90 series data. Data gap in 90 series at northern edge of study area accounts for 670 hectares or 41.88% of the 1,599 hectare unclassified component.

These acreage figures can only be viewed in a general manner as they do not indicate where pixels were misclassified. Figures 3.2-2 through 3.2-5 show these classification maps and, when compared to the control land use, give a general indication of where the classifications were accurate and inaccurate.

The most notable result of all the classifications was that, given the algorithms used, none were able to achieve the specific land use category differentiation desired for direct FMMP application. The difference between land use and land cover analysis is important to note. FMMP's desired categories are often a composite of many very different land cover classes, for example, the Urban Land category includes paving, rooftops, trees, drainage channels, etc. When given 18 or more potential classes in which to assign data, the routines will classify pixels based on the spectral signature, which may be statistically closer to dry vegetation or other classes than to that of paved material. In grouping the 18 spectral classes into like land uses, a certain amount of overlap exists such that the analyst has to balance when and how to group them to achieve the desired classification results. Subsequently, the human discrimination inherent in the 'heads up' digitizing test produces results much closer to the desired categories.

Due to the effects discussed above, the Urban class in all the automated classifiers was low compared to the control. JPL's classifier uses different methods of analysis and is discussed separately, however, it overestimated the amount of urban in the noisy far range of the 90 series data as well as in some of the agricultural areas. Marsh and tidal areas, which contain high amounts of algae and other aquatic vegetation, were often associated with agriculture or vegetated pixels in all of the classifications. The problems with discerning vineyard and orchard areas that were seen in the IHS enhancement test were also present in the automated classification tests, as these parcels were commonly categorized as dry vegetation or soils. The most homogeneous category, Water, was most accurately determined in all the automated classification trials.

All the tests of band combinations and training methods described above were run through a minimum distance classifier. This classifier computes a Euclidean distance from a given pixel's value to the mean value of each class and assigns the pixel to the closest class (Intergraph Corp., 1994). The null value threshold is three standard deviations. Training data for the combinations listed in Table 3.2-4 were also run through the maximum likelihood classifier available within the software. This classifier uses a decision function and evaluates the variance and correlation of the classes before assigning pixels to the class with the largest discriminant function. Results indicated that the maximum likelihood classifier left somewhat more of the image unclassified than the minimum distance method, but that otherwise the classification maps were identical.



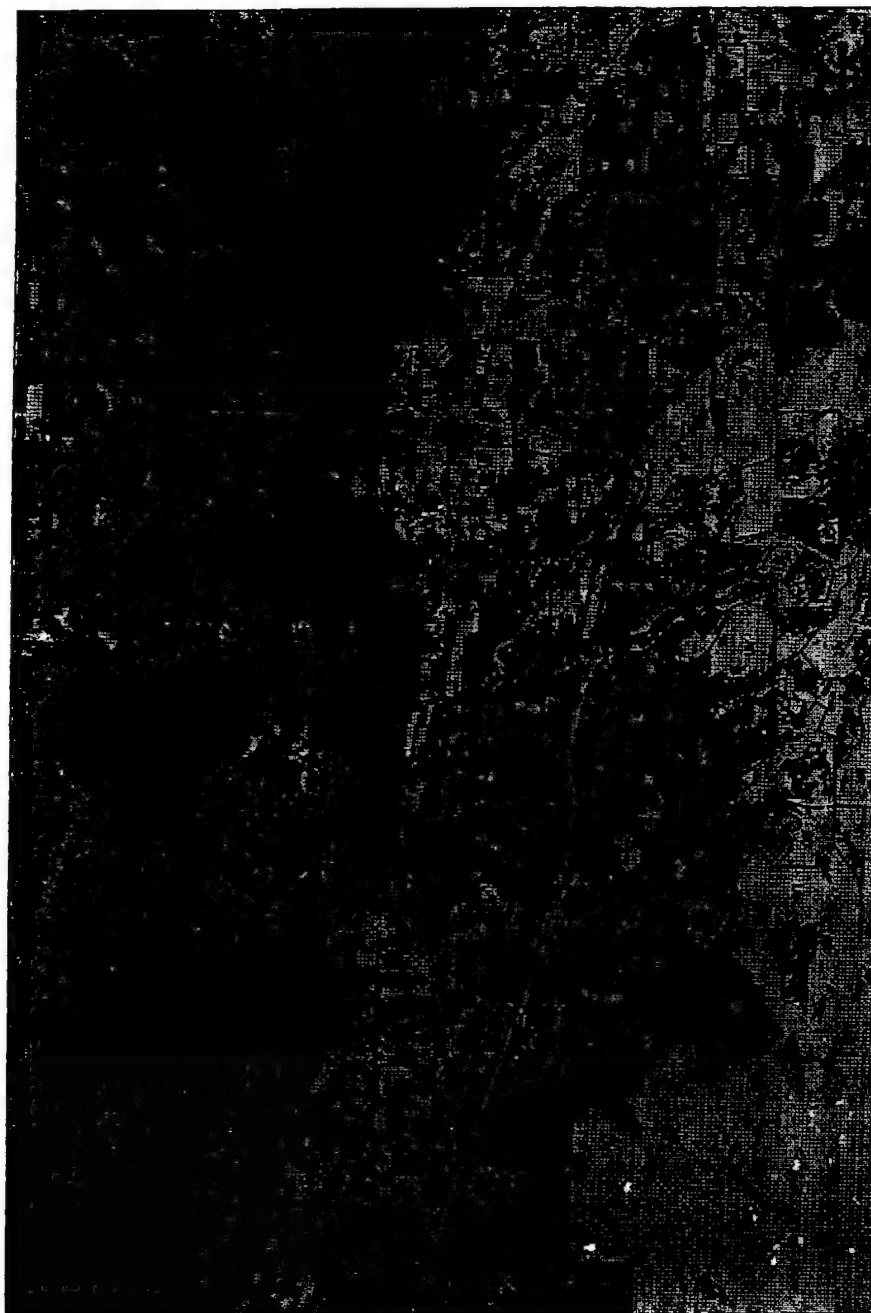
# AUTOMATED CLASSIFICATION MAP FROM 3 RADAR BANDS

## Control Land Use

- ☐ U Urban Land
- ☐ UC Urban Construction and Levelling
- ☐ OS Urban Parks and Greenspace
- ☐ RR Rural Residential
- ☐ D Orchard and Vineyard Crops
- ☐ F Annual Field and Truck Crops
- ☐ IP Irrigated Pasture
- ☐ nG Non-irrigated Grain Crops
- ☐ I Idle Farmland
- ☐ UV Urban Vacant Land
- ☐ NVI Grasslands
- ☐ NRI Marsh and Tidal Lands
- ☐ W Water

## Land Cover Classes

- ☐ Urban grouping
- ☐ Agriculture/vegetation
- ☐ Dry grasses/bare soil
- ☐ Marsh and Tidal Lands
- ☐ Water
- ☐ Unclassified



California Department of Conservation  
Farmland Mapping and Monitoring Program  
GeoSAR Study

Figure 3.2-2: Classification derived using radar magnitude, correlation, and dte with K-means algorithm and minimum-distance classifier.

# AUTOMATED CLASSIFICATION MAP FROM 6 TM BANDS

- Control Land Use**
- ☐ U Urban Land
  - ☐ UC Urban Construction and Levelling
  - ☐ OS Urban Parks and Greenspace
  - ☐ RR Rural Residential
  - ☐ D Orchard and Vineyard Crops
  - ☐ F Annual Field and Truck Crops
  - ☐ IP Irrigated Pasture
  - ☐ nG Non-irrigated Grain Crops
  - ☐ I Idle Farmland
  - ☐ UV Urban Vacant Land
  - ☐ NVI Grasslands
  - ☐ NR1 Marsh and Tidal Lands
  - ☐ W Water

- Land Cover Classes**
- ☐ Urban grouping
  - ☐ Agriculture/vegetation
  - ☐ Dry grasses/bare soil
  - ☐ Marsh and Tidal Lands
  - ☐ Water
  - ☐ Unclassified

0 500 1000 1500 2000 Meters



California Department of Conservation  
Farmland Mapping and Monitoring Program  
GeoSAR Study

Figure 3.2-3: Classification derived using 6 TM bands with Isodata algorithm and minimum-distance classifier.

# AUTOMATED CLASSIFICATION MAP FROM 6 TM AND 3 RADAR BANDS

## Control Land Use

- ☐ U Urban Land
- ☐ UC Urban Construction and Levelling
- ☐ OS Urban Parks and Greenspace
- ☐ RR Rural Residential
- ☐ D Orchard and Vineyard Crops
- ☐ F Annual Field and Truck Crops
- ☐ IP Irrigated Pasture
- ☐ nG Non-irrigated Grain Crops
- ☐ I Idle Farmland
- ☐ UV Urban Vacant Land
- ☐ NVI Grasslands
- ☐ NRI Marsh and Tidal Lands
- ☐ W Water

## Land Cover Classes

- ☐ Urban grouping
- ☐ Agriculture/vegetation
- ☐ Dry grasses/bare soil
- ☐ Marsh and Tidal Lands
- ☐ Water
- ☐ Unclassified



California Department of Conservation  
Farmland Mapping and Monitoring Program  
GeoSAR Study

Figure 3.2-4: Classification derived using 6 TM bands and 3 radar bands with Isodata algorithm and minimum-distance classifier.

# JPL AUTOMATED CLASSIFICATION MAP FROM 3 RADAR BANDS

- Control Land Use**
- ☐ U Urban Land
  - ☐ UC Urban Construction and Levelling
  - ☐ OS Urban Parks and Greenspace
  - ☐ RR Rural Residential
  - ☐ D Orchard and Vineyard Crops
  - ☐ F Annual Field and Truck Crops
  - ☐ IP Irrigated Pasture
  - ☐ nG Non-irrigated Grain Crops
  - ☐ I Idle Farmland
  - ☐ UV Urban Vacant Land
  - ☐ NVI Grasslands
  - ☐ NRI Marsh and Tidal Lands
  - ☐ W Water

## Land Cover Classes

- ☐ Urban grouping
- ☐ Agriculture/vegetation
- ☐ Dry grasses/bare soil
- ☐ Water
- ☐ Unclassified

0 500 1000 1500 2000 Meters



California Department of Conservation  
Farmland Mapping and Monitoring Program  
GeoSAR Study

Figure 3.2-5: Classification derived using radar magnitude, correlation, and DEM with JPL's classifier.

### 3.2.3.3.3 JPL Automated Classifier

Interferometric Synthetic Aperture Radar (IFSAR) data is mostly used to determine surface topography. As part of the ARPA AUTOMAP program, JPL has been developing algorithms to exploit interferometric data for land cover classification. The phase difference between interferometric channels is sufficient to derive terrain elevation images. However, there is additional information contained in the correlation coefficient between the channels which can be used together with the terrain slope and the backscatter power to infer surface properties. Land cover classifiers based on these three measurements lead to significantly better results than similar classifiers based solely on the backscatter power.

To obtain the results that were communicated to DOC using the JPL classifier, a Gaussian maximum likelihood (GML) classifier was applied to observation vectors whose elements were derived from the SAR intensity, the terrain elevation model, and the magnitude of the interferometric correlation. First and second order statistics required for the classifications were obtained from training samples drawn from forested, urban, agricultural, or bare areas. Each of these training sets was further divided into several subsets either by supervised classification or by k-means clustering in order to accommodate remaining statistical inhomogeneities due, for example, to variations in the angle of incidence. Sub-class labels were merged after classification.

#### 3.2.3.3.3.1 GML Classifier

The minimum expected error, or Bayes error  $e^*$  that can be achieved in classifying incoming observations  $\mathbf{x}$  in  $M$  classes with prior probabilities  $a_i$  and pdf's  $f_i(\mathbf{x})$  is achieved by applying the *maximum a posteriori* probability classifier (MAP):

$$\mathbf{x} \in w_i \text{ if } a_i f_i(\mathbf{x}) > a_j f_j(\mathbf{x}) \text{ for all } j \neq i$$

Class conditional pdf's and priors need to be estimated from a set of training samples, and, as a consequence, the expected error is larger than Bayes error,  $e > e^*$ .

With the assumption that the pdf of each class may be represented by a multivariate normal distribution or by a linear mixture of such normal components, the discriminant function for equal priors becomes

$$-\ln f_i(\mathbf{x}) \approx g_i(\mathbf{x}) = \ln |S_i| + d\mathbf{x}^T S_i^{-1} d\mathbf{x}$$

$$d\mathbf{x} = \mathbf{x} - \mathbf{m}_i$$

where  $\mathbf{m}_i$  and  $S_i$  are the mean vector and the covariance matrix of each normal distribution component. This is the *Gaussian Maximum Likelihood* (GML):  $\mathbf{x} \in w_i$  if  $g_i(\mathbf{x}) < g_{j \neq i}(\mathbf{x})$ .

#### 3.2.3.3.3.2 Feature Vectors

At each pixel, the SAR brightness ( $s_o$ ), the DEM height ( $h$ ), and the magnitude of the correlation between signals ( $r$ ) are used to determine an N-dimensional feature vector  $\mathbf{x}$ . The following features were considered:

1. Physical values:  $s_o$ ,  $r$ , penetration ( $d_z$ ),  $s = ||-\mathbf{h}||$
2. Spatial variabilities:  $Dh$ ,  $Ds_o$ ,  $Dr$ , and  $Ddz$ .
3. Textures: laplacians, and cooccurrence matrices of  $s_o$ ,  $r$  and  $h$ .

#### 3.2.3.3.3.3 Training Sets

1. **Supervised:** training regions with known ground truth: water, trees, field, urban area. Each class is either divided in three supervised subclasses: near, mid, and far-range, or divided by K-means.
2. **Unsupervised:** clustering by a K-means algorithm of a random set of pixels uniformly distributed throughout each class; four clusters per class have been used.

### 3.2.4 Evaluation

#### 3.2.4.1 Criteria

The purpose of this experiment is to evaluate radar and commercially available satellite imagery for their potential to be used in FMMP's land use mapping workflow, and more generally for radar's ability to substitute for or improve the accuracy of commercial satellite data in land use mapping applications. In year one, data registration, image enhancement, and classification routines would be the focus; with mapping of different geomorphic areas, land use change detection, and refinement of classification methods to follow in subsequent years.

In evaluating these technologies for possible application to FMMP's workflow, the following criteria would have to be satisfied.

1. Spatial accuracy and registration with existing vectors.

Due to the regional nature of FMMP's mapping process, image clarity and classification accuracy have greater weight than high spatial accuracies. At this time, land use changes are transferred by hand from air photos to 1:24,000 field sheets depicting previous land use. This can lead to inaccurate placement or configuration of linework. Therefore, a reasonable visual registration of raster data to the existing vector linework, in the range of 10m, would satisfy spatial accuracy criteria. Precision point and linework placement tests were used as a test of registration acceptability.

2. Image clarity and resolution.

The use of raster backdrops for digitizing, analysis, and data portrayal is expected to be one application of digital imagery for FMMP. The ability to discern land use in units as small as 4 hectares and land use changes in increments as small as .8 hectare in size is required. This standard can currently be met with 1:130,000 CIR photography. For this experiment, image clarity was assessed using the radar and satellite data as a backdrop for a 'heads up' digitizing test in which unknown or misclassified areas were measured relative the control land use vectors.

3. Automated classification capabilities.

Correct determination of Important Farmland mapping categories requires the ability to discern among land cover classes, as structured for the GeoSAR study, throughout California's geomorphic regions. Examples include discerning irrigated farmland from dryland agriculture or grazing land in summer conditions; parklands or cemeteries from agricultural land; or confined livestock facilities from industrial uses. Differences in these land uses are sometimes very subtle and significant interpreter training is involved. It is anticipated that achieving automated classification of raster data applicable to FMMP analysis will require years of experimentation and development. In the shorter term, use of time series data as a means of focusing attention on areas of change may help to reduce manual analysis.

For the GeoSAR experiment, automated image classification maps were visually compared to the control land use linework to screen out poor training parameters or classifiers. The degree to which classifiers could separate image data into the desired classes was assessed, and resultant classification maps were compared to one another.

4. Data cost, labor, and equipment requirements.

In order to become the method of choice for FMMP's land use mapping purposes, raster image technology would have to produce the same (or better) levels of accuracy, consistency, and speed as current methods; without adding significantly to the cost of analysis. Budget analysis of the 1990 to 1992 map updating cycle revealed that data acquisition, labor, travel, and supplies for the mapping process from photo interpretation through digitizing totalled about \$320,000 or 1.8 cents per hectare.



Costs of data acquisition are increasing, however; estimates for 1995 high altitude photo coverage of the Central Valley are nearly twice what they were in 1990. At the same time, computing hardware, software, and data storage costs are decreasing.

It is not possible at this time to conduct a cost assessment of GeoSAR for FMMP map updating due to the fact that the project is in a developmental as opposed to production environment. In terms of data acquisition, it is clear that GeoSAR would have to compete with commercial satellite imagery or be able to provide multiple useful data products that would promote cost sharing arrangements for limited-budget programs such as FMMP.

### 3.2.5 Discussion

Adoption of raster technologies by FMMP would require major modifications in the way Important Farmland maps are developed and updated. It would involve extensive new data acquisition and storage requirements, new notation systems, and new computer hardware on which to conduct analyses by existing staff. The potential for improvements in data accuracy and lowering labor or other costs makes exploring these technologies attractive.

The first year of the GeoSAR experiment has shown that the presence of up-to-date, rectified imagery as a backdrop for updating land use vectors would help to increase linework placement accuracy, particularly in areas where existing cultural features are limited. Linework accuracy in rapidly growing sections of southern California, the San Francisco Bay area, and the Sierra Nevada foothills, in particular, would be improved due to the fact that hillside developments are common in these regions. Precision point placement tests indicated that the radar imagery for the Antioch study had the highest spatial accuracy compared to commercial satellite imagery and would be suitable for FMMP data registration purposes.

As an imagery product, work to date indicates that noise and oversaturation effects inherent in the radar magnitude image can be decreased somewhat by mathematical substitutions among multiple passes and by use of principal components analysis. Skewed distribution of the original 32-bit floating point data can be normalized by conversion to decibel values and redistributed into the 256 bins available for 8-bit data. Other filtering and edge enhancement options will be explored in year two, including the use of different software routines than are currently available on FMMP's system.

The usefulness of radar imagery as an enhancement to TM data was shown in a 'heads up' digitizing comparison of four IHS-enhanced images. Identification of urban, dry vegetation, and marsh land categories was improved by substituting an average of TM and radar PC1 for intensity in an IHS to RGB conversion, compared with using TM intensity alone. The improvement was most dramatic in the ability to discern among dry vegetation categories, where the radar/TM average came 25% closer to the control acreage than did TM alone. However, the radar/TM average enhancement effected a 15% decline in the ability to accurately discern among irrigated agricultural categories compared with TM alone. SPOT imagery was the only intensity enhancement option which enabled analysts to discern orchards and vineyards from other irrigated land uses.

The proportion of unclassifiable pixels in all four raster backdrop trials was in the range of 8 to 10%. The proportion of uncertain areas requiring field reconnaissance using high altitude photography is below 1%. Further experience with the raster data and additional cultural information from base maps and existing vectors will help to bring the number of unclassifiable pixels closer to acceptable levels.

The capability to discern minimum land use areas of 4 hectares and land use changes in 0.8 hectare increments that is required for FMMP map updating would appear to be possible with 5m data (322 pixels per 0.8 hectare), but may not be practical with the 25m TM data (13 pixels per 0.8 hectare). The smallest polygons delineated in the 'heads up' digitizing experiment were 2 hectares. Since land use change detection with multiple acquisition dates is expected to occur in subsequent years of study, this criterion will be further explored.



Automated classification experiments with the radar and commercial sensor data were focused on using the algorithms present within in-house software on various band combinations to produce classification maps. The three test combinations included radar alone, TM alone, and combined radar and TM data. The resultant maps were visually compared to the control land use map developed using traditional air photo techniques.

Most of the trials involved classifying the image into 18 spectral classes, followed by clustering these into five major land use classes. The tests, while systematic, were not exhaustive; and the resultant classification maps all pointed to the inherent difference between land cover and land use mapping. FMMP's land use categories often contain high spectral diversity, for example, urban land was underestimated because semi-industrial areas and roadway corridors were spectrally classified as dry vegetation. Supervised classifications, in which polygons were drawn within five known land use classes to serve as the basis for classifying the rest of the image, were also conducted. Results of these tests were not significantly different than those of the unsupervised or spectral classifications.

First year classification tests pointed out the need to further refine a classification workflow with multi-step analyses that will mask out certain areas of the image to focus on areas of greatest interest. In addition, maximizing classification options by subdividing the image into a larger number (30+) of spectral classes and employing statistical as well as visual measures for clustering data may lead to more refined classification maps. These items will need to be pursued regardless of which bands of data are being used for classification.

There are a number of factors which make determining what band combination(s) are best for classification premature at this point; as first-year classification maps and acreages are inconclusive. In addition to classification technique refinements, the use of later-generation radar data and the acquisition of data in regions with a better agricultural mix would likely add to FMMP's ability to assess which options are best. Some of the enhancements to radar magnitude and correlation data that have been discussed in this report were developed after 'heads up' digitizing and automated classification experiments were underway, and taking advantage of these improvements will provide a better test of data quality. The agricultural section of the Antioch study area, where some of the worst classification results were obtained, is dominated by saturation- and saline-tolerant field crops and pasture, as well as vineyards and orchards further inland. A better differentiation among crop types and more representative agricultural conditions would give FMMP staff a better foundation on which to assess classifying these highly important categories.

Year 2 of the GeoSAR land use study is expected to focus on refining classification techniques, initiating study in new geomorphic areas, and beginning land use change detection testing at Antioch. Other items of interest for testing in year two include using the radar data for removal of slope affects from TM data, using other software routines to filter the radar data, and testing different radar wavelengths and polarimetric data.

### 3.3 VEGETATED HILLSLOPE DEM AND SLOPE HAZARDS EXPERIMENT

#### 3.3.1 ABSTRACT

A Test Site has been established to evaluate the utility of digital elevation models (DEMs) acquired by foliage-penetrating radar technology (FOPEN) for analysis of earthquake-induced slope hazards in rugged, heavily-vegetated terrain located in the Santa Cruz Mountains, California. Two targets: (1) a large landslide, and (2) Sawpit Canyon watershed, have been selected for a comparison between radar-derived and photogrammetrically-derived DEMs. Neither target is visible from the air, as they are located beneath the forest canopy. The comparison will examine the degree to which the two methods can characterize the terrain in terms of height accuracy, resolution, and completeness of coverage. Interferometric synthetic-aperture radar data were acquired using JPL's TOPSAR instrument as part of the first year effort. New aerial photography was acquired (1:40,000 scale), and a landslide inventory and vegetation survey have been conducted for specific target areas. Year 2 will acquire FOPEN data over the target areas, which, together with the field surveys, a USGS DEM, and new photogrammetric DEM, will provide the basis of the experiment.

#### 3.3.2 INTRODUCTION

##### 3.3.2.1 Purpose

The purpose of this experiment is to determine the effectiveness of using radar technology in mapping landslide hazards in rugged, heavily vegetated terrain. Unlike the experiment in Antioch Hills (see section 3.1 of this report), such conditions are generally considered "difficult" for mapping the locations of existing landslides using aerial photography or other remote sensing tools, and are conditions under which only approximate digital elevation models (DEM's) of the ground surface can be generated. Advances in radar mapping with foliage-penetrating radar (FOPEN), makes it potentially possible to develop DEMs that represent the ground surface rather than the top of the forest canopy as with photogrammetric DEM's. How well FOPEN DEM's represent the true ground surface must be demonstrated.

The Antioch Hills Test Site seismic hazard experiment introduces the State of California's Seismic Hazard Mapping Act, and addresses the data needs and issues related to mapping earthquake-induced ground failures in hillslopes. The reader is referred to section 3.1 of this report for that information. To summarize, the principal issue facing the Department's seismic zonation mandates is a deficiency of high-quality, reliable DEMs with which to perform slope hazard analysis in California. This problem is greatly magnified in forested regions where photogrammetry is of limited use, and the conventional means of acquiring high-quality elevation data by land surveying is both cost prohibitive and impractical considering the vast area to be zoned in California.

Optical imagery is of little use in mapping the occurrence of slope failures in heavily forested areas unless they are shallow, have long transport distances to carry away vegetation, and are recent enough to leave exposed, denuded terrain that contrasts with the surrounding vegetation. Within a few decades such landslide scars can become overgrown with natural vegetation and difficult to identify on aerial photography, leaving the recognition of older slope failures (decades to a few hundred years) dependent on costly and time intensive field investigation. McKean and others (1991) have investigated the use of multispectral remote sensing data to identify landslides concealed beneath the forest canopy. In some cases, changes in soil conditions and exposure to sunlight caused by the disturbance in terrain has been enough to result in the growth of different plant species having noticeably different spectral signatures. The spectral difference, together with the general

lobate shape of landslides and arcuate headscarps has been sufficient to identify concealed slope failures in forested areas (McKean, et al., 1991). This method of detection is indirect, however, and the measured effects fade with time as natural reforestation occurs. Clearly a method of seeing through the forest canopy, and imaging the ground surface would be advantageous. FOPEN technology may provide such a capability, and would be amenable to pattern recognition for direct computer-assisted detection of landslides.

### 3.3.2.2 Objectives

The principal objectives of this experiment are to test the capability of FOPEN-derived DEM's to (1) characterize, identify, and map terrain geometry associated with the occurrence of hillslope failures in heavily vegetated terrain, and (2) recognize particular terrain morphology for purposes of computer-assisted identification of hillslope failures in areas of heavily vegetated terrain.

To address these objectives will require the development of "ground truth", which will be accomplished by geodetic surveying, GPS surveying, and production of a photogrammetric DEM. Currently, it is not possible to develop a photogrammetric DEM in this area that represents the ground surface because of the dense forest cover. However, during the 1930's and 1940's, aerial-photo surveys were conducted when a portion of the study area was clear-cut by logging operations. The ground surface is readily exposed in these vintage air-photos, and a secondary objective is to develop stereo models and DEM's from these early aerial surveys.

### 3.3.2.3 Site Description

The Laurel Quad includes a part of the Santa Cruz Mountains south of the San Francisco Bay Area and north of the city of Santa Cruz (Figure 1.4-3). The area is characterized by rugged topography with elevations ranging from 60 to 700m. Most of the area is covered with dense vegetation with deciduous and conifer forests the dominant vegetation. Also common are brush, cleared grasslands for grazing, orchards, and low density residential development.

Regional geology controls the topography and geologic hazards of the area. The San Andreas fault crosses the northeast corner of the quadrangle and the epicenter of the 1989 Loma Prieta earthquake is within the quadrangle. Local geometry of the San Andreas fault has led to rapid uplift of the Santa Cruz Mountains. Uplift of young, weak sedimentary rocks to substantial elevations has helped create a serious landslide hazard. Periodic earthquake shaking has also stimulated movement of existing landslides.

Two target sites have been selected to test FOPEN capabilities; (1) a large landslide, hereafter called "Giveaway Landslide", located in the northwest quarter of the USGS 7.5-minute Laurel Quad as shown in Figure 3.3-1, and (2) a watershed hereafter called "Sawpit Drainage", located in the northeast quarter of the Laurel Quad. The Giveaway Landslide is typical of the slope failures in the Santa Cruz Mountains, and has a well defined head scarp and the characteristic hummocky terrain that would make this feature easily identifiable from the air were it not for the heavy tree cover (Figure 3.3-2). Sawpit Drainage was chosen because of the available vintage aerial photography covering the site taken when the ground surface was exposed as a result of logging. Photogrammetric DEM's from that era will estimate the height of the true ground surface, which is now covered by 20-40m - tall evergreens, presenting a unique comparison with FOPEN capabilities.

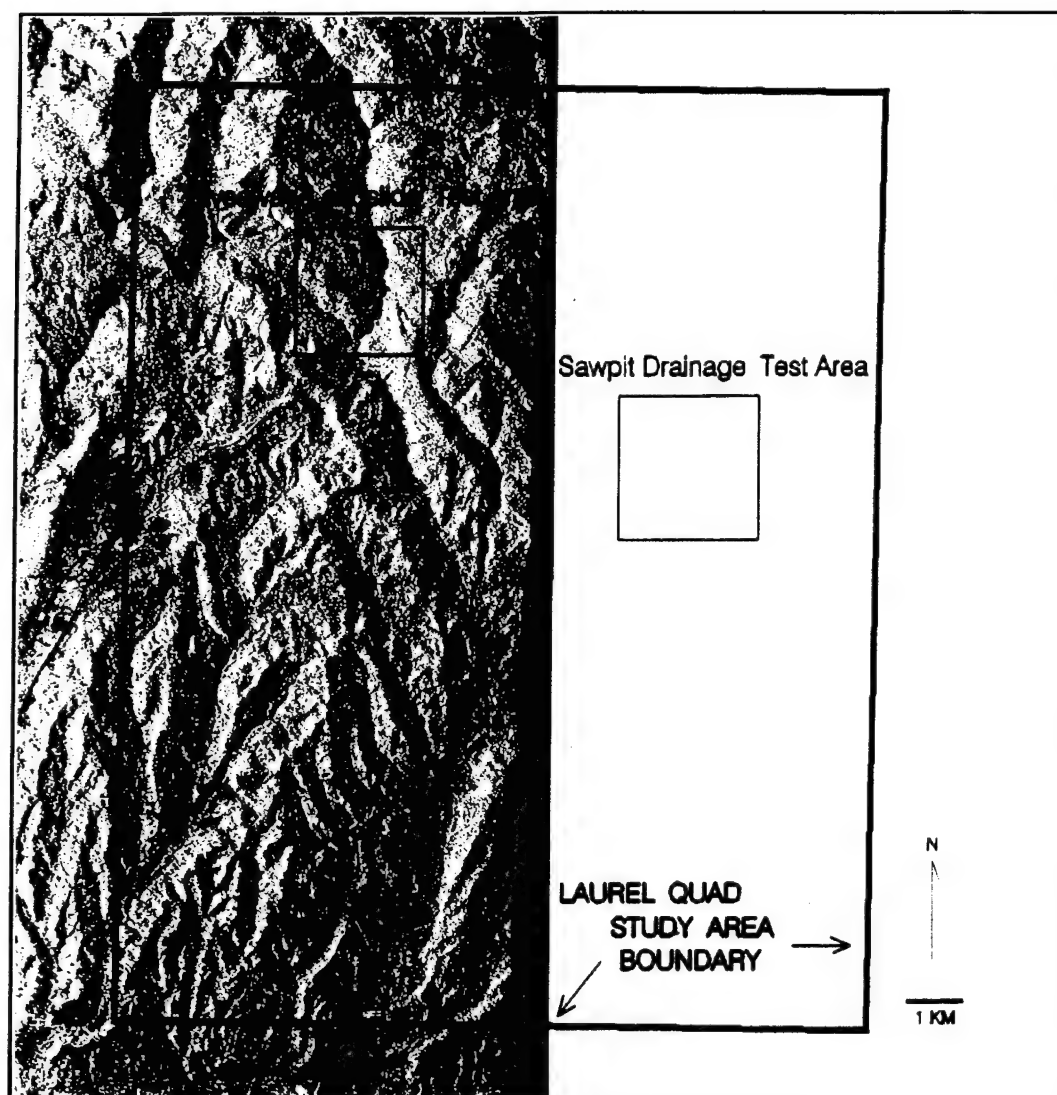


Figure 3.3-1: Location of test areas within the Laurel Quad.



Figure 3.3-2: Debris flow chute to Soquel Creek East of Jarvis Road.

### 3.3.3 User Experiment

#### 3.3.3.1 Methodology

The basic approach used to compare FOPEN DEMs with "ground truth" will be similar to that used in the Antioch Hills seismic experiment described in section 3.1.3.2 of this report. Height differences will be examined visually and statistically as before, only this time vegetation will be added as a spatial variable to analyze for possible effects on DEM accuracy. Comparisons will be made between FOPEN DEMs, IFSAR DEMs, photogrammetric DEMs (vintage photography and new), variations of the USGS DEM for the Laurel Quad, and elevation checkpoints acquired using GPS and detailed ground surveys.

Ground-truth is being acquired by 1) vintage aerial photography, 2) field ground surveying, and 3) a field vegetation survey. Vintage photography for aerial surveys flown in 1931, 1939, and 1943, have been acquired and digitally scanned at 15 microns (see section 3.1.3.1 of this report for a description of softcopy photogrammetry and DEM collection used in this study). DOC helped Calgis plan the ground surveys and vegetation transects. Ground surveying to define the morphology of the Giveaway Landslide and vegetation transects to classify types of foliage were carried out by Calgis, and are described in sections 2.2.2.2 and 2.2.2.3, respectively.

Because so much of the study area is affected by landslides, and because ground truth for Sawpit Drainage is being defined by decades-old photography, it is important to confirm that no hillslope movement has occurred since the vintage photography was acquired. This will be determined by comparing results of the ground survey with the vintage photography DEM.

##### 3.3.3.1.1 Landslide Inventories

The Laurel Quad was chosen for the GeoSAR experiment because it is an area of well known landslide hazards which are difficult to map using traditional aerial photo based techniques. In order to evaluate the effectiveness and accuracy of using IFSAR and FOPEN technologies for recognizing landslide topography (part of Year 2 of the experiment), we have prepared or acquired three separate landslide inventories. The three inventories were prepared using different techniques each of which have advantages and disadvantages.

The first of these landslide inventories could more accurately be termed an inventory of topographic features suggestive of landsliding. Landslides cause distinctive topographic features such as scarps, benches high on hillslopes, and hummocky topography. In some cases, these can be distinguished from the contour lines on a 7.5-minute topographic map. A geologist who is aware of the distinctive signature of landsliding on a topographic map can very rapidly interpret an area. Our inventory for the Laurel Quad was prepared by one geologist in 10 hours. The obvious advantage of this technique is speed, its disadvantage is lack of accuracy. Only those landslides large enough to affect topography at 1:24,000 scale are visible, and the effects of vegetation on preparation of the topographic map are ignored. The result is an inventory in which large bedrock landslides are recognized but small or shallow slides are not. This inventory probably also includes features that superficially resemble landslides, but were formed by other processes. Although the inventory of topographic features appears to produce an unsatisfactory landslide map when prepared from the existing USGS topographic map, this technique used with a more detailed and accurate DEM generated by FOPEN technology should result in a more accurate landslide inventory.

The second of our landslide inventories was prepared using the "traditional" technique of aerial photo interpretation using a mirror stereoscope. Our inventory for the Laurel Quad using this technique was prepared by one geologist in 98 hours. For this interpretation we used aerial photos taken in 1931, 1939, 1943, 1975 and 1985 at scales ranging from 1:12,000 to approximately 1:30,000.



It is important to interpret landslides from photos of varying ages and scales in this area because of changes in vegetation cover over time and for ease of interpreting different scales of landslides. The earlier photos are most useful for interpreting areas that had been logged in the 1920's and 1930's. The larger scale photos are most useful for interpreting small slides but larger landslides, which do not fit in a single print, are difficult to map.

Our aerial-photo landslide inventory (Figure 3.3-3) represents a reasonably accurate reconnaissance level map of landslides in the area, given the difficulties of mapping landslides through heavy vegetation. Landslides are classified by type, recency of movement and confidence of interpretation using the system of Wieczorek (1984).

This aerial photo based inventory shows some distinct patterns in the distribution of landslides, patterns that are at least partly artifacts of the interpretation method. Figure 3.3-3 shows that landslides in the southwestern one-third of the quadrangle are less common and generally smaller, but debris flows appear to be more abundant. The pattern of debris slides in the southwest and large bedrock slides in the northeast appears to be caused by an actual decrease in large bedrock slides from northeast to southwest and an apparent decrease in debris flows from southwest to northeast. Debris flows and other small, shallow slides are simply much harder to map through the dense forest cover on the northeastern two-thirds of the map. Preliminary field data and analysis of other mapping suggests that the actual abundance of debris flows may increase to the northeast.

The third landslide inventory that we have acquired will serve as ground truth for the landslide inventories prepared from aerial photos and FOPEN. This inventory covers the Forest of Nisene Marks State Park in the southeast part of the Laurel Quad, overlapping into the adjacent Loma Prieta Quadrangle. It was prepared by geologists from Weber and Associates under a grant from USGS. Geologists mapped landslides in this area on the ground, generally walking over the area to recognize landforms related to sliding. This technique is extraordinarily time-intensive and is virtually never done for large areas of undeveloped land. It is, however, very accurate for locating landslides, especially the smaller and more active slides. We estimate the inventory for the Laurel Quad using this method took the equivalent of one geologist 883 hours to complete.

### 3.3.3.2 Analysis

Nearly all of the first-year activities for the Laurel Quad Site have been confined to site selection, development of ground, and data acquisition. The only radar data set acquired thus far is IFSAR from JPL's TOPSAR instrument. These data only cover a portion of the test area, missing the Sawpit Drainage entirely, and have not yet been analyzed.

### 3.3.3.3 Results

No results are available for the Laurel quad Test Site because; (1) the first year was devoted entirely to data acquisition, (2) FOPEN has not yet been acquired, and (3) no analysis has been made yet the IFSAR DEM.

## 3.3.4 Evaluation

### 3.3.4.1 Criteria

The criteria used to evaluate the usefulness of radar DEMs and imagery will be the same as that used for the Antioch Hills Experiment. Refer to Section 3.1.4.1 of this report.



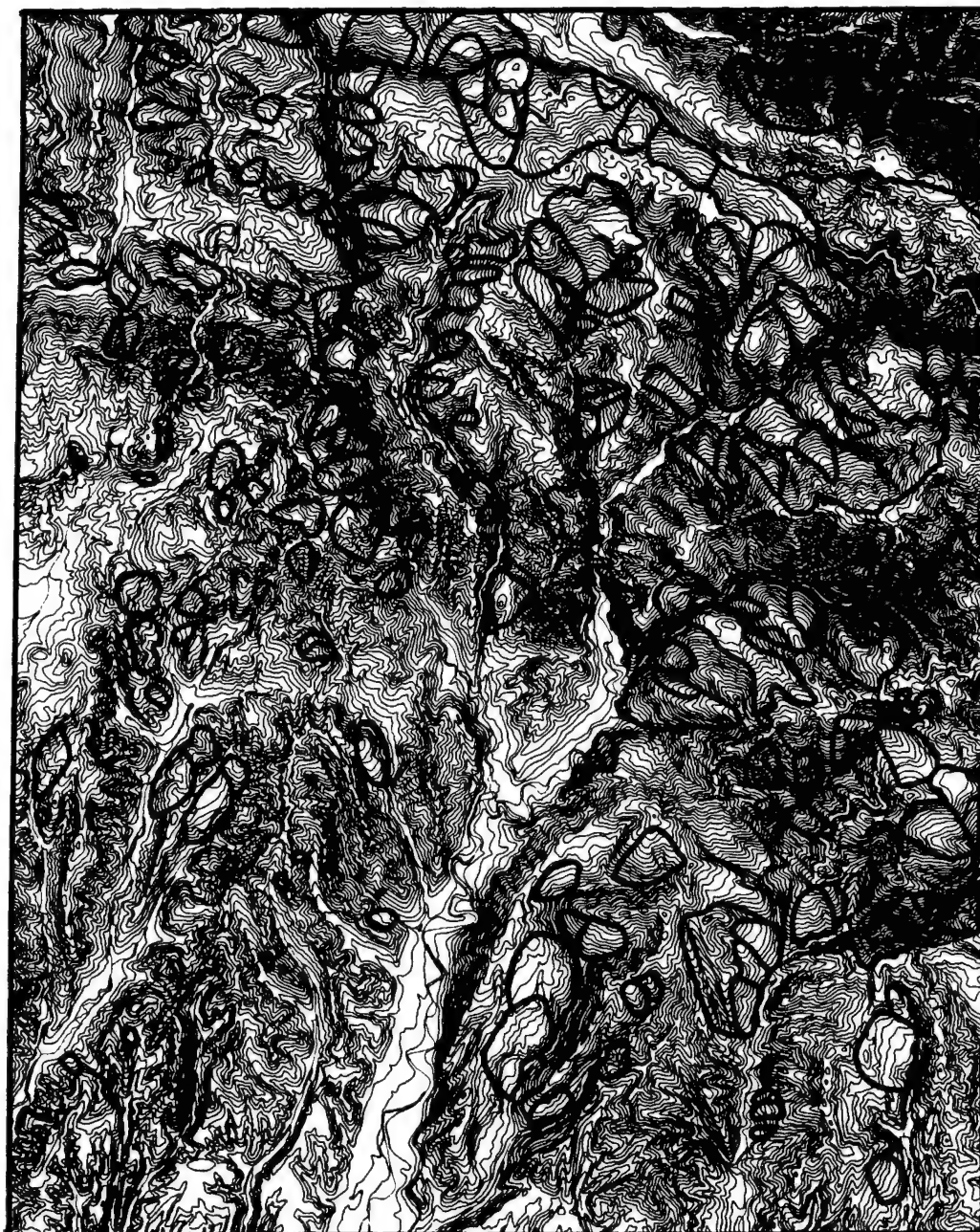


**Figure 3.3-3:** Aerial photo reconnaissance inventory of landslides in the study area.

### 3.3.4.2 Discussion

The third landslide inventory will be a key test for evaluating interpretations from a DEM generated from FOPEN in Year 2. We expect that landslide interpretation based on FOPEN technology will produce a more accurate and detailed inventory than our first inventory. If it can equal or surpass the accuracy and detail of our second inventory it will be a sign of significant potential. If interpretations based on FOPEN technology can approach the detail and accuracy of this third inventory, this will indicate that this technique is by far the most effective for mapping of landslide hazards in forested terrain.

### 3.3.5 Year 2 Work

During Year 2 the following tasks will be completed; (1) development of stereo models and DEMs for vintage photography, (2) rectification of new 1:40,000-scale aerial photographs and production of DEM, (3) comparison of FOPEN DEM with IFSAR DEM, photogrammetric DEM, and USGS DEM, and height differences will be examined to determine possible correlation with terrain and vegetation, (4) radar products will be evaluated for overall utility in seismic hazard mapping in wooded areas.

A final report will be prepared that considers the usefulness of IFSAR and FOPEN to mapping seismic hazards, considering cost, accuracy, and efficiency as a routine tool for use in DOC's Seismic Hazards Evaluation and Zonation Program.

### 3.4 GUALALA RIVER BASIN, TIMBER HARVEST EROSION EXPERIMENT, TIMBER HARVEST PLAN PROGRAM

#### 3.4.1 Abstract

Radar imagery will be used to analyze the watershed of the north fork of the Gualala River for slope instabilities by visual inspection and by searching for parameters of known landslide features within each watershed. True ground surface DEMs obtained using FOPEN Radar will be used as a topographic base for field work, modeling debris flow potential and to identify existing roads and skid trail under the forest canopy. These features are the primary sources of non point source discharges within forested areas for analysis of erosion problems resulting from timber harvesting

#### 3.4.2 Introduction

##### 3.4.2.1 Purpose

The purpose of the Gualala River experiment is to evaluate the utility of using foliage penetrating radar to generate a true ground surface DEM for assessing landslide initiation and stream sedimentation. An additional purpose for this experiment will be the comparison of TOPSAR and FOPEN derived vegetation canopy and ground surfaces, and incorporating this with multi-spectral imagery for quantifying biomass and habitat characteristics.

##### 3.4.2.2 Objectives

This experiment is directed to aid in evaluating the impacts of logging on debris flow landslide initiation and in testing the effectiveness of the California Forest Practice Rules in protecting water quality from non-point sources.

IFSAR imagery and soft copy photogrammetry will be used to analyze the watershed for slope instabilities by visual inspection and by searching for parameters of known landslide features within each watershed. The digital terrain models of the true ground surface obtained using FOPEN Radar will be used as a topographic base for field work, and for modeling debris flow. FOPEN-derived digital terrain models of the true ground surface and radar imagery will be used to identify existing roads and skid trail. These features are the primary sources of non point source discharges within forested areas.

Three watersheds, of which the Gualala River is one, have been selected for in-stream and hill slope monitoring by the Monitoring Study Group of the California Board of Forestry. The objectives of the Gualala River experiment are:

1. Define the processes by which hill slope activities can affect stream channels utilizing field reconnaissance.
2. Provide a geomorphic overview of the entire pilot monitoring program so that normal spatial and temporal variations are not mistaken for simple cause-and-effect slope processes. Define high-risk areas by preparing maps of geologic and geomorphic features related to land sliding, soil erosion, and sediment yield for the pilot watersheds using radar derived DEM modeling in a GIS.
3. Conduct field reviews of these high risk areas in the watersheds to evaluate the radar DEM in addressing potential erosion problems. Document this on a database developed for the Division of Mines and Geology's Effectiveness Study of the Timber Harvesting Plan Review Project.

4. Document conditions at high-risk sites to aid in defining appropriate monitoring locations. This would involve developing a photographic library of types of geomorphic conditions that represent high-risk sites.

#### 3.4.2.3 Description

The proposed test site is the north fork of the Gualala River Basin and its watershed in southwestern Mendocino County and northwestern Sonoma County. This watershed has supported a long history of logging and agriculture. The current cycle of logging has been challenged because of concerns regarding salmonid spawning and rearing habitats. The Gualala River Basin is underlain by the Franciscan Complex, a highly variable sedimentary bedrock that has been tectonically accreted to North America. Debris flows are very common on steep slopes in areas underlain by the Franciscan Complex. Logging-related land-use activities have contributed to debris flow activities within the watershed.

The vegetation in the test site includes conifer forests of various ages and logging histories, hard wood stands, and scattered grass openings and brush fields. The experiment will test if Soft Copy Photogrammetry, IFSAR, and FOPEN can produce high-resolution digital terrain models for surface geometry analyses, landslide mapping, and biomass evaluation in the Gualala River watershed.

#### 3.4.3 Year 2 Work Plans

It is planned for JPL to process the Gualala River C-Band IFSAR data to make them available for distribution and use by other researchers. Year 2 budget restraints preclude DOC from pursuing detailed investigations with this data.

### 3.5 SITE #4 - IRON MOUNTAIN MINE, CONTAMINATED MINE RUNOFF EXPERIMENT, OFFICE OF MINE RECLAMATION

#### 3.5.1 Abstract

Radar imagery will be used to identify and quantify lands disturbed by mining and to develop a digital elevation model (DEM) of the watershed surrounding the Iron Mountain Mine near Redding, California. The DEM will then be used develop a digital terrain model (DTM) that serves as the foundation for a GIS based ecohydrological simulation model to assess mining impacts on watersheds. Radar imagery will also be evaluated for its utility in characterizing hydrologic parameters of surface roughness, lineament density, drainage density, and vegetation type and density. The data extracted from the radar imagery will be combined with other literature and remote sensing information as GIS input for a ecohydrological simulation assessing mining impacts on the watershed, the risks of contamination, and remediation alternatives.

#### 3.5.2 Introduction

##### 3.5.2.1 Purpose

The purpose of the Iron Mountain Mine experiment is to investigate the use of digital elevation models developed from IFSAR and FOPEN imagery to construct high resolution digital terrain models of mountain watersheds disturbed by mining activities, and to integrate the digital terrain model into a Geographic Information System (GIS) that can be used to assess and rank abandoned mine sites based on the potential risks to environmental quality and public safety, and to aid in evaluation of remediation alternatives.

##### 3.5.2.2 Objective

The objectives of the Iron Mountain Mine experiment are to develop and evaluate the effectiveness of IFSAR and FOPEN in identifying, evaluating and classifying environmental impacts of mined lands and the effectiveness of remediation alternative. Specific objectives include:

- a. Produce IFSAR and FOPEN based digital terrain models in disturbed mined lands and the adjacent forest watershed.
- b. Develop a watershed hydrologic model based on radar DTM for mined lands.
- c. Develop a contaminant risk assessment model based on DTM and hydrologic model.
- d. Evaluate the use of radar in detecting mine openings and mining structures, such as metal buildings.
- e. Evaluate the accuracy of radar in detecting larger lands areas disturbed by mining.
- f. Evaluate the ability of multifrequency IFSAR to characterize terrain roughness and lineaments.

### 3.5.2.3 Site Description

First mined in 1879, this 1,780 hectare site is located in the Klamath Mountains approximately 14.4km northeast of Redding. The mine proper is located on a northwest-to-southeast trending ridge with two adjacent watersheds drained by Slickrock Creek to the west and Boulder Creek to the east. The west and east drainage basins are approximately 4.3 and 5.6km long and cover approximately 550 and 789 hectares, respectively. Elevations in the mine area range from 457 to 1097m. The mean annual precipitation is approximately 190cm. The surface runoff from the mine site discharges into Spring Creek, which drains a large watershed to the east, and eventually into Keswick Reservoir located on the Sacramento River northwest of Redding. Figure 1.4-5 shows the watershed boundary of the Iron Mountain experiment along with the major drainages.

The mine site has several features that are typical of lands disturbed by mining. Located on the west side of the mountain are several waste tailing dumps. The largest dump covers approximately 26.3 hectares with an elevation change of 122m and fills the drainage channel of Slickrock Creek.

This waste dump consists of large boulders and rocks with interstitial fines sidecast off Iron Mountain. Located within the waste pile are several early workings shafts, roadways and mill sites. The waste pile is highly eroded and has reportedly failed in the past as a massive landslide.

Waste dumps typically have not revegetated although scattered shrubs and conifers do occur. The undisturbed lands are typically covered by dense conifer forest.

A smaller 4 hectare hematite waste pile located 0.4km to the east has been highly eroded creating a badlands type topography. Near the top of Iron Mountain is the Brick Flat open pit covering approximately 4 hectares. In the eastern portion of the mine site Boulder Creek has been filled with tens of meters of mine waste for approximately 0.8km. This area of Boulder Canyon has numerous destroyed mine buildings and several mine portals. The largest intact group of mine buildings occur at the Richmond Mine located approximately halfway up the eastern slope of Iron Mountain. Other smaller mine waste dumps, roadways, mill site and underground entrances are scattered throughout the mine area.

### 3.5.3 Year 2 Work Plans

A follow-up flight using the improved TOPSAR instrument is planned for the spring of 1995, to acquire C, L and P-band radar data for use in Year 2. It is planned to conduct the original Iron Mountain contaminated surface runoff experiment at a reduced scope of work to accommodate budget reductions.



## REFERENCES

- Adkins, K.F. and Merry, C.J., 1994, Accuracy Assessment of Elevation Data Sets Using the Global Positioning System: Photogrammetric Engineering and Remote Sensing, Vol. 60, No. 2, p. 195-202.
- American Society of Photogrammetry, 1980, Manual of Photogrammetry, Fourth Edition.
- Bolstad, P.V. and Stowe, T., 1994, An Evaluation of DEM Accuracy: Elevation, Slope, and Aspect: Photogrammetric Engineering and Remote Sensing, Vol. 60, No. 11, p. 1327-1332.
- Brown, D.G. and Bara T.J., 1994, Recognition and Reduction of Systematic Error in Elevation and Derivative Surfaces from 7 1/2-Minute DEMs: Photogrammetric Engineering and Remote Sensing, Vol. 60, No. 2, p. 189-194.
- California Department of Conservation, Farmland Conversion Reports, 1984 through 1992. California Department of Conservation, Sacramento CA, June 1988, 1990, 1992 and 1994.
- Carrara, A., Cardinali, M., Detti, R., Guzzetti, F., Pasqui, V., and Reichenbach, P., 1991, GIS Techniques and Statistical Models in Evaluating Landslide Hazard: Earth Surface Processes and Landforms, Vol. 16, p. 427-445.
- Chang K.T. and Tsai, B., 1991, The Effect of DEM Resolution on Slope and Aspect Mapping: Cartography and Geographic Information Systems, Vol. 18, No. 1, p. 69-77.
- Crane, R. C., 1994a, Geologic Map of the Antioch South Quadrangle, unpublished, scale 1:24,000.
- Crane, R. C., 1994b, Geologic Map of the Clayton Quadrangle, unpublished, scale 1:24,000.
- Dibblee, T. W., Jr., 1980a, Preliminary Geologic Map of the Antioch South Quadrangle, Contra Costa County, California: U. S. Geological Survey Open File Report 80-536, scale 1:24,000.
- Dibblee, T. W., Jr., 1980b, Preliminary Geologic Map of the Clayton Quadrangle, Contra Costa County, California: U. S. Geological Survey Open File Report 80-547, scale 1:24,000.
- Dikau, R., 1989, The Application of a Digital Relief Model to Landform Analysis in Geomorphology, in Raper, J., ed., Three Dimensional Applications in Geographical Information Systems, p. 51-77.
- Ellen, S.D. and Wieczorek, G.F., 1988, Landslides, Floods and Marine Effects of the Storm of January 3-5, 1982, in the San Francisco Bay Area Region, California: U. S. Geological Survey Professional Paper 1432, 310 p., 14 plates.
- Fryer, J.G., Chandler, J.H., and Cooper, M.A.R., 1994, On The Accuracy of Heighting From Aerial Photographs and Maps: Implications to Process Modellers: Earth Surface Processes and Landforms, Vol. 19, p. 577-583.
- Gao, J., 1993, Identification of Topographic Settings Conducive to Landsliding From DEM in Nelson County, Virginia, U.S.A.: Earth Surface Processes and Landforms, Vol. 18, p. 579-591.
- Glass, C.E. and Slemmons, D.B., 1978, State-of-The-Art For Assessing Earthquake Hazards in The United States, Report 2, Imagery in Earthquake Analysis, U.S. Army Engineer Waterways Experiment Station Miscellaneous Paper S-73-1.
- Graymer, R.W., Jones, D.L., and Brabb, E.E., 1994, Preliminary Geologic Map Emphasizing Bedrock Formations in Contra Costa County, California: A Digital Database: U. S. Geological Survey Open File Report 94-622.
- Intergraph Corporation, p. 10-87 to 89.
- Intergraph Corporation, ImageStation Match-T (ISMT) User's Guide, September 1994, Section 1 and Appendix B.
- Intergraph Corporation, Modular GIS Environment/Image Station Imager-3 User's Guide, Vol. II, June 1994; Intergraph Corporation, Huntsville Alabama, chapter 10.2.
- Isaacson, D.L. and Ripple, W.J., 1990, Comparison of 7.5-Minute and 1-Degree DEMs: Photogrammetric Engineering and Remote Sensing, Vol. 56, No. 11, p. 1523-1527.